2011

The characterization of dry powder magnesium hydroxide suspensions using sedimentation, thermal analysis and other techniques

Yingzhe Wang
The University of Toledo

A Thesis

entitled

The Characterization of Dry Powder Magnesium Hydroxide Suspensions Using Sedimentation, Thermal Analysis and Other Techniques

by

Yingzhe Wang

Submitted to the Graduate Faculty as partial fulfillment

of the requirements of the Master of Science degree in Pharmaceutical Sciences

with Industrial Pharmacy Option

Dr. Jerry Nesamony, Committee Chair

Dr. Kenneth S. Alexander, Committee Member

Dr. Sai Hanuman Sagar Boddu, Committee Member

Dr. Patricia R. Komuniecki, Dean
College of Graduate Studies

The University of Toledo

December 2011

An Abstract of

The Characterization of Dry Powder Magnesium Hydroxide Suspensions Using Sedimentation, Thermal Analysis and Other Techniques

by

Yingzhe Wang

Submitted to the Graduate Faculty as partial fulfillment
of the requirements of the Master of Science degree in Pharmaceutical Sciences
with Industrial Pharmacy Option

The University of Toledo
December 2011

Dry powder magnesium hydroxide suspensions in various media were characterized by their settling behavior as determining their particle size in the dispersed phase by sedimentation and other techniques, as well as thermal analysis. Several different methods were used for the particle size determination, including sieve analysis, sedimentation, scanning electron microscopy (SEM), and laser diffraction (LD). The settling behavior of the concentrated flocculated suspensions is termed hindered settling, where Stokes' law cannot be applied. Several different theories were utilized for the interpretation of the hindered settling phenomenon by correlating the observed rate of fall of the interface and Stokes' limiting velocity. The best matches for the case of dry powder magnesium hydroxide suspensions were the theories of Steinour, Richardson and Zaki, and Dollimore and McBride.

The particle size determined by sieve analysis was much greater than that determined by sedimentation due to the clustered porous nature of the dry powder magnesium hydroxide. Thus, sieve analysis is not a suitable method for particle size determination for suspensions since the vehicle associates with the dry powder to cause it to break apart

into its individual granules. Sedimentation methods were verified to be more consistent with both SEM and LD results although the un-spherical shape of the particles casued the precision of the sedimentation results to vary to some extent. The unbound and bound water associated with the suspensions in various media were determined by thermal techniques such as differential scanning calorimetry (DSC) and thermogravimetry (TG). The thermal results showed that the dried sediments decomposed after heating at temperatures above 350 °C, which made it difficult to determine the interstitial water content. X-ray powder diffraction (PXRD) was used to verify the decomposition of magnesium hydroxide as the dry powder and dried sediments before and after heating by comparing the peak patterns with standards.

All the efforts put in this work

are dedicated to my beloved parents

Guoyu Wang & Juhui Tan

Acknowledge

I give my sincere thanks to my advisor Dr. Kenneth S. Alexander for his encouragement, guidance and patience during my two years' study here in The University of Toledo. Without his willingness to help and motivate me in both my work and life, nothing could have been easily achieved. I would give my thanks to Dr. Alan Riga for his enthusiastic help and valuable advice in thermal analysis, Dr. Timothy Fisher, and Dr. Pannee Burckel, for their help in instrumentation usage. I would also give my thanks to Dr. Curtis D. Black for his kindness, help and encouragement. It has been a wonderful experience to be a teaching assistant in his neat and comfortable Pharm.D teaching lab. I give my thanks to Dr. Jerry Nesamony, Dr. Sai Hanuman Sagar Boddu for being my Committee members, and Dr. Vincent Mauro to be my graduate faculty representative. I would like to thank all of the faculty and staff of the College of Pharmacy for the help they provided me during this opportunity to study in the United States. I would extend my thanks to all senior students and lab-mates for the help and laugh they provided.

Finally, I would like to take this opportunity to thank Dr. Ping Tong for her recommendation to this program. I am deeply grateful to my beloved parents for all their love and support, and all my friends here in the United States and back in China.

Contents

List of Tables

List of Figures

Chapter 1

Introduction

The aim of this study was to characterize suspensions prepared from dry powder magnesium hydroxide using various methods for the determination of the dispersed particle size as well as by thermal analysis.

Magnesium hydroxide suspension is widely known as an antacid or laxative in the form of milk of magnesia in the pharmaceutical industry. Dry powder magnesium hydroxide is also used in a wide range of industries and applications as well as in combinations with other elements to create a versatile substance.

A pharmaceutical suspension is a coarse dispersion in which insoluble particles, generally greater than 1 μm in diameter, are dispersed in a liquid medium. An aqueous suspension is a useful formulation system for administrating an insoluble or poorly soluble drug. The large surface area of the dispersed drug ensures a high availability for dissolution and hence absorption. [1] Such coarse suspensions are thermodynamically unstable due to the large surface energy and the tendency of settling for the dispersed particles.

Dry powder magnesium hydroxide suspensions are concentrated systems and the settling behavior is quite different from that of a dilute poly-dispersed system, thus it cannot be discribed easily by Stokes' Law. The concentrated dispersed particles makes free settling of a single particle impossible. The settling of a single particle will be effected by the surrounding particles. [2] This phenomenon is termed hindered settling, and is further discussed in Chapter 2.

The behavior and properties of particulate materials are, to a large extent, dependent on particle morphology (shape, texture, etc.), as well as size and size distribution. [3] Therefore, particle size and size distribution of the dispersed phase is an essential parameter for the characterization of a suspension. Several different methods were used and compared for the determination of particle size. Such methods as sieve analysis, sedimentation, scanning electron microscopy (SEM), and laser diffraction (LD) are discussed in Chapter 4.

Thermal techniques such as differential scanning calorimetry (DSC) and thermogravimetry (TG) are used for the characterization of the thermal stability of dry powder magnesium hydroxide suspensions.

TG is a technique in which the mass change of a substance is measured as a function of temperature while the substance is subjected to a controlled temperature program. [4] This method is suitable for the determination of the various waters associated with the suspension sediments. It was the water loss with temperature increase as a means to

verify total water composition. It also allows us to investigate the decomposition of magnesium hydroxide under high temperature.

DSC is used to measure heat flow rates (power) and determine the characteristic temperature of a reaction or a transition. This methods was also used in this study to determine the water content of magnesium hydroxide sediments.

The decomposition of magnesium hydroxide was also verified by X-ray powder diffraction (PXRD) for the sample compositions of dry powder magnesium hydroxide, magnesium hydroxide suspension sediment before and after decomposition by pattern comparisons.

Chapter 2

Hindered Settling Theory

2.1 Introduction

Suspensions are heterogeneous systems consisting of two phases. The continuous or external phase is generally a liquid or semisolid, and the dispersed or internal phase is made up of particulate matter that is essentially insoluble in, but dispersed throughout, the continuous phase. The dispersed phase may consist of discrete particles, or it may be a network of particles resulting from particle-particle interactions. [1]

For pharmaceutical purposes, physical stability of suspensions may be defined as the condition in which the particles do not aggregate and in which they remain uniformly distributed throughout the dispersion. [2] However, sedimentation is the most obvious sign that a dispersion contains large particles. Since most solids have a higher density than the external liquids, no dispersant can negate the pull of gravity. The rate of sedimentation decreases for smaller particles or higher viscosities but is never eliminated. [3] Thus, it is necessary and essential to consider the factors affecting the process of sedimentation.

An acceptable suspension possesses certain desirable qualities, including [2]:

1) The suspended material should not settle rapidly;
2) The particles that do settle to the bottom of the container must not form a hard cake, but should be readily re-dispersed into a uniform mixture when the container is shaken;
3) The suspension must not be too viscous to pour freely from the orifice of the bottle or to flow through a syringe needle.

Two distinct theoretical approaches are possible for considering solid particles settling under the force of gravity in a liquid. [4] In dilute suspensions, containing less than 2 g of solid per 100 mL of liquid, it is statistically possible to consider each particle falling unhindered from its initial position to the bottom of the container. The particles do not interfere with one another during sedimentation and free settling occurs. This process of free settling obeys Stokes' law. [2] In concentrated suspensions, however, there is a real possibility that the fall of any particle will be hindered by the other particles in its path, and Stokes' law no longer applies. There is one single observation which allows this transition to be noted, namely that under hindered fall the suspension settles "*en bloc*" with an interface, above which is a clear supernatant liquid. [2,4]

Two observations are at once apparent in hindered settling, namely the rate of fall of the interface and the final settled volume of the sediment. When fall is hindered then the mode of settlement may be affected by the following factors: [4]

1) Concentration of the suspension;
2) Tendency of the particles to flocculate;
3) Physical properties of the suspending liquids, e.g. viscosity, surface tension and dielectric constant;
4) Chemical properties of the suspending liquids;
5) Size relation between the smallest range of particles present and the larger particles (i.e. do the smaller particles fit in between the close-packed larger particles?);
6) The lapse of time since settling began (a consequence of "compression" or increase in concentration in the lower levels).

2.2 Stokes' Law

In dilute suspensions, the fall of a single isolated spherical particle under gravity in an infinite viscous fluid is described by Stokes' Law. [5]

This sedimentation process depends on an application of Stokes' law for the viscous drag on a moving spherical particle. [3] At constant velocity, the frictional force (F_f) is proportional to the radius (r), the velocity (Vs), and the viscosity (η) of the medium. The proportionality constant for conditions of laminar flow is equal to (6π),

$$F_f = 6\pi r V_s \eta \qquad \text{Eqn. 2.1}$$

The gravitational force (F_g) acting on a sphere in a medium is

$$F_g = \frac{4}{3}\pi r^3(\rho_s - \rho_l)g \qquad \text{Eqn. 2.2}$$

where (ρ_s) is the density of the dispersed particle, and (ρ_l) is the density of the medium.

Under conditions of steady state,

$$F_f = F_g \qquad \text{Eqn. 2.3}$$

Therefore,

$$6\pi r V_s \eta = \frac{4}{3}\pi r^3(\rho_s - \rho_l)g \qquad \text{Eqn. 2.4}$$

$$V_s = \frac{2r^2(\rho_s - \rho_l)g}{9\eta} \qquad \text{Eqn. 2.5}$$

or

$$\mathrm{r} = \sqrt{\frac{9\eta V_S}{2g(\rho_s - \rho_l)}} \qquad \text{Eqn. 2.6}$$

Stokes' law applies only to spherical particles, and non-spherical particles are described in terms of an equivalent diameter; this is the Stokes' equivalent diameter (d_{St}). [5]

$$d_{St} = \sqrt{\frac{18\eta V_S}{g\,(\rho_s - \rho_l)}} \qquad \text{Eqn. 2.7}$$

One of the most significant limitations of Stokes' law is that the particles are assumed to settle under laminar flow conditions, i.e. that no turbulence is induced in the medium by their movement. [5] In other words, the rate of sedimentation of a particle must not be so rapid that turbulence is set up, since this in turn will affect the sedimentation of the particle. Whether the flow is turbulent or laminar is indicated by the dimensionless Reynolds number (Re). Stokes' law cannot be used if (Re) is greater than 0.2, since turbulence appears at this value. [6]

$$R_e = \frac{V_S d_{St} \rho_l}{\eta}$$ Eqn. 2.8

As the particle increases in size or becomes irregular in shape, turbulence begins to develop. The assumption that the resistance or fractional force (F_f) to the motion of the particle is entirely due to the viscosity of the medium is no longer valid. [7] This invalidation also happens to concentrated suspensions.

2.3 Experimental Observations on the Rate of Settling

In concentrated suspensions, the obvious parameter to note is the rate of fall of the "sludge line" (the interface). The normal curve for the position of the interface plotted against time is seen in Figure 2.1. However, an alternative curve which often occurs is seen in Figure 2.2. In this plot the initial portion is followed by a linear region which corresponds to the initial linear region in Figure 2.1. [4]

A qualitative analysis indicates three regions, an initial region (A), a subsequent "linear" region (B) and finally a "compressive" region (C) in which only small changes take place when considered against time. [4]

Region (A) is probably seen in many of the flocculated systems. The usual explanation is that in region (A) the suspension is adjusting itself to a steady state. It will have been recently agitated and flocs may have been broken up. In region (A), reflocculation is taking place with a corresponding increase in the rate of fall of the interface. Region (B) should be considered the hindered settling region from which the particle size may be

calculated. Region (C) represents the approach to saturation and the final settled volume. Figure 2.1 differs from Figure 2.2 only in that the initial region (A) is absent in Figure 2.1. [4]

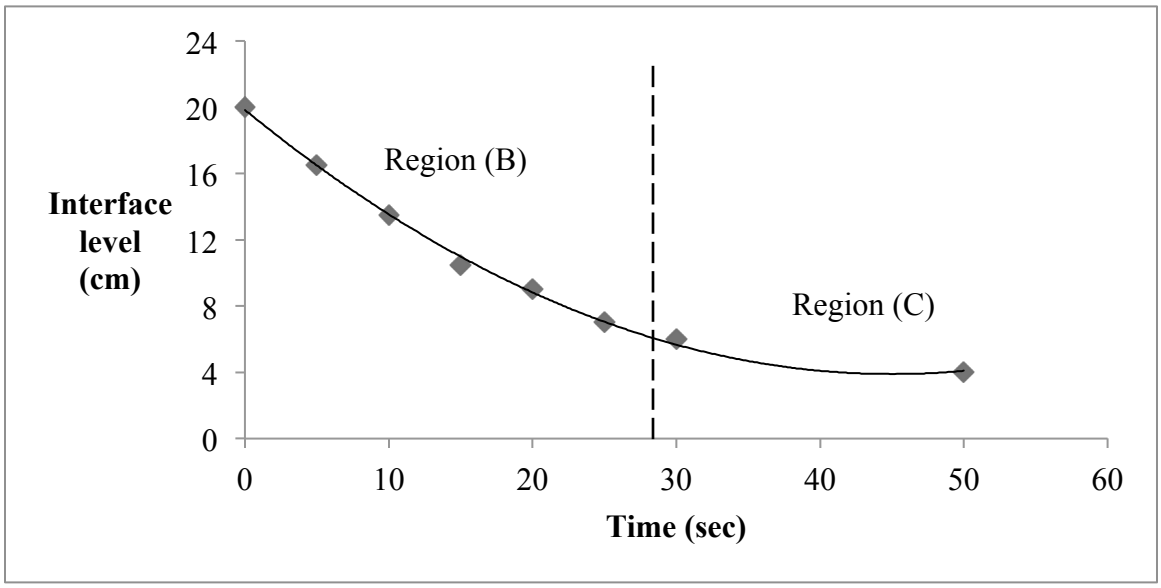

Figure 2.1 A "normal" plot of the position of the interface against time in hindered settling [4]

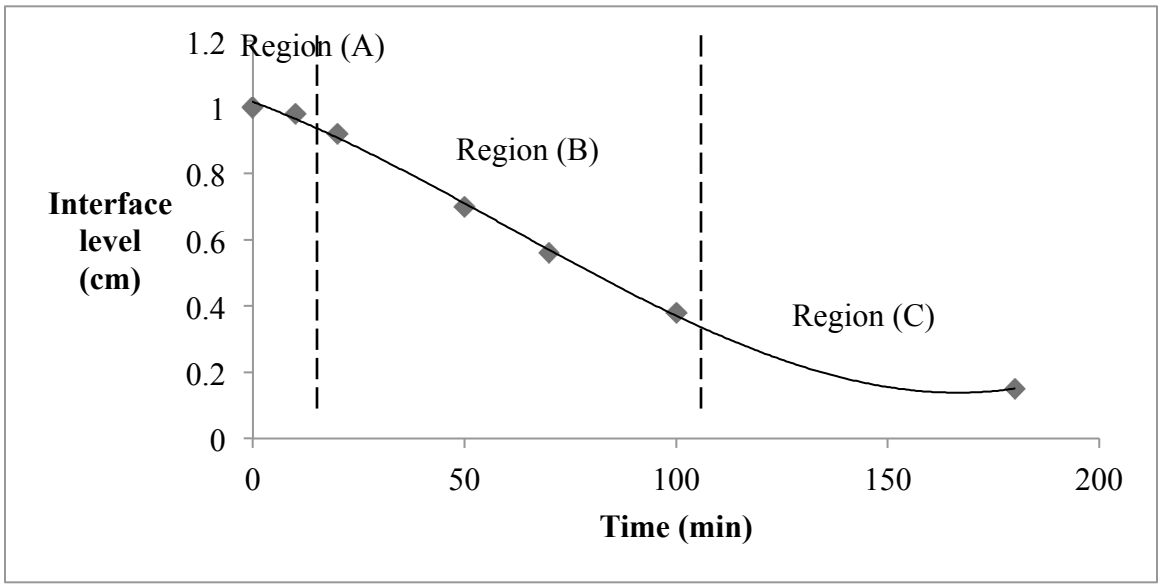

Figure 2.2 An alternative plot of the position of the interface against time in hindered settling [4]

Therefore, Davies et al. [8] defined hindered settling as a process of sedimentation in which a clear suspension-supernatant interface forms early. The interface settles at a linear rate (Q values or negative of the slope of the linear region from the observation plot) for a considerable portion of the period during which sedimentation occurs.

At lower concentrations in hindered settling, the linear regions may not be apparent during sedimentation. An intermediate state occurs when not all particles are associated with flocs or due to different sized particles. The intermediate state is denser at lower concentrations, where the small particles pass between larger particles and the interface is not clear. As the concentration of the suspension increases, however, the interface is clearly observed. The space available for the particle to fall decreases and the rate of fall of the interface decreases. [9, 10]

Thus, a minimum suspension concentration to form a clear interface with an apparent linear region is essential for the application of hindered settling theory.

2.4 Modifications to Stokes' Law

The kinetics of sedimentation of solid particles in liquid media and the characteristics of the resultant sediments are of wide applicability in industry, being of importance in such activities as ore processing, chemicals and ceramics manufacture, and sewage treatment. [8] For concentrated suspensions with particles of different sizes, the conditions which govern the fall of the interface are very complicated due to the possible particle-liquid

and particle-particle interactions. [9]

As a result of a number of investigations, various equations have been proposed to represent the relationships between settling rate and such variables as initial suspension concentration, Stokes' law limiting velocity, container dimensions, concentration of settled sediments, shape of the particle, bulk viscosity of the suspension, etc.. [8]

The relationship of the rate of fall of the interface (Q) and suspension concentration is expressed as,

$$Q = V_s[f(c)] \qquad \text{Eqn. 2.9}$$

where [f(c)] is the function of the suspension concentration. One of the applications for such a relationship is the determination of the mean particle or aggregation size. If such a dependence is established, extrapolation to infinite dilution would transform (Q) into the Stokes' limiting velocity (V_s) and the corresponding particle or aggregation size could be calculated. This [f(c)] was replaced by other terms in most studies based on their considerations of suspension concentrations and other properties. [11]

The equations based upon Eqn. 2.9 to modify Stokes' law, which had been proved to be most efficient and reliable in previous studies of inorganic suspensions include: Steinour's equation [12], Richardson and Zaki's equation [13, 14], and the Dollimore and McBride equation [10, 15].

2.4.1 Steinour's Equation

Steinour [12] modified Stokes' law by involving a dimensionless "shape factor". [8] A series of assumption was made by Steinour in this modification which included: the distribution of spheres in an actual suspension under the best conditions of a fixed arrangement and a closely maintained constant velocity of fall. The fluid space to maintain a constant shape within which a steady laminar flow pattern is established. The flow velocities relative to the sphere increase from zero at the sphere surfaces to a maxima in the intervening regions; and the arrangement of the spheres in different suspensions are identical.

Steinour [12] concluded that at a given concentration the average velocity (V) is proportional to the average velocity gradient or rate of shear at the sphere surface, and to the average spacing between spheres. When the volume concentration is changed, the flow space necessarily changes in shape. Therefore, the term, shape factor [$\phi(\varepsilon)$] is introduced into this modification, which is a function only of the proportion of fluid (ε), also known as internal liquid volume fraction or internal porosity.

Since the concentration of solid by volume is (1-ε), [$\phi(\varepsilon)$] presents a function of the concentration. Another effect of concentration is implicit in the rate of shear at the surface of a sphere, which is evaluated in terms of the viscous resistance (R), which is expressed as:

$$R = \frac{6\pi r V}{\phi(\varepsilon)} \qquad \text{Eqn. 2.10}$$

Viscous resistance (R), also known as fluid friction equals the motive force, which is the weight of the sphere minus its buoyancy. Steinour pointed out that the hydrostatic pressure developed by a layer of mixture is determined by the density of the mixture (ρ_g) rather than by the density of the liquid (ρ_l) alone.

Therefore,

$$R = \frac{4}{3}\pi r^3(\rho_s - \rho_m)g \qquad \text{Eqn. 2.11}$$

but

$$\rho_s - \rho_m = \rho_s - [(1-\varepsilon)\rho_s + \varepsilon\rho_l] = (\rho_s - \rho_l)\varepsilon \qquad \text{Eqn. 2.12}$$

Substituting Eqn. 2.12 into Eqn. 2.11, and into Eqn. 2.10 and solving for (V),

$$V = \frac{2g(\rho_s - \rho_l)r^2\varepsilon\phi(\varepsilon)}{9\eta} \qquad \text{Eqn. 2.13}$$

(V) was defined as the average relative velocity between spheres and fluid, whereas the measured velocity is that of the particles relative to a fixed horizontal plane. The velocity of which will here be represented by (Q). The relationship between (Q) and (V) may be derived by equating the volumes of solid and fluid that move in opposite directions past a unit of horizontal cross section in unit of time.

That is,

$$(1-\varepsilon)Q = \epsilon(V - Q) \qquad \text{Eqn. 2.14}$$

or

$$Q = \varepsilon V \qquad \text{Eqn. 2.15}$$

Substituting Eqn. 2.15 into Eqn. 2.13,

$$Q = \frac{2g(\rho_s - \rho_l)r^2\varepsilon^2\phi(\varepsilon)}{9\eta} \quad \text{Eqn. 2.16}$$

In terms of Stokes' law (V_s), as seen in Eqn. 2.5:

$$Q = V_s\varepsilon^2\phi(\varepsilon) \quad \text{Eqn. 2.17}$$

Steinour also evaluated the effect of size and part of the effect of shape by use of the hydraulic radius; only a residual undetermined shape factor [θ(ε)] is left in [ϕ(ε)], and which remains nearly constant for concentrated suspensions.

$$\phi(\varepsilon) = \frac{\varepsilon}{1-\varepsilon}\theta(\varepsilon) \quad \text{Eqn. 2.18}$$

Substituting Eqn. 2.18 into Eqn. 2.17,

$$Q = V_s\left[\frac{\varepsilon^3\theta(\varepsilon)}{1-\varepsilon}\right] \quad \text{Eqn. 2.19}$$

The shape factor [θ(ε)] was reported to be constant at approximately 0.123 over a considerable range of high concentrations with the (ε) value in the range of 0.3 to 0.7. [14, 16]

An empirical equation was also developed in this modification [17], which took the form of:

$$Q = V_s\varepsilon^2 10^{-A(1-\varepsilon)} \quad \text{Eqn. 2.20}$$

or in logarithmic form:

$$Log\left(\frac{Q}{\varepsilon^2}\right) = A\epsilon - (LogV_s - A) \quad \text{Eqn. 2.21}$$

where (A) is a constant for a given system.

A plot of $\left[Log\left(\frac{Q}{\varepsilon^2}\right)\right]$ against (ε) should be linear and provide data for (A) and (V_s) from the slope and intercept. The value of (A) was determined by Steinour as 1.82, but this

value does not apply to all systems. However, the value does not affect the particle size calculation when evaluated by extrapolation of the data to unit porosity. Thus, the particle size can be easily calculated using Stokes' law. [17, 18]

2.4.2 Richardson and Zaki's Equation

Richardson and Zaki [13] assumed that all the particles in the same horizontal layer are settling at the same constant velocity and that a statistically stable arrangement is maintained based on the fact that a sharp interface forms during the settling of a suspension.

There are two possible arrangements: one is that the vertical distances between the layers were taken as equal to the distance between the particles in a horizontal direction; the other is that the particles were arranged in adjacent horizontal layers so as to offer minimum resistance to the motion of a fluid flowing through the system.

With mathematical simplifications made to both arrangements, Richardson and Zaki concluded this relationship between the linear rate of settling (Q) of the interface and the Stokes' limiting velocity (V_s) to be:

$$Q = V_s(\varepsilon)^{4.65} \qquad \text{Eqn. 2.22}$$

The value of 4.65 was further generalized into a dimensionless quantity (n), thus Richardson and Zaki [14] proposed another empirical equation as follows:

$$Q = V_s(\varepsilon)^{n} \qquad \text{Eqn. 2.23}$$

or

$$LogQ = nLog\varepsilon + LogV_s \qquad \text{Eqn. 2.24}$$

This empirical equation is more tractable than Steinour's equation Eqn. 2.19. The linear rate of settling (Q) of the interface will increase with increasing initial porosity (ε) of the mixed suspension.

Davies et al. [8] investigated (n) at various conditions of (ε). Since (1- ε) decreases (to zero) as (ε) increases, a plot of the function [Q(1-ε)] against ε (see Figure 2.3) will pass through a maximum at some (ε). The quantity [Q(1-ε)ρ_s], known as the "solid flux", indicates the mass transfer of solid per unit time down the sedimentation column. It is therefore of importance as a measure of solid transport.

If the system obeys Richardson and Zaki's equation (Eqn. 2.23), then,

$$\frac{d[Q(1-\varepsilon)]}{d\varepsilon} = \frac{d[V_s\varepsilon^n]}{d\varepsilon} = -V_s\varepsilon^n + nV_s\varepsilon^{n-1}(1-\varepsilon) \qquad \text{Eqn. 2.25}$$

The maximum value for [Q(1-ε)] occurs when $\frac{d[Q(1-\varepsilon)]}{d\varepsilon} = 0$.

Defining the porosity at this point as (ε_1) gives,

$$V_s{\varepsilon_1}^n = V_s{\varepsilon_1}^n\, n{\varepsilon_1}^{-1}(1-\varepsilon_1) \qquad \text{Eqn. 2.26}$$

the form of which is simplified as:

$$n = \frac{\varepsilon_1}{1-\varepsilon_1} \qquad \text{Eqn. 2.27}$$

and

$$\varepsilon_1 = \frac{n}{n+1} \qquad \text{Eqn. 2.28}$$

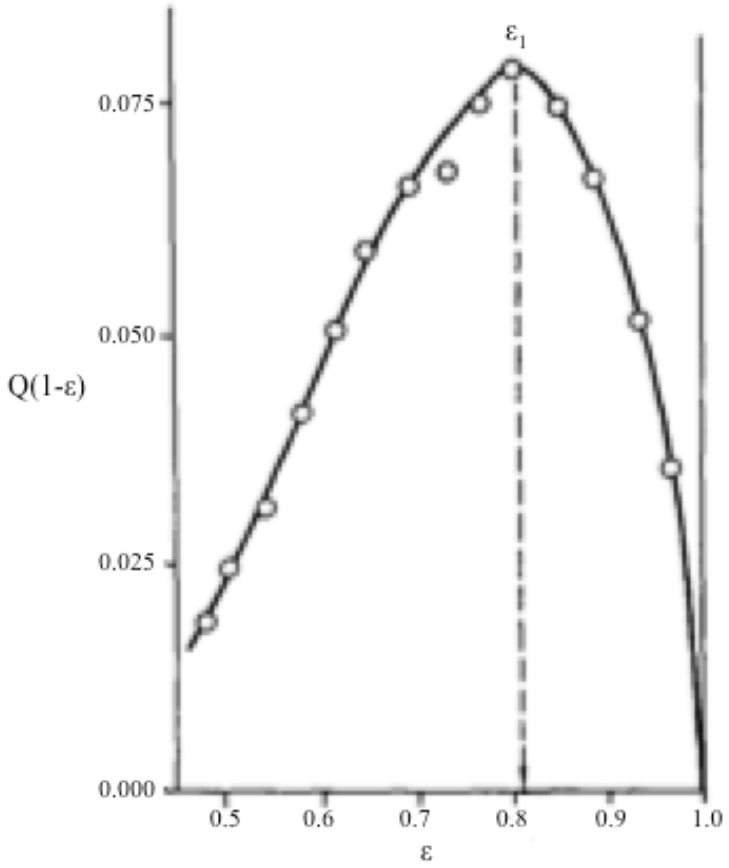

Figure 2.3 Plot of the function [Q(1-ε)] against (ε) [4]

Hence (n), which has been assumed to have no physical significance, is in fact a function of the porosity (ε_1) at which [Q(1- ε)], and hence solids flux has a maximum value for a system. Richardson and Zaki's equation (Eqn. 2.23) may thus be rewritten as:

$$Q = V_s \varepsilon^{\varepsilon_1/(1-\varepsilon_1)} \qquad \text{Eqn. 2.29}$$

Therefore, (ε_1) appears to be an important parameter in describing the settling rates of suspensions. A relationship should exist between (ε_1) and the chemical system parameters which determine its magnitude. Additionally, (ε_1) is of importance since it represents the initial suspension concentration for maximum solid flux.

Davies et al. [8] therefore provided the following conclusions:

1) The power number (n) for the Richardson and Zaki equation is a useful indication of the effect of an increment of solids concentration in reducing the settling of a suspension.
2) The term (ε_1), the initial porosity at which the function [Q(1-ε)] has a maximum value. It is a useful indication of the tendency of a system to show hindrance. It is in fact, the value of (ε) at which solid flux has a maximum value for a suspension, if the latter obeys the Richardson and Zaki equation.
3) The term (ε_1) has an advantage over (n) as an index of hindrance. The approach to maximum hindrance corresponds to (ε_1) converging to an upper boundery of unity, where (n) diverges to indefinitely large values.
4) Hindrance to settling increases as (ε_1) increases, and tends (as (ε_1) approaches unity) to a maximum represented by the ratio of the settling rate (Q) at (ε_1) to Stokes' limiting rate (V_s) having a maximum value of $\exp^{-1}$.
5) Hindrance to settling is directly proportional to system polarity.
6) Surface areas may not be applicable in any simple way to the interpretation of the hindered settling behavior.
7) The charge density on the solid surface exposed to the bulk liquid is probably the dominant factor in determining hindrance to sedimentation.

2.4.3 Dollimore and McBride's Equation

Dollimore and McBride [10] proposed a further empirical equation using results from the observation that plots of the logarithm of the rate of fall of the interface (Log Q) against the concentration of the suspension (C) are linear. Hence, [4, 15, 19]

$$Log\ Q = a - bC \qquad \text{Eqn. 2.30}$$

so that,

$$Q = 10^{a}10^{-bc} \qquad \text{Eqn. 2.31}$$

where (a) and (b) are constants.

At infinite dilution,

$$a = LogQ \qquad \text{Eqn. 2.32}$$

and

$$Q = V_s \qquad \text{Enq. 2.33}$$

whence,

$$10^{a} = 10^{logV_s} = V_s \qquad \text{Eqn. 2.34}$$

and therefore

$$Q = V_s 10^{-bC} \qquad \text{Eqn. 2.35}$$

The initial porosity (ε) of a settling particulate system is given by,

$$\varepsilon = \frac{V_{sn} - V_{sd}}{V_{sn}} \qquad \text{Eqn. 2.36}$$

where (V_{sn}) is the volume of suspension, (V_{sd}) is the volume of solid.

However,

$$V_{sd} = \frac{mass\ of\ solid}{density\ of\ solid} = \frac{M_s}{\rho_s} \qquad \text{Eqn. 2.37}$$

whence

$$\varepsilon = \frac{V_{sn} - M_s/\rho_s}{V_{sn}} = 1 - \frac{M_s}{\rho_s V_{sn}} \qquad \text{Eqn. 2.38}$$

Since $\frac{M_s}{V_{sn}} = C$, it follows that,

$$\varepsilon = 1 - \frac{C}{\rho_s} \qquad \text{Eqn. 2.39}$$

or

$$C = \rho_s(1 - \varepsilon) \qquad \text{Eqn. 2.40}$$

Using this in Eqn. 3.35 gives

$$Q = V_s 10^{-b\rho_s(1-\varepsilon)} \qquad \text{Eqn. 2.41}$$

or

$$LogQ = LogV_s - b\rho_s(1 - \varepsilon) \qquad \text{Eqn. 2.42}$$

The behavior in terms of this law (Eqn. 3.41) may be noted with reference to the plot of [Q(1-ε)] against (ε) as shown in Figure 2.3. The value of [Q(1-ε)] is given from Eqn. 3.41 as,

$$Q(1 - \varepsilon) = V_s 10^{-b\rho_s(1-\varepsilon)}(1 - \varepsilon) \qquad \text{Eqn. 2.43}$$

Differentiation then gives,

$$\frac{d[Q(1-\varepsilon)]}{d\varepsilon} = 2.303 b\rho_s V_s 10^{-b\rho_s(1-\varepsilon)} \left(1 - \varepsilon - \frac{1}{2.303 b\rho_s}\right) \qquad \text{Eqn. 2.44}$$

According to Figure 2.3, the valued of $\frac{d[Q(1-\varepsilon)]}{d\varepsilon} = 0$ at a maximum of [Q(1-ε)] which occurs at (ε_1), therefore,

$$\varepsilon_1 = 1 - \frac{1}{2.303 b \rho_s} \qquad \text{Eqn. 2.45}$$

Substituting Eqn. 2.45 into Eqn. 2.40 gives the solid concentration for maximum solid flux ($C\varepsilon_1$) as:

$$C_{\varepsilon_1} = \frac{1}{2.303 b} \qquad \text{Eqn. 2.46}$$

2.5 Other Theories for Concentrated Suspensions

2.5.1 Permeability

Davies et al [20] classified the explanation of the behavior of the concentrated suspensions into two distinct classes of theories. The first set of theories regard this problem as essentially a modification which must be applied to the classical equations for dilute suspensions based on Stokes' law. [21] The second set of theories regard the suspensions as a packed bed through which a fluid is allowed to flow and is based on the phenomenon of permeability. [22]

The Kozeny-Carman equation may be represented in the case of fluid flow through settled beds of solid particles by [20, 21]:

$$u = \left[\frac{\varepsilon^3}{k\eta S^2}\right]\left[\frac{\Delta p}{L}\right] \qquad \text{Eqn. 2.47}$$

where (u) is the volume of fluid flowing through the bed per second divided by the total cross-section of the container ($cm \cdot s^{-1}$) or the apparent fluid flow velocity through a

motionless bed; (ε) is the volume of pore space per unit volume of bed (i.e. initial porosity); (k) is the Kozeny constant originally stated as 5.0; (η) is the fluid viscosity ($g \cdot cm^{-1} \cdot s^{-1}$); (S) is the particle surface area per unit bed volume (cm^{-1}); (Δp) is the pressure differences across the bed depth ($g \cdot cm^{-1} \cdot s^{-2}$); and (L) is the bed depth (cm).

The value of (S) can be expressed for a bed of spheres having radius (r) and porosity (ε). Let a bed volume (V) contain one sphere. The sphere volume is given by [(1- ε)V] and $V = \frac{\frac{4}{3}\pi r^3}{1-\varepsilon}$. Therefore,

$$S = \frac{4\pi r^2}{V} = \frac{4\pi r^2(1-\varepsilon)}{\frac{4}{3}\pi r^3} = \frac{3(1-\varepsilon)}{r} \qquad \text{Eqn. 2.48}$$

In any cubic centimeter of the bed there is an additional mass (as compared with the situation in motionless fluid of density (ρ_l)) due to the element of volume (1- ε) having an additional density of (ρ_s - ρ_l) since (ρ_s) represents the solid density. This creates pressure difference [(1- ε)(ρ_s - ρ_l)gL] across the bed depth, and hence,

$$\frac{\Delta p}{L} = (1-\varepsilon)\left(\rho_s - \rho_l\right)g \qquad \text{Eqn. 2.49}$$

where (g) is the acceleration due to gravity ($cm \cdot s^{-2}$).

Substituting in Eqn. 2.47 for (S) and and $\left[\frac{\Delta p}{L}\right]$ then gives,

$$u = \left[\frac{1}{k}\right]\left[\frac{\varepsilon^3}{1-\varepsilon}\right]\left[\frac{gr^2(\rho_s-\rho_l)}{9\eta}\right] \qquad \text{Eqn. 2.50}$$

In hindered settling, the particles move under laminar flow conditions (i.e. where Reynolds number is ≤ 0.2) with a measured velocity (Q) relative to a fixed horizontal plane, through a liquid volume, as compared with the flow of liquid at velocity (u) through a motionless bed; therefore (u = Q). Since the Stokes' limiting velocity (V_s) was

given in Eqn. 2.5, then:

$$Q = (V_s)\left[\frac{1}{k}\right]\left[\frac{\varepsilon^3}{1-\varepsilon}\right] \qquad \text{Eqn. 2.51}$$

There is a difference between a sedimenting mass and a settled bed, in that in the former the particles can adjust their positions to the fluid flow, which is impossible in the bed. However, in the hindered settling condition, particles of different masses settle at one velocity and show very little or no sideways motion. The sedimenting plug is therefore comparable to a fluidized bed through which laminar flow is occurring. [20]

2.5.2 Compartment Model

Ping Tong et al. [23, 24] developed a new compartment model theory to model the hindered settling behavior. This theory supported the presence of a mean floc radius in the concentrated suspensions and proved the non-linearity of the settling profile.

According to Ping Tong [23] the sedimentation process in a concentrated suspension exhibiting hindered settling can be influenced by two interactions: 1) hindered settling, in which hydrodynamic interactions such as the formation of clusters and flocculation have been included; and 2) diffusion, which is caused by the concentration gradient down the sedimentation column and thus causes an impetus for particles or clusters to resist sedimentation. Each of theses interactions may be visualized independently as a separate "compartment" to account for the two sedimentation processes as shown in Figure 2.4. The diffusion compartment moves down with a net settling rate (q) relative to the liquid

and the sedimentation compartment with an apparent settling rate (Q).

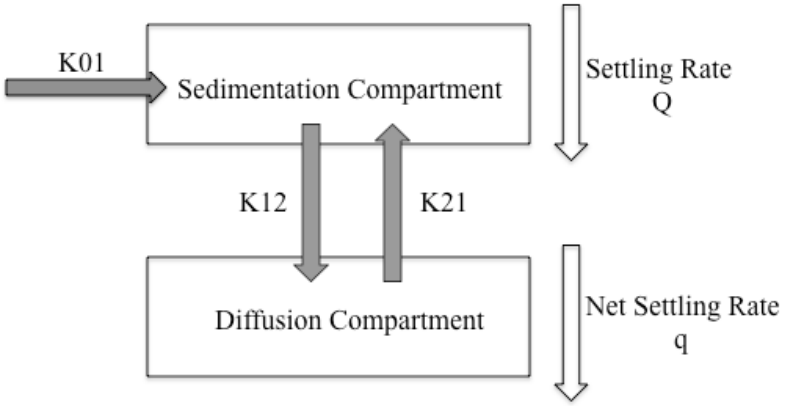

Figure 2.4 Schematic drawing of a "Two-Compartment" settling process (K01 = the first order rate constant of the movement particles into the sedimentation compartment, K12 = the first order rate constant of the movement particle from the sedimentation compartment to the diffusion compartment, K21 = the first order rate constant of the movement particles from the diffusion compartment to the sedimentation compartment)

A bi-exponential model was developed, which gives the following equations:

For the sedimentation compartment,

$$\frac{dQ}{d(1-\varepsilon)} = K_{01}Q + K_{21}q - K_{12}q \qquad \text{Eqn. 2.52}$$

For the diffusion compartment,

$$\frac{dQ}{d(1-\varepsilon)} = K_{12}Q - K_{21}q \qquad \text{Eqn. 2.53}$$

Thus,

$$Q = Ae^{-\alpha(1-\varepsilon)} + Be^{-\beta(1-\varepsilon)} \qquad \text{Eqn. 2.54}$$

where (α), and (β) are hybrid rate constants expressed as,

$$\alpha = \frac{1}{2}\left[(K_{01} + K_{12}+K_{21}) + \sqrt{(K_{01} + K_{12}+K_{21})^2 - 4K_{21}K_{01}}\right] \qquad \text{Eqn. 2.55}$$

$$\beta = \frac{1}{2}\left[(K_{01} + K_{12}+K_{21}) - \sqrt{(K_{01} + K_{12}+K_{21})^2 - 4K_{21}K_{01}}\right] \qquad \text{Eqn. 2.55}$$

Since (α >> β), as the initial porosity (ε) decreases, the exponential term $[Ae^{-\alpha(1-\varepsilon)}]$

will tend to zero more quickly than the other exponential term $[Be^{-\beta(1-\varepsilon)}]$. Thus below certain (ε),

$$Q = Be^{-\beta(1-\varepsilon)} \qquad \text{Eqn. 2.56}$$

or

$$LnQ = LnB - \beta(1-\varepsilon) \qquad \text{Eqn. 2.57}$$

Therefore, a terminal line plot of (Ln Q) against (1- ε) is linear with the slope of (-β) and the intercept of (Ln B).

The method of residuals is used to determine (A) and (α). The straight line obtained form Eqn. 2.57 is extrapolated back to the Y-axis with the (ε) above certain values which are not included in the terminal line. The difference between the observed settling rate (Q) and the extrapolated rates ($Q_{extrp} = Be^{-\beta(1-\varepsilon)}$) at different values of (1- ε) give different residual rates (Q_{Re}).

Therefore,

$$Q_{Re} = Q - Q_{extrp} = Ae^{-\alpha(1-\varepsilon)} \qquad \text{Eqn. 2.58}$$

or

$$LnQ_{Re} = LnA - \alpha(1-\varepsilon) \qquad \text{Eqn. 2.59}$$

The residual line plot of (Ln Q_{Re}) against (1- ε) is linear with with the slope of (-α) and the intercept of (Ln A).

At infinite dilution, when (ε=1), Stokes' limiting velocity (V_s) will be,

$$V_s = Q = A + B \qquad \text{Eqn. 2.60}$$

Basu et al. [24], however, considered the sedimentation processes in a concentrated suspension exhibiting hindered settling to be influenced by three interactions. In addition to the previously stated two interactions by Ping Tong [23], Basu included a third interaction, that of the associated liquid phase. This becomes an integral part of the sedimenting floc and alters the density of the aggregates. The associated liquid phase around a sedimenting particle is shown in Figure 2.5.

The application of the compartment theory, as discussed above, to the three compartment model whose the calculation is much more complicated, it is possible to determine of $V_s = A + B + C$.

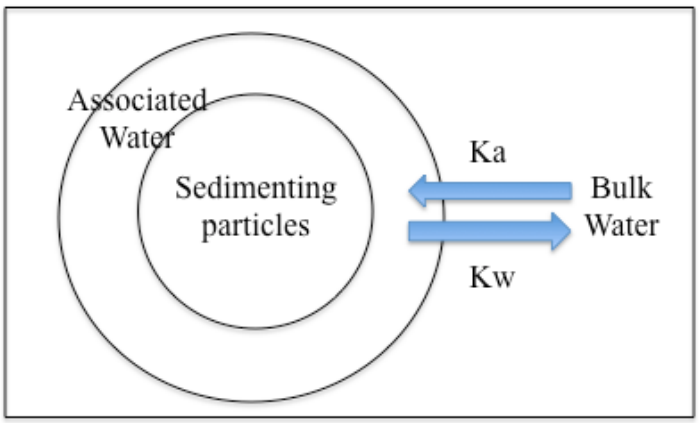

Figure 2.5 Schematic drawing of the associated liquid phase around a settling particle (K_a = the first order rate constant for the movement of water from the bulk water phase to the associated water phase of the sedimenting particle, K_w = the first order rate constant for the movement of water from the associated water phase of the sedimenting particle to the bulk water phase)

Chapter 3

Wetting and Flocculation of Suspensions

3.1 Wetting Process

A frequently encountered difficulty that is a factor of prime importance in suspension formulation concerns the wetting of the solid phase by the suspension medium. [1] By definition, a suspension is essentially an incompatible system, but to exist at all, it requires some degree of compatibility, and good wetting of the suspended material is important in achieving this end. [1] When strong affinity exists between a liquid and a solid, the liquid easily forms a film over the surface of the solid. When the affinity is non-existent or weak, however, the liquid has difficulty displacing the air or other substances surrounding the solid, and there exists an angle of contact between the liquid and the solid. This angle results from the combination of interfacial tensions, including the liquid/solid, the liquid/air, and the solid/air. [1]

For a liquid to wet a powder completely there should be a decrease in the surface free energy as a result of the immersion process. Once the particle is submerged in the liquid, the process of spreading and wetting becomes important. [2]

Suspensions should be allowed to wet sufficiently before any investigation can be made. [3] For dispersed solids which are able to absorb water and transfer into associated water attached to the individual particle by hydrogen bonding, wetting time is especially important for the validation and accuracy of the preparation of suspensions. Aging of suspensions over time, due to the possibility of changes in associated water, is of great importance in the determination of the stability of the suspension system, as well as the shelf life.

Most insoluble solids will exhibit varying degrees of hydrophobicity and will not be easily wetted. Some particles will form large porous clumps within the liquid, whereas others remain on the surface and become attached to the upper part of the container. To ensure adequate wetting, several types of wetting agents can be used [4]:

1) Surface-active agents, with HLB (Hydrophilic-Lipophilic Balance) values between 7 to 9, will lower the interfacial tensions between the solid and the liquid to a lesser extent than between the liquid and air.
2) Hydrophilic colloids, include acacia, bentonite, tragacanth, alginate, xanthan gum and cellulose derivatives, will behave as protective colloids by coating the solid hydrophobic particles with a multi-molecular layer.
3) Solvents, such as alcohols, glycerol and glycols, will reduce the interfacial tension between the liquid and air.

3.2 Flocculation

3.2.1 Particle-Particle and Particle-Liquid Interactions

In colloidal dispersions frequent encounters between the particles occur as a result of Brownian movement. [5] Whether these collisions result in permanent contact of particles

(coagulation), which leads eventually to the destruction of the colloidal system, or temporary contact (flocculation), or whether the particles rebound and remain freely dispersed (a stable colloidal system), depends on the forces of interaction between the particles. [5] These forces can be divided into three types [6]:

1) Repulsion forces due to the interaction of the electrical double layer surrounding the particles;
2) Van der Waals attractive forces based on electrical interaction, but which do not involve two net charges;
3) Steric effects, mainly due to (adsorbed) polymers;

In considering the interaction between two colloidal particles, Derjaguin, Landau, Verwey, and Overbeek produced a quantitative approach to the stability of hydrophobic sols, known as the DLVO theory of colloidal stability. [5] It is assumed that the only interaction involved are electrical repulsion and van der Waals attraction, and that these parameters are additive (see Figure 3.1).

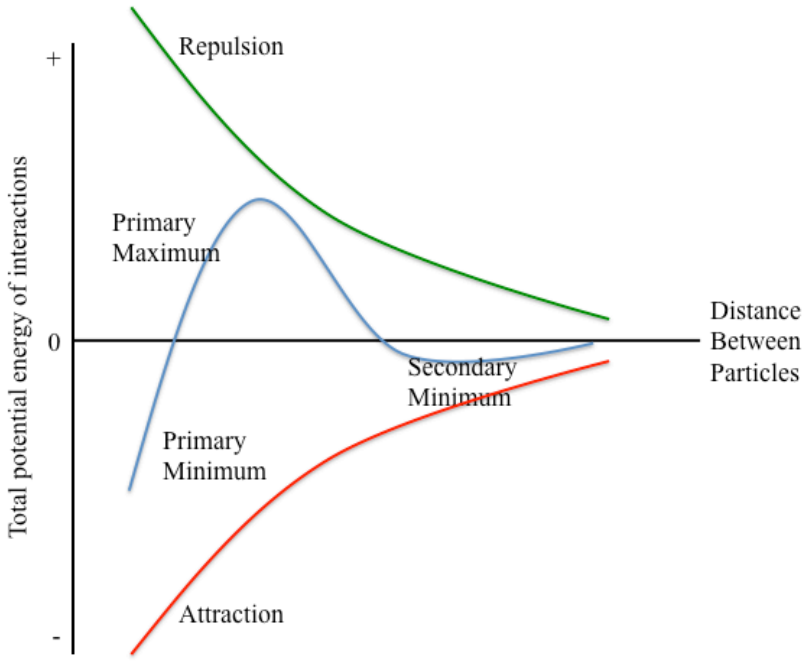

Figure 3.1 Schematic curve of total potential of interaction energy [5]

Repulsion between particles arises because of the osmotic effect produced by the increase in the number of charged species on overlap of the diffusion parts of the electrical double layer. [5] The electronic potential gradient on and near a solid-liquid interface results in the formation of an electric double layer as seen in Figure 3.2. [7]

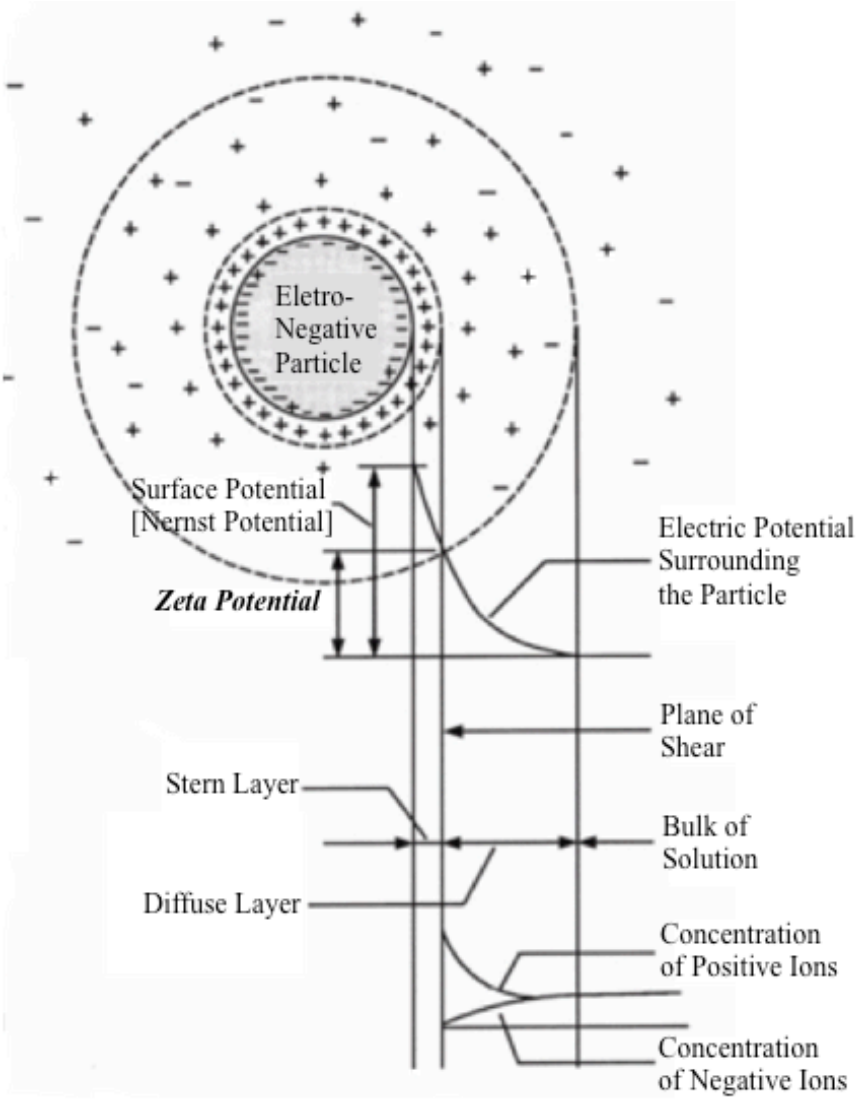

Figure 3.2 Electric double layer and zeta potential of a charged particle [7]

The potential between the surface of a tightly bound layer and the eletroneutral region of the solution is termed the zeta potential (ζ). [8] The zeta potential governs the degree of repulsion between adjacent, similarly charged particles. The energy of attraction arises

from van der Waals universal forces of attraction, the so-called dispersion forces, the major contribution to which is the electromagnetic attractions. [5] If the zeta potential is reduced below a certain value, the attractive forces exceed the repulsive forces, and particles may undergo flocculation. [9]

The overall interfacial area between the liquid and the solid control the degree of interactions. Small particles will give relatively larger interfacial area per unit mass which results in a higher degree of interaction, compared to larger particles where the interaction is reduced and their settling will be more influenced by other physical factors such as size, shape and concentration of solid particles in suspension. [10]

3.2.2 Flocculation and Aggregation

It is necessary to define the terms aggregation, coagulation and flocculation to better understand suspensions. Aggregation is a general term signifying the collection of particles into groups. Coagulation signifies that the particles are closely aggregated and difficult to redisperse, a primary minimum phenomenon of the DLVO theory of colloidal stability. In flocculation, the aggregates have an open structure in which the particles remain a small distance apart from one another. This may be a secondary minimum phenomenon or a consequence of bridging by a polymer or polyelectrolyte (see Figure 3.2). [5]

The large surface area of the particles in a suspension is associated with a surface free energy that makes the system thermodynamically unstable. This means that the particles are highly energetic and tend to regroup in such a way as to decrease the total area and reduce the surface free energy. The particles in a suspension therefore tend to flocculate. They tend to form light, fluffy conglomerates that are held together by weak Van der

Waals forces. Under certain conditions – in a compacted cake, for example – the particles may adhere by stronger forces to form what are termed aggregates. [11]

Pharmaceutical suspensions are coarse disperse systems which would sediment because of the size of the particles. The electrical repulsive forces between the particles allow them to slip past one another to form a close-packed arrangement at the bottom of the container, with the small particles filling in the voids between the larger ones. The supernatant liquid may remain cloudy after sedimentation owing to the presence of colloidal particles that remain dispersed. Those particles lowermost in the sediment are gradually pressed together by the weight of the ones above. The repulsive barrier is thus overcome, allowing the particles to pack closely together. Physical bonding, leading to "cake" or "clay" formation, may then occur owing to the formation of bridges between the particles. This can result from crystal growth and hydration effects, forces greater than agitation usually being required to disperse the sediment. [2] Such cakes tend to resist breaking on shaking, and form rigid aggregations of particles which are of larger dimensions and less re-dispersible than the original particles.

On the other hand, particles flocculated in the secondary minimum form a loosely bonded structure, called a floc or floccule. A suspension consisting of particles in this state is said to be flocculated. Although sedimentation of flocculated suspensions is fairly rapid, a loosely packed, high-volume sediment is obtained in which the flocs retain their structure and the particles are easily re-dispersed. The supernatant liquid is clear because the colloidal particles are trapped within the flocs and sediment with them. Secondary minimum flocculation is therefore a desirable state for a pharmaceutical suspension. [11]

Factors for the secondary minimum for flocculation to occur includes [11]:

1) Particles with a size greater than 1 μm radius should, unless highly charged, show a sufficiently deep secondary minimum flocculation.
2) Particle shape: Asymmetric particles, especially those that are elongated, are more satisfactory than spherical ones;
3) Concentration: The rate of flocculation depends on the number of particles present, so that greater the number of particles the more collisions there will be and the more flocculation is likely to occur.

The production of a satisfactory secondary minimum leading to floc formation in this manner is termed controlled flocculation. [11] In concentrated flocculated suspensions, the particles exist not as individual particles, but rather as aggregates. The number of particles in an aggregate depends on: the concentration and properties of the flocculating agent if used; the viscosity and density of the medium; and the density and nature of the charge on the particles. [12]

3.2.3 Flocculated and Deflocculated Systems

Having incorporated a suitable wetting agent, it is then necessary to determine whether the suspension is flocculated or deflocculated. This depends on the relative magnitudes of the forces of repulsion and attraction between the particles as previously discussed, and is concluded in Table 3.1. [4] Figure 3.3 illustrates the appearance of both flocculated and deflocculated suspensions at given times after shaking.

Deflocculated systems have the advantage of a slow sedimentation rate, thereby enabling a uniform dose to be taken from the container, but when settling does occur, the sediment is compacted and difficult to re-disperse. Flocculated systems form loose sediments which are easily re-dispersible, but the sedimentation rate is fast and there is a danger of

an inaccurate dose being administrated; also, the product will look inelegant. [4]

Table 3.1 Comparison of flocculated and deflocculated systems [13]

Comparison	Flocculated system	Deflocculated system
Particles	Compressed of particles	In discrete units of particles
Size	Larger due to aggregation	Small
Rate of settling	Rapid	Slow
Supernatant	Clear	Cloudy for an appreciable time
Nature of sediments	Loose flocs with high porosity	Compact sediments
Final sediment	Larger volume	Smaller volume
Re-dispersibility	Easy by shaking	Very difficult

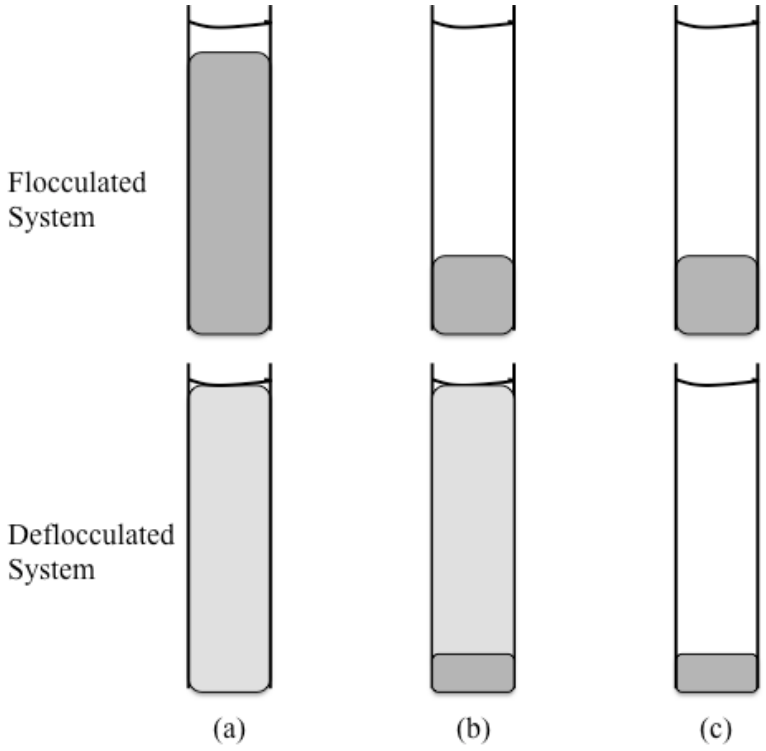

Figure 3.3 The sedimentation behavior of flocculated and deflocculated systems ((a) is a few minutes after shaking, (b) is after several hours, (c) is after prolonged storage). [4]

A deflocculated system which has a sufficiently high viscosity to prevent sedimentation would be an ideal formulation. It cannot be guaranteed, however, that the system would

remain homogeneous during the entire shelf-life for the product. Flocculating agents may be added to ensure that the product exhibits the correct degree of flocculation. [4]

Materials that can be added into suspensions to produce flocculation includes [4, 14]:

1) Electrolytes: Used to alter the zeta potential of the dispersed particles, and if the value is lowered sufficiently, flocculation may occur.
2) Surfactants: Both ionic and nonionic surfactants have been used to bring about flocculation of suspended particles. The concentration to achieve this effect is critical since these compounds also act as wetting and deflocculating agents.
3) Polymers: These long chain high molecular weight compounds containing active groups spaced along their molecular length can be used to flocculate the suspension, and include such materials as starch, alginates, cellulose derivatives, tragacanth, carbomers and silicates.

3.2.4 Steric Stabilization of Suspensions

Colloidal particles may be stabilized against coagulation in the absence of a charge on the particle by the use of polymeric materials, which involves the concept of steric stabilization or protective colloid action. This concept may be applied to pharmaceutical suspensions where naturally occurring gums such as tragacanth, and synthetic materials such as surfactants and cellulose polymers, may be used to produce satisfactory suspensions. These materials may increase the viscosity of the aqueous vehicle and thus slow the rate of sedimentation of the particle. However, they will also form adsorbed layers around the particles so that the approach of their surfaces and aggregation to the coagulated state is hindered. [11]

Controlled flocculation cannot be produced by all polymeric materials. Deflocculated and

caked systems may also be produced. The balance of repulsive forces and attraction forces depends on both the thickness and the concentration of the polymer in the adsorbed layer. [11]

There are two possible mechanisms for flocculating agents:

1) Soluble polymeric materials adsorb onto more than one solid particle surface because of the repeating nature of the basic monomeric unit in the polymer structure and their high molecular weight;
2) The multivalent ionic compounds transfer a charge by ionic adsorption onto the surface of the particles.

Bridges are formed by adsorption of two or more remote sites on the polymer chain with the surfaces of the particle, thus forming a loosely connected floc. At higher polymer concentrations the individual particles are enveloped by polymer and the bridging mechanism cannot operate since no adsorption sites are available for bridging to other particles. The system is then considered to be stabilized. [15, 16]

Chapter 4

Particle Size Analyses

4.1 Introduction

A pharmaceutical suspension is a coarse dispersion in which insoluble particles, generally greater than 1 μm in diameter, are dispersed in a usually aqueous liquid medium. [1] Polydisperse suspensions have a board range of size, shape and mass characteristics. This is especially true for dry powder suspensions. The behavior and properties of particulate materials are, to a large extent, dependent on particle morphology (shape, texture, etc.), as well as size and size distribution. [2] The stability of the suspension depends on the size of the dispersed material. The forces between colloidal particles depend on their dimensions. The settling rate of the particles depends on their size and density. [3]

A number of methods can be used for particle size measurement, the most commonly used include:

1) Microscopy and image analysis: optical microscopy, transmission electron microscopy (TEM), scanning electron microscopy (SEM).
2) Sieve analysis.

3) Interaction between fluids and particles: sedimentation method.

4) Interaction between particles: stream scanning, field scanning.

5) Light scattering: laser diffraction (LD), dynamic light scattering (DLS).

4.2 Microscopy and Image Analysis

Microscopy is often used as an absolute method for particle size measurement using image analysis. It is useful not only for particle size measurement but also for particle shape and particle texture evaluation collectively called morphology. [4] The major advantage that microscopic techniques possess over most other methods for size analysis is that the particle profile itself is measured, rather than some property which is dependent on particle size. [5] Optical microscopy, transmission electron microscopy (TEM), and scanning electron microscopy (SEM) are the most commonly used microscopic techniques for particle size analysis by imagery. The range of particle sizes suitable for these techniques is shown in Figure 4.1.

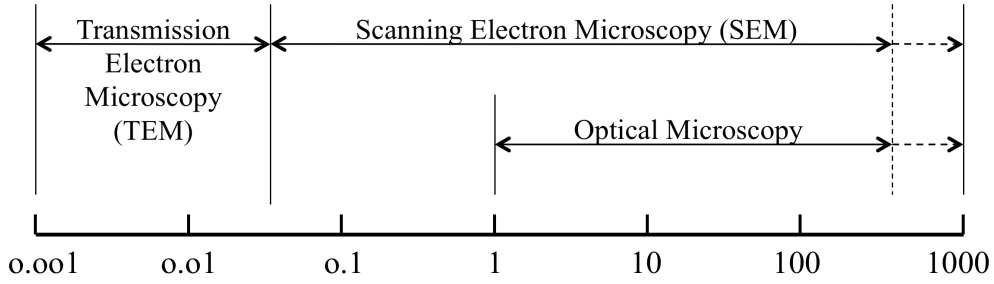

Figure 4.1 Range of particle sizes [6]

4.2.1 Optical Microscopy

Optical microscopy is most often used for the examination of particles from about 3 μm to 150 μm. The theoretical lower limit is approximately 0.2 μm but the diffraction halo around the particle gives a gross overestimation of the particle size. Above 150 μm a simple magnifying glass is suitable. [4] The size of particles which can be imaged by microscopy is limited by the diffraction of the light used to form this image.

The maximum magnification for optical microscopy is 2000×. A significant problem for microscopic analysis is that it may only examine a rather small number of particles, especially for samples with a large range of particle sizes, due to the small depth of focus [5], which is about 250 μm at a magnification of 10×, about 10 μm at 100×, and about 0.5 μm at 1000×. Thus, microscopy cannot provide a precise size distribution for particles, and sample preparation requires special consideration.

The number of particles in a given size range can be counted using a screen or a hemocytometer slide, and the arithmetic mean diameter can be calculated by:

$$A_d = \frac{\sum n_d}{\sum d} \qquad \text{Eqn. 4.1}$$

Where (A_d) is the arithmetic mean diameter; (n_d) is the number of particles in a given size range with a diameter d; (d) is the diameter of a given size range.

A disadvantage of optical microscopy is that the size analysis is carried out on two-dimensional images of particles which are generally assumed to be randomly oriented in three dimensions. Under such conditions, size analysis is carried out accepting

that they are viewed in their most stable orientation. This will lead to an overestimation of size, since the largest dimensions of the particle will be observed. [6] In addition, the number of particles that must be counted (300 to 500) to obtain a good estimation of the distribution makes the method somewhat slow and tedious. [7]

4.2.2 Transmission Electron Microscopy (TEM)

Both TEM and SEM analysis have lower particle size limits than optical microscopy, but sample preparations are more complicated. Many interesting materials do not absorb electrons and specialized methods such as replica casting or shadowing have to be employed. [5]

In TEM, a thin solid specimen (≤ 0.2 μm thick) is bombarded in a vacuum with a focused electron beam of sufficient energy to penetrate through the specimen. The transmitted electrons form an image of the internal and external structure of the particles due to differences in the interaction between the electrons and the atomic constituents of the sample. [8]

TEM is used for the direct examination of particles in the 0.001μm to 5 μm size range. TEM operates by flooding the sample with an electron beam, most commonly at 100-200 keV, and generating an image on a fluorescent screen or photographic plate behind the sample. TEM operates in the magnification range from about 600× to 1,000,000×. [9]

Considering the size range of TEM, this technology was not used in this study.

4.2.3 Scanning Electron Microscopy (SEM)

4.2.3.1 Introduction

Scanning electron microscopy (SEM) is a versatile electron microscopic technique that provides on one hand surface information such as texture, topography, etc. (up to a length scale of few tens of nanometers), and on the other hand, it provides a three dimensional effect to the images due to depth of focus of the SEM instruments. [10]

The theoretical magnifications of SEM vary from 10× to 800,000× at resolutions of 5 to 7 nm. It also has a much greater depth of focus compared to optical microscopy, which is about 1000 μm at a magnification of 10×, and about 10 μm at 10,000×. [6]

With additional detectors, elemental analysis can be performed at local spots on the surface of particles. SEM is particularly appropriate when a three-dimensional particle image is required. The combination of high resolution, an extensive magnification range, and high depth of focus makes SEM uniquely suited for the study of surfaces. [11]

4.2.3.2 Basic Principle

Electrons can be “reflected” (back-scattered) from a bulk specimen, as in the original experiments of Davisson and Germer in 1927. [12] However, another possibility is for the incoming (primary) electrons to supply energy to the atomic electrons present in a solid, which can then be released as secondary electrons. These electrons are emitted with a range of energies, making it more difficult to focus them into an image by electron

lenses. [12]

However, there is an alternative mode of image formation that uses a scanning principle (see Figure 4.2):

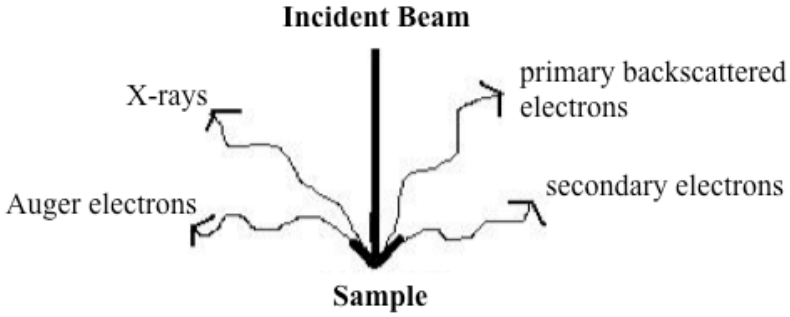

Figure 4.2 Electron "reflected" from sample specimen [13]

A scanning electron microscope (SEM) is a type of microscope which images a sample by scanning it with a high-energy (20–30 keV) beam of electrons in a raster scanning pattern over a rectangular area. [14]

When accelerated electrons enter a solid, they are scattered both elastically (by electrostatic interaction with atomic nuclei) and inelastically (by interaction with atomic electrons. Most of this interaction is "forward" scattering, which implies deflection angles of less than 90°. But a small fraction of the primaries are elastically backscattered (> 90°) with only a small fractional loss of energy. Due to their high kinetic energy, these backscattered electrons have a reasonable probability of leaving the specimen and re-entering the surrounding vacuum, in which case they can be collected as a backscattered-electron (BSE) signal. [15]

Any energy lost by a primary electron will appear as a gain in energy of the atomic

electrons that are responsible for the inelastic scattering. If these are the outer-shell (valence or conduction) electrons, weakly bound (electrostatically) to an atomic nucleus, only a small part of this acquired energy will be used up as potential energy, in order to release them from the confines of a particular atom. The remainder will be retained as kinetic energy, allowing the escaping electrons to travel through the solid as secondary electrons.

Primary electrons are focused into a small-diameter electron probe that is scanned across the specimen. This makes use of the fact that electrostatic or magnetic fields, applied at right angles to the beam, can be used to change its direction of travel. [13] By scanning simultaneously in two perpendicular directions, a square or rectangular area of specimen (known as a raster) can be covered. Thus, an image of this area can be formed by collecting secondary electrons from each point on the specimen. [15]

The same raster-scan signals can be used to deflect the beam generated within a cathode-ray tube (CRT), in exact synchronism with the motion of the electron beam that is focused on the specimen. If the secondary-electron signal is amplified and applied to the electron gun of the CRT (to change the number of electrons reaching the CRT screen), the resulting brightness variation on the phosphor represents a secondary-electron image of the specimen. [15] In raster scanning, the image is generated serially (point by point) rather than simultaneously, as in the TEM or light microscope. A similar principle is used in the production and reception of television signals. [13]

In summery, the electrons create various signals from the specimen, viz. back-scattered primary electrons, secondary electrons (low energy, up till about 50 eV), internal currents and photon emission, etc., all of which can be detected. The back-scattered signals are used to modulate the brightness of a cathode ray tube, which is scanned in synchronism with the electron beam. [8]

4.2.3.3 Instrument Set-up

The SEM consists basically of four systems; a schematic diagram of which is shown in Figure 4.3:

1) The *illuminating/imaging system* produces the electron beam and directs it onto the sample. It comprises an electron gun and several magnetic lenses that serve to produce a collimated, coherent beam of electrons, which can be focused onto the specimen. [15]
2) The *information system* includes (1) the sample, which releases a variety of data signals resulting from interaction with the imaging beam, and (2) a series of detectors, which recognize and analyze the data signals. [15]
3) The *display system* consists of one or two cathode-ray tubes (CRT) for observing and photographing the surface of interest. Permanent records or scanning electron micrographs are recorded by photographing either the visual CRT or second high-resolution record CRT. [15]

4) The *vacuum system* removes gases from the microscope column, which would otherwise interfere with high-resolution imaging. The microscope column and specimen chamber are operated under high vacuum ($\geq 10^{-4}$ torr). [15]

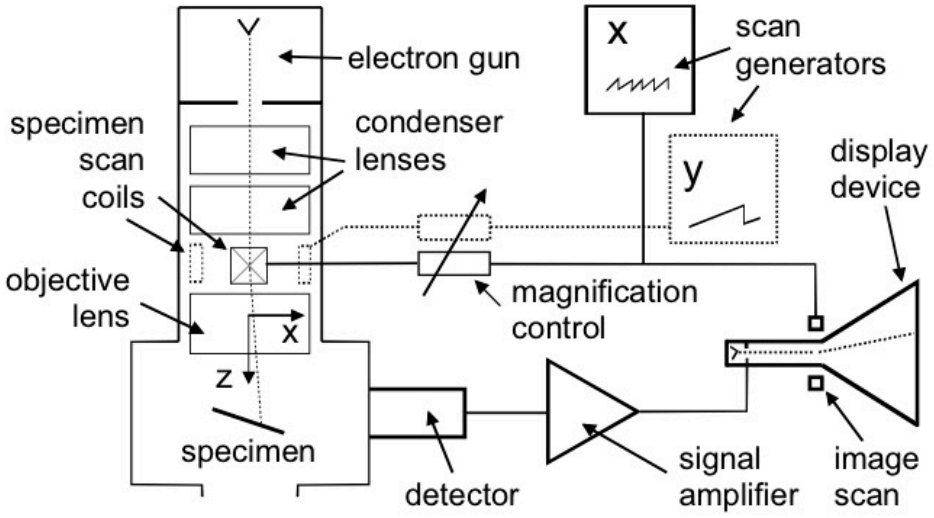

Figure 4.3 A schematic diagram of SEM with a CRT display [15]

4.2.3.4 Sample Preparation

Only particles that do not change their size or shape during the preparative and electron irradiation stages can be analyzed. [8] A very obvious criterion is that the sample cannot exceed the size of the specimen chamber. There are three steps for sample preparation: cleaning, mounting, and coating. [16]

Any contaminants on a specimen surface will affect the good imaging, and deposit during vacuum exposure on detectors, apertures, column liner tubes and etc.. In the SEM, contamination is manifested as areas of charging caused by the presence of

nonconductive particles or films, which obscure the sample surface. This can be avoided by cleaning the specimen with organic solvents in an ultrasonic bath followed by a blast of compressed gas. [16]

The specimen is then mounted on a substrate, which can be secured in the SEM specimen stage. Aluminum or carbon stubs are the standard specimen supports with various sizes and configurations. [16]

Conductive thin film coatings (10-20 nm thick) increase the density and conductivity of nonmetallic specimen, which would otherwise act as beam absorbers during irradiation. Gold is the metal most commonly used for coating, and conductive thin films are prepared using either the evaporative or sputter coating technique. [16]

Uncoated materials such as plastics, ceramics, glasses and replicas are poor conductors that exhibit charging artifacts under normal operating conditions. Such specimens may be examined at low accelerating voltage, but magnifications and resolutions are limited. [16]

4.2.3.5 Applications

SEM is an indispensable imaging tool in the fields of metallurgy, material science, biology, agriculture and geology. [16]

In this study, a Cold Cathode Field Emission Scanning Electron Microscope (JEOL JSM-7500F) is used for particle size analysis for the magnesium hydroxide dry powder and suspension sediments.

4.3 Sieve Analysis

Sieve analysis, or sieving, is the most widely used method for measuring particle size distribution because it is inexpensive, simple and with little variation between operators. [17] It is one of the few principal methods in which a relatively large quantity of material is physically subdivided in size classes. The separated fractions can be accurately weighed and, thus, the determination of the size distribution function (based on mass) may be accurately obtained. [18]

Sieves are generally used for grading coarser particles, in a range from about 40 to 9500 μm. The openings in the screen are described by a U.S. Mesh Number, calibrated by the National Bureau of Standards, which indicates the number of strands per inch (see Table 4.1). [19]

Table 4.1 U.S. mesh openings [20]

Mesh No.	Opening (mm)	Mesh No.	Opening (mm)	Mesh No.	Opening (mm)	Mesh No.	Opening (mm)
4	4.750	16	1.200	45	0.354	140	0.104
6	3.350	18	1.000	50	0.297	170	0.089
7	2.810	20	0.853	60	0.251	200	0.075
8	2.380	25	0.710	70	0.211	230	0.066
10	2.000	30	0.599	80	0.178	270	0.053
12	1.680	35	0.500	100	0.152	325	0.044
14	1.400	40	0.422	120	0.125	400	0.037

Sieve analysis utilizes a woven, punched or electroformed mesh, often in brass o stainless steel, with known aperture diameters, which form a physical barrier to particles.

Most sieve analyses utilize a series, stack or “nest” of sieves, which has the smallest mesh above a collector pan at the bottom followed by meshes that become progressively coarser towards the top of the series. [6]

According to the method of the U.S. Pharmacopeia for testing powder fineness, a definite mass of sample is placed on the proper sieve in a mechanical shaker. The powder is shaken for a definite period of time, with the material passing trough one sieve and being retained on the next finer sieve. Another custom is to assign the particles on the lower sieve the arithmetic or geometric mean size of the two screens. [7] This method is used in this study to investigate the particle size distribution of the dry powder magnesium hydroxide.

Size distribution by sieving is reported as the mass of material retained on the mesh of a given size, or as the cumulative mass retained on all sieves above a mesh size, or as the cumulative mass fraction above a given mesh size. [21]

To illustrate the sieving results, one can plot either the percentage of sample retained on each sieve in a histogram plot (see Figure 4.4 a) or the cumulative distribution as a function of sieve size (see Figure 4.4 b). Sieving results are most commonly plotted on 3-cycle log paper (see Figure 4.4 c) to compare the particle size with the cumulative percentage of undersize particles. If the plot is linear throughout the entire range, then the material is characterized by a log-normal distribution. If the line is curved or consists of two or more linear segments, then the distribution is polymodal. [22]

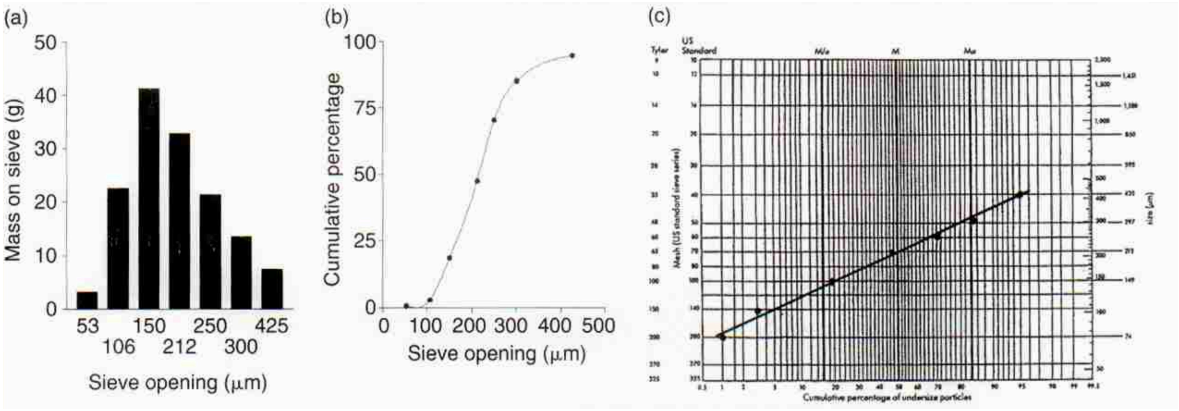

Figure 4.4 Representations of the particle size distribution of a sieve analysis ((a) histogram plot, (b) cumulative distribution plot, (c) 3-cycle log plot) [22]

There are several errors and problems associated with the sieve analysis:

1) Errors in the sieve:

   Sieves are subject to many errors in manufacture, which has been closely studied. Leschonski [23] studied the range of orifice sizes in typical woven sieves and found a coefficient of variation of around 10% for the smaller sizes, falling to 3-5% for millimeter-sized sieves. This obviously sets a limit on the sharpness of the cut which can be achieved. The errors are further compounded by damage and wear during use.

2) Sieve load:

   The mass of material placed in the sieve can have a considerable influence on the final results. [23] Sieves work best when there is only a thin layer of well-separated material on the mesh; however, if there is very little material present, the error in its weighing is relatively large. A good starting point is 50 – 100 g for 100 mm sieves, and 200 g for 200 mm sieve.

3) Sieving time:

The time-dependence of the sieving process has been investigated [23], and found that most powders show a biphasic behavior if the fraction of material passing through the sieve is plotted against time (Figure 4.5). The first phase is due to the passage of particles which are smaller than the sieve mesh in all dimensions. The second phase is due to particles with two dimensions smaller than the sieve mesh but larger then the three dimensions. As a result of this effect, particle shape influences sieving time. Spherical particles show a pronounced first phase and little or no second phase. Needle-like crystalline materials can be mainly second phase. Sieving time needed for the two shapes to obtain equal percentage passing through sieve will be quite different.

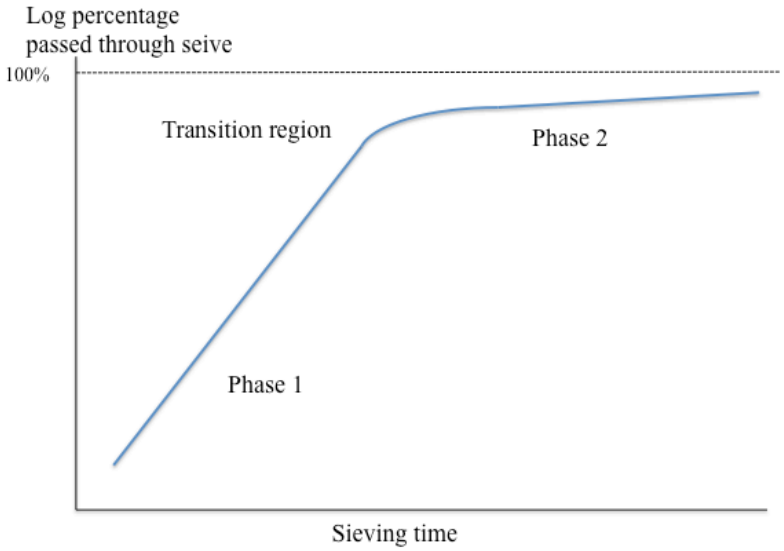

Figure 4.5 Effect of sieving time on mass passing through sieve [23]

Therefore, sieve analysis needs a predetermined sieving time to obtain the

necessary results.

4) Properties of the material:

   Many sieving errors are due to properties of the material. [23] Many materials adhere to themselves or to the sieve mesh, which can prolong sieving time considerably and cause major loses. Results can be improved by the addition of a small amount of colloidal silica, or by wet sieving. Humidity can also cause powder adherence, and low-temperature drying may improve the behavior of the powder.

4.4 Sedimentation Method

The sedimentation method is one of the oldest methods of particle size measurement and classification. [24] It is based on the settling behavior of a single falling sphere under gravity in a fluid. Particle size determined by this method ranges from 0.8 to 300 μm. This is the main method used in this study for particle size analysis. [7]

The sedimentation method, based on the dependence of the rate of sedimentation of the particles on their size, is expressed by Stokes' equation as discussed in Chapter 2:

$$r = \sqrt{\frac{9\eta V_S}{2g(\rho_s - \rho_l)}} \qquad \text{Eqn. 2.6}$$

where (r) is the particle radius, (η) is the viscosity, (ρ_s) is the density of the solid, (ρ_l) is the density of the media, and (Vs) is Stokes' law velocity of sedimentation.

Stokes' law applies only to spherical particles, and nonspherical particles are described in

terms of an equivalent diameter; this is the Stokes' equivalent diameter, (d_{St}). [24]

$$d_{St} = \sqrt{\frac{18\eta V_S}{g\,(\rho_s - \rho_l)}} \qquad \text{Eqn. 2.7}$$

One of the most significant limitations of Stokes' law is that the particle suspension must be dilute. The reason for this is that the derivation of any viscous drag forces assumes that the fluid is infinite in extent, or that the particles are isolated. [24]

For concentrated suspensions under hindered settling conditions, several theories have been discussed in order for the Stokes' law to be applied by correlating observed rate of fall of interface (Q) with Stokes' limiting velocity (V_s), as discussed in Chapter 2, and is summarized as follows:

Method 1, Steinour's equation: A plot of $\left[Log\left(\frac{Q}{\varepsilon^2}\right)\right]$ against (ε) should be linear and provide data for (A) and (V_s) from the slope and intercept.

$$Log\left(\frac{Q}{\varepsilon^2}\right) = A\epsilon - (LogV_s - A) \qquad \text{Eqn. 2.21}$$

Method 2, Richardson and Zaki's equation: A plot of (Log Q) against (Log ε) should be linear and provide data for (n) and (V_s) from the slope and intercept.

$$LogQ = nLog\varepsilon + LogV_s \qquad \text{Eqn. 2.24}$$

Method 3, Dollimore and McBride's equation: A plot of (Log Q) against (1- ε) should be linear and provide data for (V_s) from the intercept.

$$LogQ = LogV_s - b\rho_s(1-\varepsilon) \qquad \text{Eqn. 2.42}$$

Method 4, "Compartment" Model: when ε =1, at infinite dilution.

$$V_s = Q = A + B \qquad \text{Eqn. 2.60}$$

A further source of error arises from temperature variations. Temperature enters Stokes' law through fluid viscosity. The viscosities of most fluids fall as the temperature rises. All sedimentation experiments should be performed at a controlled temperature if this error is to be minimized. [7]

4.5 Light Scattering

Light scattering techniques have been used for many decades to measure the size of small particulates, molecular weights and diffusion coefficients, and generally to obtain an enormous amount of information about macromolecular and particle systems. When using lasers as a light source, light scattering techniques become sufficiently straightforward and can be used by non-specialists. [25] Laser diffraction (LD) and dynamic light scattering (DLS) are the most common methods used for the determination of small particle size and size distribution. Both of these methods are non-imaging methods.

4.5.1 Laser Diffraction (LD)

4.5.1.1 Introduction

Laser diffraction (LD), also known as "Static Laser Light scattering", low-angle laser light scattering (LALLS), Fraunhofer diffraction, are non-intrusive and simple to implement and are frequently employed to assess the size of particles in the 0.1 to 2000 μm range. [26]

4.5.1.2 Basic Principles

LD is a scientific technique which utilizes properties of the diffraction patterns of a laser beam passed through a substance, to measure the size of its particles. [27]

In this technique, the scattering pattern of monochromatic laser light by an ensemble of dispersed particles is measured on a series of detector elements positioned at different angles, mostly in the forward direction. The measured detector signals are then converted to a particle size distribution by using a model-based matrix. This matrix contains the calculated signals at all detector elements per unit volume of spherical particles for each of a defined set of size classes. [28]

Between light and a particle, four types of interactions can be distinguished (see Figure 4.6):

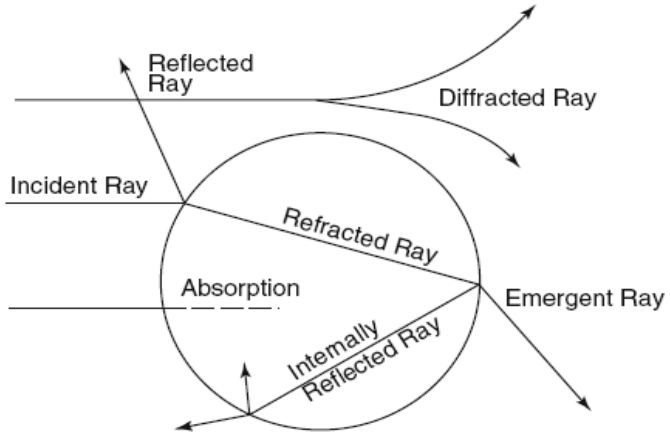

Figure 4.6 Interaction between light and a particle [28]

1) Diffraction of light at the contour of the particle, known as (Fraunhofer)

diffraction;

2) Reflection of light at the particle's surface, both inside and outside the particle;
3) Refraction of light at the interface of particle and dispersion medium; and
4) Absorption of light inside the particle.

These interactions lead to an interference phenomena, which gives rise to a characteristic scattering pattern in the far field. In the pattern, the scattered light intensities at different angles are dependent on the size, shape and optical properties of the particle. [28]

LD is accurately described by the Fraunhofer Approximation and the Mie theory, with the assumption of spherical particle morphology. The Fraunhofer approximation assumes the particles are opaque, two dimensional, and large circular discs and describes light scattering from the edges of an object. [29] The Mie theory gives the rigorous solution for light scattering by homogeneous spheres, where it accounts for all types of light interaction. As a consequence, this theory requires full knowledge of the optical properties of the particles and the dispersion medium. The Mie theory holds true for spherical, isotropic particles illuminated by monochromatic light. [28]

4.5.1.3 Instrument Set-up

The typical set up for a LD instrument is shown in Figure 4.7. The typical light source is a laser, generating a monochromatic, coherent light beam. A beam processing unit follows the light source. It usually consists of a beam expander with integrated pinholes

and lenses to produce an extended parallel light beam. The detector elements convert the scattered light intensities into electrical signals that can be read and processed in a computer. [28]

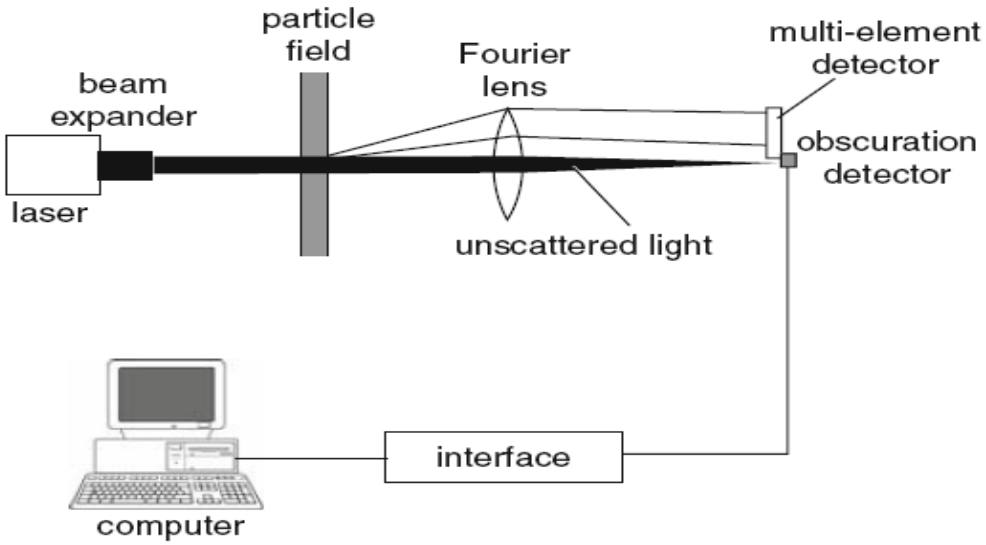

Figure 4.7 Typical set-up of a LD instrument [28]

4.5.1.4 Sample Preparation

LD has different possibilities for size measurement. Particulate materials can be dispersed in a gas stream or in a transparent liquid. Measurements can be performed off-line, on-line and in-line. Also, sprays, aerosols and gas bubbles in a liquid can be measured. There are three requirements: 1) the particulate concentration is at an adequate level between stated limits; 2) the dispersion medium is transparent; and 3) the refractive index of the dispersion medium differs from that of the particulate material. The measured sample should be representative for the bulk material or many samples should be measured to give adequate representation. [27]

4.5.1.5 Applications

The advantages for the LD technique are its large flexibility to different sample types, wide size range, rapidity and high precision.

The application of the forward laser diffraction technique in monitoring the particle size distribution in industrial processes is however restricted to dilute suspensions, since in concentrated suspensions; the occurrence of multiple light scattering modifies the angular distribution of light intensity. The phenomenon of multiple scattering is illustrated in a simplified way in Figure 4.8.

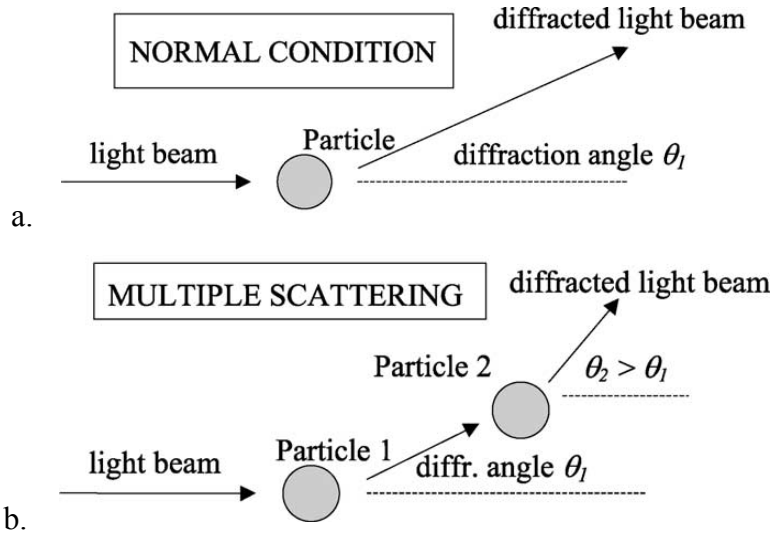

Figure 4.8 a: Normal condition occurring in dilute suspensions;
b: Multiple scattering observed in concentrated suspensions. [30]

In dilute particle-fluid suspensions composed of spherical particles, the diffracted light beam reaches the detector at angles that depend on the wavelength of the light source and the particle diameter, besides the optical properties of the fluid and particle. As the suspension concentration increases, there is an increasing probability that the diffracted

beam intercepts other particles in the suspension. In order to measure the particle size distribution in concentrated suspensions, it is necessary to dilute the suspension to acceptable levels. [30]

In this study, a Malvern Mastersizer 2000 particle size analyzer was used to determine the particle size of the dry powder magnesium hydroxide in various media.

4.5.2 Dynamic Light Scattering (DLS)

Dynamic light scattering (DLS), also known as photon correlation spectroscopy or quasi-elastic light scattering, is a technique in physics, which can be used to determine the size distribution profile of small particles in suspension or polymers in solution. [31]

DLS is used to determine the particle size, and size distribution. It can also measure the polydispersity index of various types of samples including nanoparticles, colloids, gels, emulsions, pigments, liquid crystals, DNA, polymers and proteins. It can measure submicron particles in the range of 0.6 nm to 6 μm. [32] Considering the size range of DLS, this technique is not used in this study.

Chapter 5

Thermal Analyses

5.1 Introduction

Thermal analysis is a group of techniques in which one or more properties of a sample are studied while the sample is subjected to a controlled temperature program. [1] Thermal analysis techniques are used for the characterization of drugs and drug products. [2] It provides essential data on the properties of substances used in processing. Its application is related to their structures.

The application of thermal analysis includes the determination of thermal data, thermal stability, investigation of a phase changes, as well as characterization and identification of materials, and kinetics and thermodynamic studies. [3]

Because there are many properties that a sample may posses, which can be measured, the number of techniques (and associated methods) is quite large. [4] For example, thermometry measures temperature; differential thermal analysis (DTA) measures temperature difference; differential scanning calorimetry (DSC) measures heat flow differences; thermogravimetry (TG) measures mass loss or gain; thermomechanometry

(TM) measures dimensions or mechanical properties; and etc.. [5]

The two techniques mainly used in pharmaceutical analysis are: differential scanning calorimetry (DSC) and thermogravimetry (TG). [6]

5.2 Differential Scanning Calorimetry (DSC)

5.2.1 Introduction

DSC measures the change of the difference in the heat flow rate to the sample and to a reference sample while they are subjected to a controlled temperature program. In addition to the measurement of heat, DSC is used to measure heat flow rates (power) and characteristic temperature of a reaction or a transition. The precise measurement of heat capacities including integral (total) heats of reaction or transition, and partial heats – important for kinetic evaluations, determination of crystallinity and purity, which is of an increasing importance, has distinctly been improved with modern DSC. [7] The modern DSC technique was first developed by E.S. Watson and M.J. O'Neill in 1962. [8]

5.2.2 Basic Principles

The concept underlying the technique is simple enough: to obtain information on thermal changes in a sample by heating or cooling it alongside an inert reference. Figure 5.1 is a schematic representation of the main parts of such an instrument.

The sample and reference are contained in the DSC cell; temperature sensors and the means of heating the sample and reference are also incorporated into the cell. [9]

Two basic methods of measurement are generally used in modern DSC. If the sample pan and the reference pan are heated linearly, they will initially be at the same temperature. If a change such as melting occurs in the sample, energy is used by the sample because the

process is endothermic. Due to the need for energy for melting the temperature remains constant in the sample pan. Thus, a difference in temperature occurs between the sample pan and reference pan.

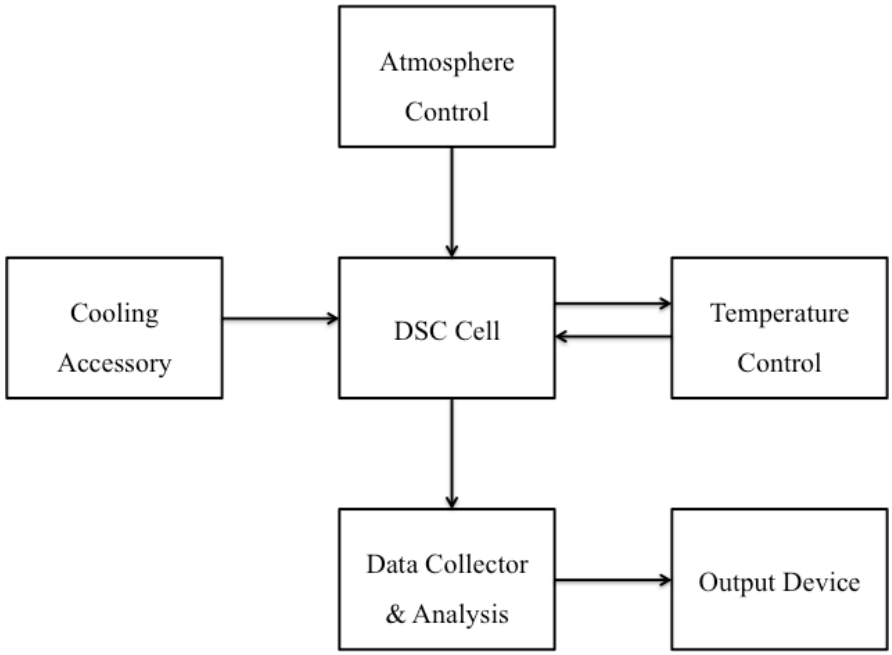

Figure 5.1 A Schematic representation of a DSC instrument

The first method is called "heat-flux DSC" (as shown in Figure 5.2), in which the instrument measures this temperature difference. The temperature difference is converted to energy flow via a mathematical equation. [6] There are three types of measuring systems based on sample shape: disc type, turret type and cylinder type. [10] The Mettler DSC 822e used in this study is this type of instrument.

The second method is called "power-compensated DSC" (as shown in Figure 5.3), in which two individual heaters are used in order to monitor the individual heating rates. A control system regulates the temperature difference between the sample and reference. When an endothermic or exothermic process occurs, the instrument delivers the compensation energy, which must be given in order to maintain equal temperature in both

pans. Thus, the primary measurement is energy. [6]

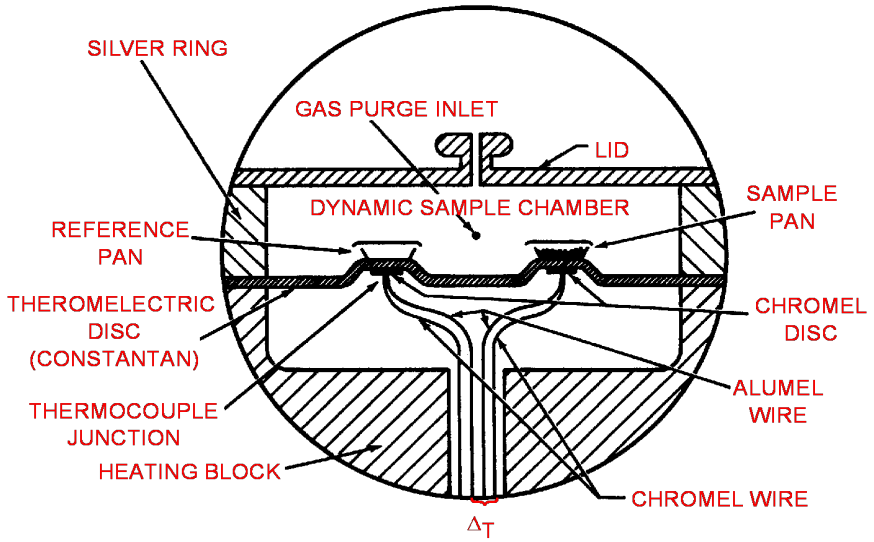

Figure 5.2 DSC cell of the heat-flux type method [11]

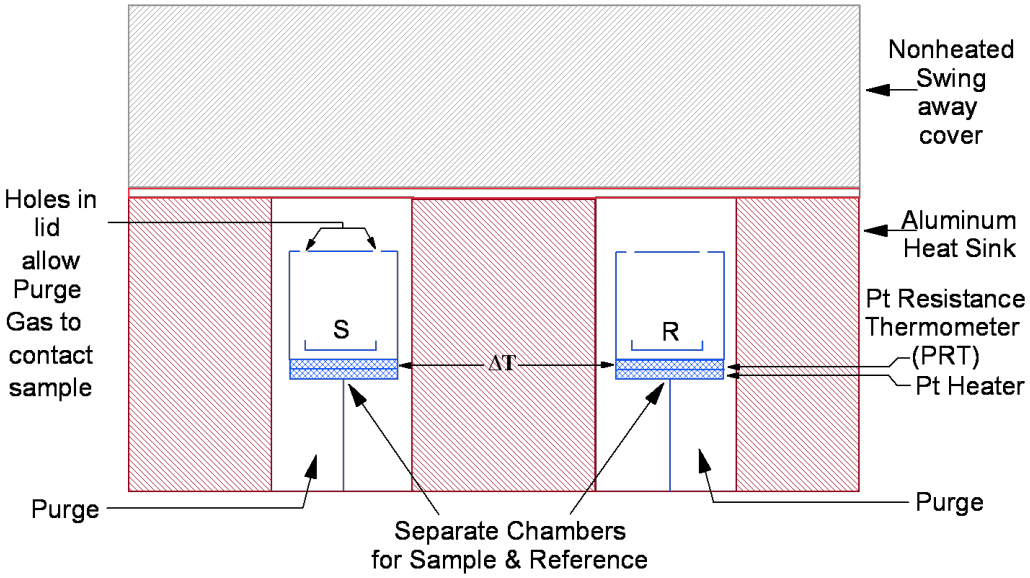

Figure 5.3 DSC cell of the power-compensated type method [11]

A characteristic common to both types of DSC methods is that the measured signal is proportional to a heat flow rate (Φ) and not to a heat as is the case with most of the classic calorimeters. [10]

Heat flow rate (Φ) is going to be shown in units of heat (q) supplied per unit time (t).

Assuming that heat capacity of a sample is greater than that of the reference ($C_S > C_R$),

and that heat flow is governed by Newton's law:

$$\Phi = dq/dt = (1/R)\Delta T \quad \text{Eqn. 5.1}$$

where, R = thermal resistance, $\Delta T = (T_S - T_R)$ = temperature difference between sample and reference. [12]

Considering that calorimetry is generally based on the heat capacity (C) which can be expressed as the following equation:

$$dq = C \cdot \Delta T \quad \text{Eqn. 5.2}$$

thus,

$$\Phi = dq/dt = C(dT/dt) = C\beta \quad \text{Eqn. 5.3}$$

where (β) is the scanning or heating rate of the instrument. [12]

For heat-flux DSC, the condition is $T_S \neq T_R$, $R \neq 0$.

The signal is:

$$\Delta T = R\,(dT/dt)(C_S - C_R) \quad \text{Eqn. 5.4}$$

where (R) only depends on the instrument, and not on the characteristics of the sample.

For power-compensated DSC, the power is modified to make $T_S = T_R$, therefore there is no thermal resistance, R=0. [12]

The signal is then:

$$\Delta(dq/dt) = (dT/dt)(C_S - C_R) \quad \text{Eqn. 5.5}$$

There are two modes of operation depending on the heating rates: constant and variable.

In the constant heating rate mode, the relationship between temperature and time is linear. Both heat-flux and power-compensated DSC belong to the constant heating rate mode.

DSC using variable heating rate mode is called modulated temperature DSC (MTDSC or mt-DSC). The heating program is modulated by superimposing a sine wave (or other

periodic waveform) of small amplitude on the linear rise. [13]

5.2.3 Instrumentation

The maximum operating temperature of both types of DSC is limited to about 750°C. However, high-temperature DSC can measure temperatures up to 750-1600°C.

The choice of crucible depends on the construction of the DSC cell, reactivity of the sample and temperature range over which the measurements are to be made. The most frequently used crucibles for low and moderate temperatures, −150 °C to about 600°C, are made of aluminum and can be of a shallow (e.g. 2 mm) or deep (e.g. 10 mm) design. The temperature, 600°C, is still well below the melting temperature of aluminum (660°C) but at higher temperatures there is the risk of irreversible damage to temperature sensors arising from alloying reactions. Crucibles made of platinum are used for high temperature measurements. Crucibles made of silver, gold, quartz, alumina, copper and graphite are all available commercially.

Heating rates from 0.1 to 500°C/min can be selected depending on the particular equipment. The high heating rates are used in specific measurements to allow for temperature regions of interest to be reached quickly, and to minimize kinetic reactions, e.g. formation of polymorphs. [14]

DSC calibration must be performed frequently before the experiment begins for the purpose of accuracy and reliability.

5.2.4 Thermogram & Interpretation

DSC curves, also known as thermograms, are expressed by plotting heat flow (Φ) versus temperature or time. Some characteristic terms are used to describe a measured DSC curve (see Figure 5.4).

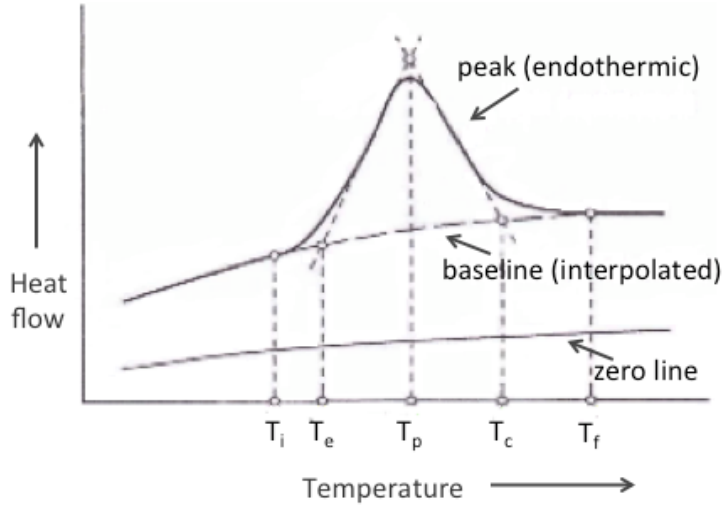

Figure 5.4 Characteristic terms used to describe a DSC curve [15]

The zero line is the curve measured with the instrument empty; the (interpolated) baseline is the line constructed in such a way that it connects the measured curve before and after a peak, as if no peak had developed. A peak in the curve appears when the steady state is disturbed by some production or consumption of heat by the sample.

The characteristic temperatures of a DSC curve are: initial peak onset temperature (T_i); extrapolated peak onset temperature (T_e); peak maximum temperature (T_p); extrapolated peak completion temperature (T_c); and final peak temperature (T_f). [15,16]

In a DSC thermogram, the plot (see Figure 5.5) of heat flow (Φ) versus temperature of heating, have peaks associated with endothermic processes, e.g. melting and denaturation, are plotted downwards; while peaks with exothermic processes, e.g. crystallization, crosslinking, oxidation or decomposition, are plotted upwards. Some transitions, such as glass transitions, lead to changes in the shape of curve, rather than to distinguishable peaks. [11, 15]

For chemicals and drugs, most frequently measured transitions include: glass transition temperature (T_g), glass transition size (ΔC_p), melting temperature (T_m), crystallization temperature (T_c), crystallinity (J/g), and polymorphic transitions. [11]

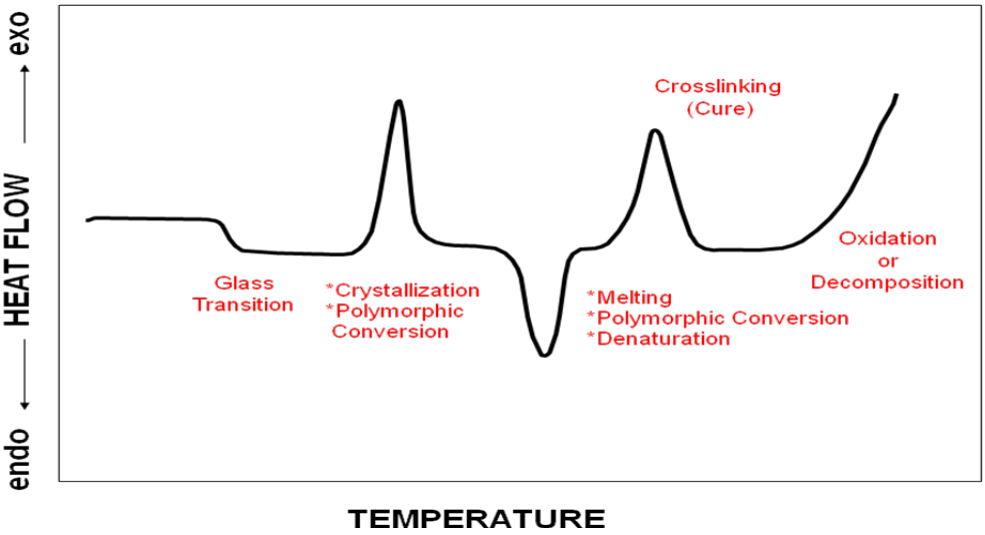

Figure 5.5 Typical transitions observed in a DSC thermogram [11]

5.2.5 Applications

DSC allows reaction heats and heats of transition, or heat flow rates and their changes at characteristic temperatures, to be quickly measured on small sample masses (milligram range), over a wide temperature ranges and with an accuracy which is usually sufficiently high for the respective purpose. DSC can be applied to the following fields:

1) Characterization of materials (in particular polymers),
2) Comparison (relative) measurements (quality control, identification of substances or mixtures),
3) Stability investigation,
4) Evaluation of phase diagrams,
5) Purity determination,
6) Kinetic investigations,
7) Safety investigation,
8) Determination of heat capacity and complex heat capacity. [17]

5.3 Thermogravimetry (TG)

5.3.1 Introduction

Thermogravimerty (TG) is an experimental technique used in a complete evaluation and interpretation of results. It is usually referred to as Thermal Gravimetric Analysis (TGA). The technique has been defined by ICTAC (the International Confederation for Thermal Analysis and Calorimetry) as a technique in which the mass change of a substance is measured as a function of temperature while the substance is subjected to a controlled temperature program. [18] Mass loss is only seen if a process occurs where a volatile component is lost. [19]

5.3.2 Basic Principles & Instrumentation

The basic instrumental requirements for thermogravimetry are a precision balance, a furnance capable of being programmed for a linear rise of temperature with time, and a recorder. [20]

Measurements of changes in sample mass with temperature are made using a thermobalance. A thermobalance is a combination of a suitable electronic microbalance with a furnace, a temperature programmer and computer control, that allows the sample to be simultaneously weighed and heated or cooled in a controlled manner, and the mass, time, temperature to be captured (see Figure 5.6). The sensitivity of a thermobalance and the maximum load which it can accept, without damage, are related. Typical values are maximum loads of 1 g and sensitivities of the order of 1 μg. [21]

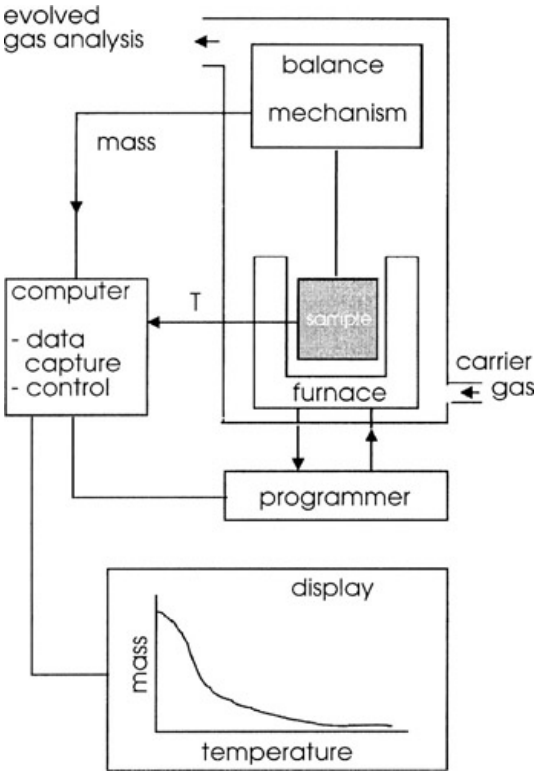

Figure 5.6 A schematic of a thermobalance [21]

Two weighing systems are used: the deflection balance and the null-point balance (see Figure 5.7).

a.

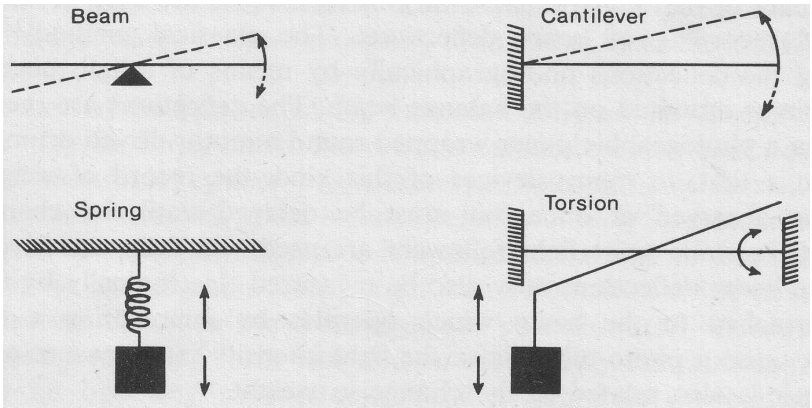

b.

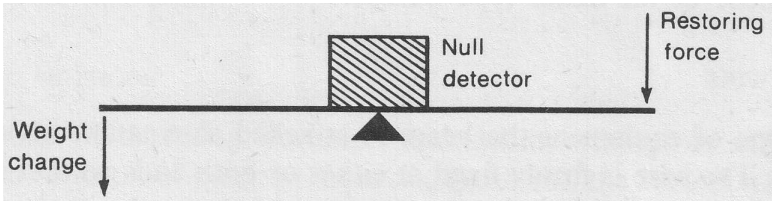

Figure 5.7 Two types of weighing systems in TG
(a. Deflection balances, b. Null-point balance.) [20]

The deflection balances depend on measuring a deflection from the norm by an appropriate technique; while the null-point balance incorporates a sensor to detect the deviation of the balance beam from its null position. The latter system is favored for modern TG. [20]

The furnace and control system must be designed to produce a linear heating rate over the whole working temperature range of the furnace and provision should also be made to maintain any fixed temperature. The choice if material for the furnace winding is governed by the maximum required working temperature. Furnaces, intended to work up to 1100°C, use resistive alloy wire or ribbon such as Kanthal or Nichrome, wound on a ceramic or silica tube. For higher temperatures, those reaching 1600°C, platinum or platinum/rhodium alloy is used. [20, 21]

The simplest TG experiment would be to heat the sample in static air. However, the sample may react with air in oxidizing or burning. Usually an inert gas such nitrogen or argon is used. [21]

Crucibles are made of various materials. The best ones are made of platinum. These are inert with respect to most gases and molten inorganic materials, and only melt at 1769°C. Alternative materials are metals, fused alumina, silica or ceramics. They must never be heated to high temperature in on oxidizing atmosphere, such as air, even in inert gases, such as nitrogen from a cylinder where traces of oxygen still exists. [21]

5.3.3 Thermogram & Interpretation

TG thermograms are presented as a plot of mass against temperature or time. The mass then appears as a step. [19] It is also plotted as the percentage mass loss or fractional decomposition against the temperature.

Actual TG curves obtained may be classified into various types as illustrated in Figure 5.8. Possible interpretations for these curves are as follows [22]:

Type (i) curve: The sample undergoes no decomposition with loss of volatile products over the temperature range shown. No information is obtained, however, on whether solid phase transitions, melting, polymerization or other reactions involving no volatile products have occurred.

Type (ii) curve: The rapid initial mass-loss observed is characteristic of desorption or drying, It could also arise, when working at reduced pressures, from effects such as thermomolecular flow or convection.

Type (iii) curve: It represents decomposition of the sample in a single stage. The curve may be used to define the limits of stability of the reactant, to determine the stoichiometry of the reaction, and to investigate the kinetics of reaction.

Type (iv) curve: It indicates multi-stage decomposition with relatively stable intermediates. Again, the temperature limits of stability of the reactant and of the intermediates can be determined from the curve, together with the more complicated stoichiometry of reaction.

Type (v) curve: It also represents multi-stage decomposition, but in this example stable intermediates are not formed and little information on all but the stoichiometry of the overall reaction can be obtained.

Type (vi) curve: It shows a gain in mass as a result of reaction of the sample with the surrounding atmosphere.

Type (vii) curve: It is not often encountered. The product of an oxidation reaction decomposes again at higher temperature.

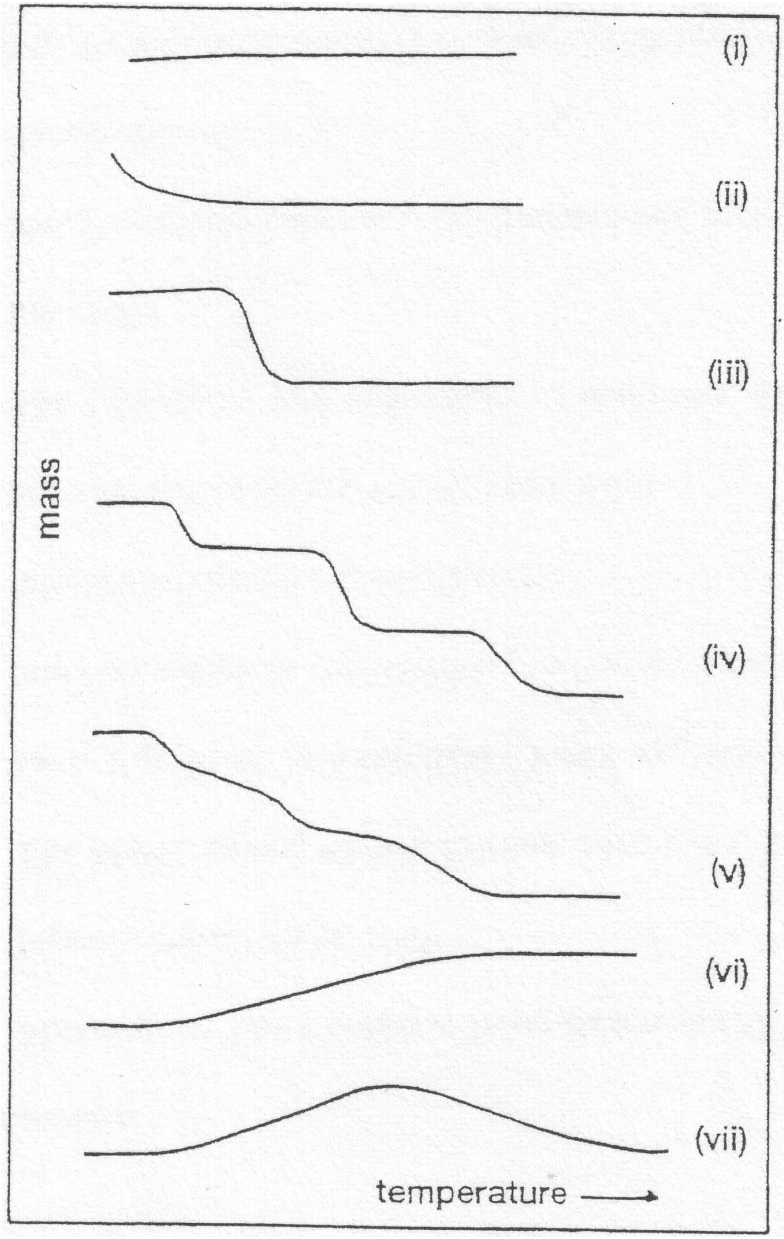

Figure 5.8 The main types of TG curves [22]

5.3.4 Applications

Thermogravimetry techniques have a very wide field of application. [23]

1) To examine the absorptive surfaces, together with the nature and processes involved in thermal decomposition and oxidation processes.
2) To examine water of crystallization and in forensic work involving the

identification and comparison of varnishes and other surface coating.

3) The determining the age of art treasures, particularly paintings and in determining the stability of explosives.
4) To control the dehydration procedures for crops particularly in the control of the drying processes used for tobacco.
5) To examine the drug stability and the rate of degradation of certain drugs when expose to air in the pharmaceutical industry.

Chapter 6

X-Ray Powder Diffraction (PXRD)

6.1 Introduction

X-ray powder diffraction (PXRD) is a scientific technique which uses X-rays diffracted on powder or microcrystalline samples to determine structural characterization of the materials. [1] Powder diffractometry is used mainly for the identification of compounds by their specific diffraction patterns. [2] PXRD is an extremely important technique in the field of material characterization to obtain information on an atomic scale from both crystalline and noncrystalline (amorphous) materials. PXRD is also applied to derive information concerning the fine structure of materials, including: crystalline size; lattice strain; chemical composition; state of ordering; etc. The X-ray diffraction by crystals was discovered in 1912 by Max von Laue, and its immediate application to structure determination was made by W. L. Bragg in 1913. [3] This technique was used to identify the sample composition of a powder before and after high temperature heating in thermal analysis comparing it to the standard diffraction patterns.

6.2 Basic Principles

X-rays are relatively short-wavelength, high-energy beams of electromagnetic radiation. [3] They have energies ranging from 200 eV to 1MeV. [4]

Diffraction is a general characteristic of all waves and can be defined as the modification of the behavior of light or other waves by its interaction with an object. Using the concept of a photon, an X-ray photon is absorbed during incident radiation, and another photon will be reemitted in another direction. This process is known as scattering. [3]

The three dimensional structure of a crystalline substance causes a crystal to diffract a monochromatic wave in a number of directions. [4] The angles of diffraction will only depend on the various arrangements of the atoms in the crystal lattice. [5]

The oscillating electric field of X-rays will interact with the electrons in matter to cause a coherent scattering of more than one atom. [4] They interfere in a constructive way and the diffracted beams will be in a specific direction. These directions are governed by the wavelength (λ) of the incident radiation and the nature of the crystalline sample. Bragg's law, relates the wavelength of the X-rays to the spacing of the atomic planes, and can be expressed mathematically as: [6]

$$n\lambda = 2d \sin\theta \qquad \text{Eqn. 6.1}$$

where the integer (n) is the order of the diffraction beam, (d) is the distance between adjacent planes of atoms, (θ) is the angle of the incident beam to the atomic lattice planes. This is demonstrated in Figure 6.1.

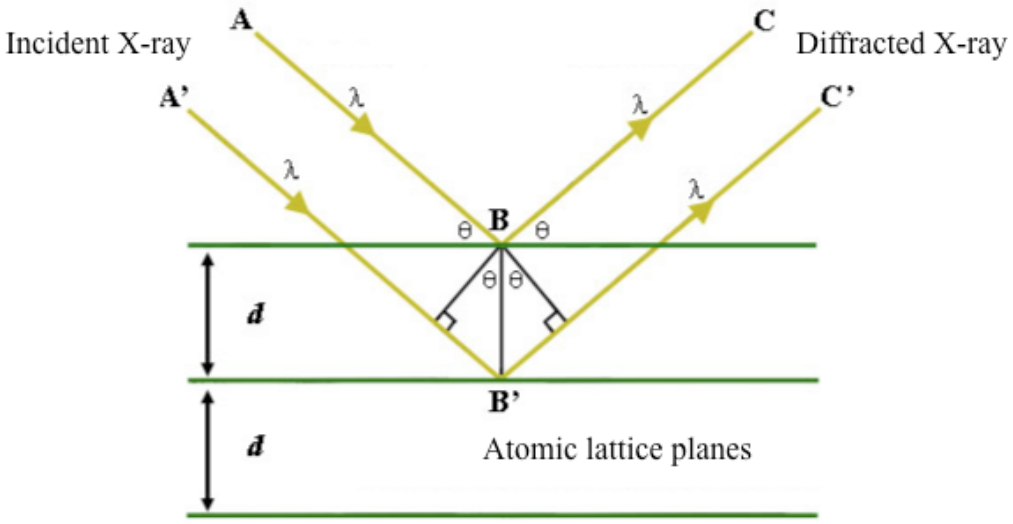

Figure 6.1 Diffraction of X-ray by a crystal [7]

6.3 Instrument Set-up

The three basic components of an X-ray diffractometer include the X-ray source, specimen and x-ray detector (see Figure 6.2). They all lie on the focusing circle. [8]

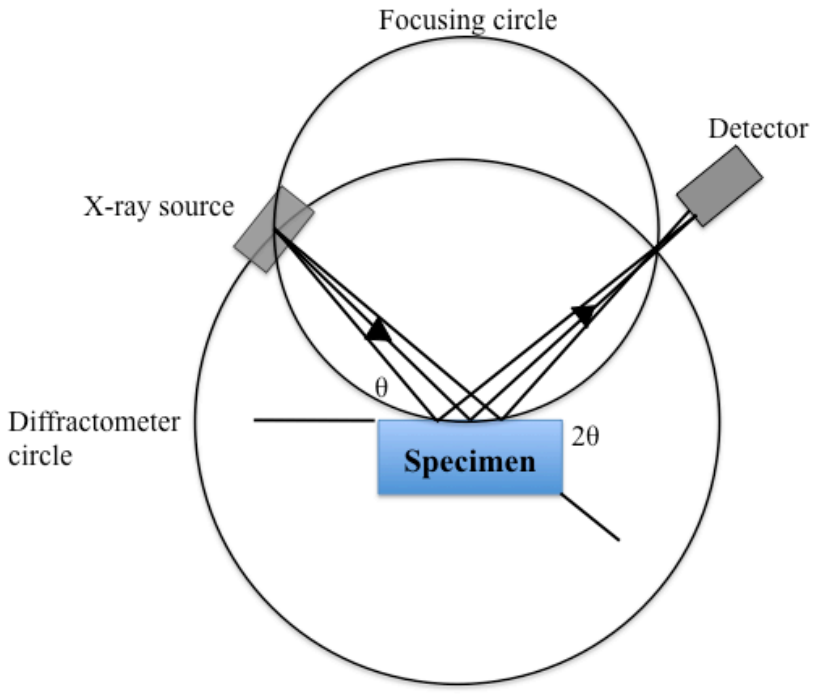

Figure 6.2 Geometry of an X-ray diffractometer

The angle between the plane of the specimen and the X-ray source is the Bragg angle (θ). The angle between the projection of the X-ray source and the detector is (2θ). The X-ray diffraction patterns produced in this geometry are often known as (θ-2θ) scans. In the (θ-2θ) geometry the X-ray source is fixed, and the detector moves through a rang of angles. The (2θ) measurement range is typically from 0° to about 170°. The diffraction pattern for the material is obtained from this (2θ) measurement. [8, 9]

Besides the three basic components, there are also a series of optics between the X-ray source and specimen as well as the specimen and the detector. In this study, PANalytical X'Pert Pro MPD was utilized, and a detailed instrument set-up is given in Figure 6.3. The Soller slits consist of a series of closely spaced parallel metal plates that define and collimate the incident beam. The divergence slit and mask controls the size on the sample to be measured, while the anti-scatter slit reduces the background radiation. [8]

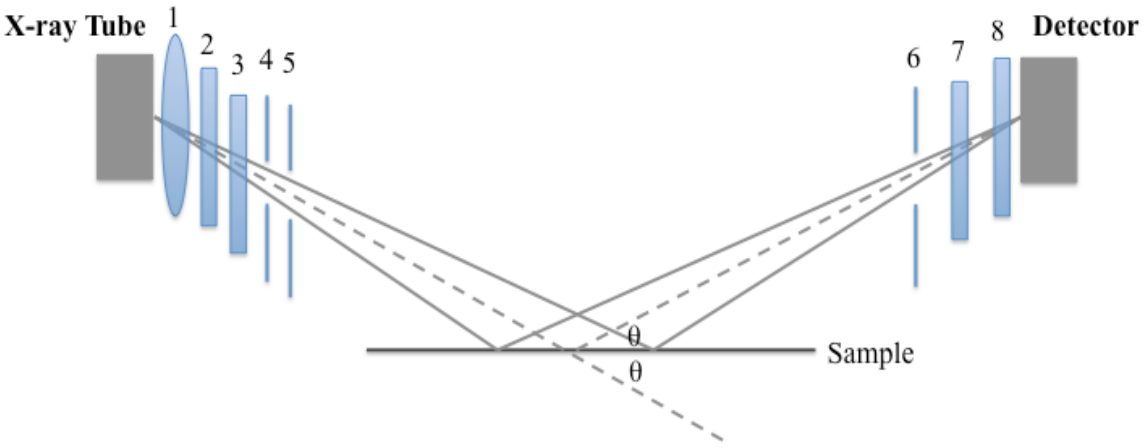

Figure 6.3 Instrument set-up for PANalytical X'Pert Pro MPD (1. Focus; 2. Soller slits; 3. Mask; 4. Anti-scatter slit; 5. Divergence slit; 6. Anti-scatter slit; 7. Soller slits; 8. Filter)

6.4 Sample Preparations

Various methods can be used for the preparation of the sample specimen. The success of a given diffraction experiment will invariably depend on the correct choice of preparation

method for the sample being analyzed and for the instrument conditions being used for the analysis. [10] The specimen preparation may involve a number of steps such as drying, grinding, sieving, dilution and mounting. [11]

Materials with equal crystal shapes and no cleavages that produce flat samples usually yield random samples using any specimen preparation method. However, if the particles have any crystalographically related shape, the shape will make achieving randomness difficult. As the difference between the maximum and minimum dimensions of the particle increases, it becomes more difficult to make a random sample. One possible resolution to this problem is to mix the sample with a viscous binder before mounting it into the sample holder. [10, 12]

6.5 Applications

PXRD is most widely used for characterization and identification of unknown materials. It is used on materials in such fields as metallurgy, mineralogy, forensic science, archeology, condensed matter physics, and the biological and pharmaceutical sciences. [1]

Its applications include: [13]

1) Identification of single-phase materials - minerals, chemical compounds, ceramics or other engineered materials;
2) Identification of multiple phases in microcrystalline mixtures (i.e., rocks);
3) Determination of the crystal structure of identified materials;
4) Identification and structural analysis of clay minerals; and
5) Recognition of amorphous materials in partially crystalline mixtures.

Chapter 7

Materials & Methods

7.1 Materials

7.1.1 Magnesium Hydroxide Powder USP

7.1.1.1 Physical and Chemical Properties

Magnesium hydroxide is a white fine amorphous powder, as seen in Figure 7.1. It is tasteless and odorless; has a molecular weight of 58.32, specific gravity of 2.36; and decomposes into magnesium oxide at temperatures above 350 °C. [1]

Figure 7.1 Dry powder magnesium hydroxide

Magnesium hydroxide; Magnesium hydrate; Marinco H.; $Mg(OH)_2$ contains Mg 41.69%; H 3.46%; O 54.85%; and MgO 69.12% (Figure 7.2). It is practically insoluble in water (1:80,000; K_{sp} of 1.5×10^{-11}) and alcohol; soluble in dilute acids, and imparts a slight alkaline reaction to water. The pH value of an aqueous slurry is 9.5-10.5. [2]

Magnesium hydroxide dissociates into magnesium ions and hydroxide ions in aqueous solutions, all of the magnesium hydroxide that does dissolve does dissociate.

$$Mg(OH)_2 \leftrightarrow Mg^{2+} + 2\,OH^- \qquad \text{Eqn. 7.1}$$

The solubility of magnesium hydroxide changes when the equilibrium is disturbed. The addition of sodium hydroxide or potassium hydroxide reduces the solubility by increasing the presence of hydroxide ions to shift the equilibrium in the reverse direction; while the addition of ammonia or ammonium chloride increases the solubility by combining with hydroxide ions to form non-ionized ammonium hydroxide to move the equilibrium in the forward direction. [3] Magnesium hydroxide absorbs carbon dioxide in the presence of water, partially forms magnesium carbonate, which requires it to be kept in well-closed, airtight containers. [2]

Magnesium hydroxide powder was obtained from Spectrum Chemical Mfg. Corp., CAS 1309-42-8, Lot No. YS1082, with the parameters given in Table 7.1.

Table 7.1 Maximum limits of magnesium hydroxide powder

Molecular Weight	58.32
Assay (Dried Basis)	95.0 – 100.5%
Loss on Ignition	30.0-33.0%
Microbial Limits (Escherichia Coli)	to pass test
Loss on drying	2.0%
Soluble Salts	to pass test (≤10 mg)
Carbonate	to pass test
Calcium	1.5%
Heavy Metals	20 ug/g
Lead	1.5ppm
Residual Solvents	to pass test

7.1.1.2 Natural Occurrence

Magnesium hydroxide occurs naturally as the mineral called brucite, in a ratio of 1:2:1 in clay minerals amongst others (e.g. in chlorite), in which it occupies the interlayer position normally filled by monovalent and divalent cations such as Na^+, K^+, Mg^{2+} and Ca^{2+}. [4]

It is a common alteration product of periclase in marble; a low-temperature hydrothermal vein mineral in metamorphosed limestones and chlorite schists; and is formed during the serpentinization of dunites. [5]

The crystal habit of brucite can be divided into three categories [5]: 1) platy or foliated masses and rosettes - layered structure, parting into thin sheets; 2) fibrous - extremely slender prisms; 3) massive - shapeless, no distinctive external crystal shape. [6]

The crystal mostly appears in layers; consists of double OH layers per single Mg layer. The layers are packed as a hexagonal crystal system. Each Mg atom or O atom is attached to six H atom (Figure 7.2), which has an analogy to the center ion coordinates with ligands in a complex. [7]

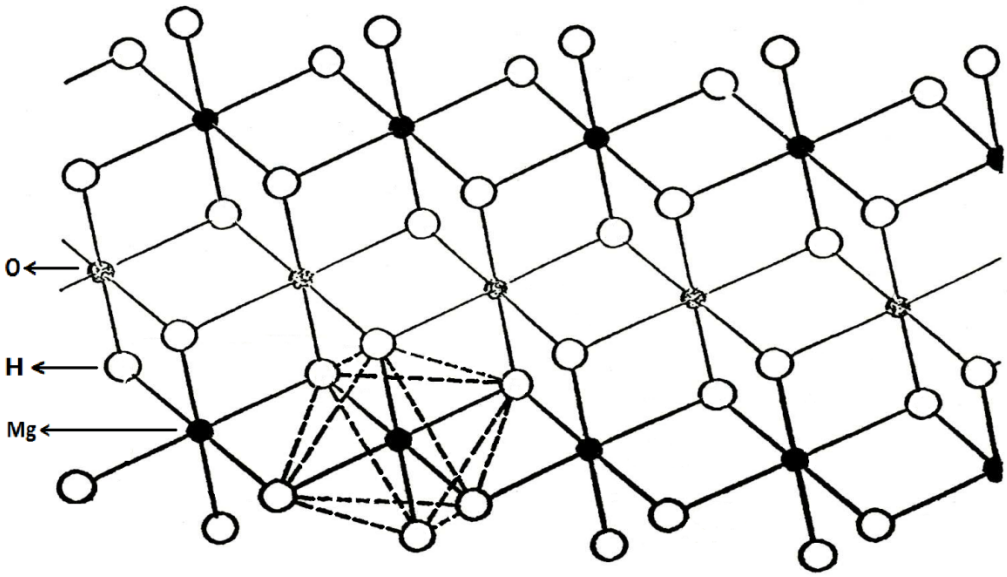

Figure 7.2 Crystal structure of magnesium hydroxide

7.1.1.3 Uses of Magnesium Hydroxide

Liquid dispersions of magnesium hydroxide is widely known as an antacid or laxative in the form of milk of magnesia. The combination of the element magnesium (an alkaline earth metal) with other elements or compounds creates a versatile substance that is useful for a wide range of industries and applications. All its uses include:

1) As an antacid, saline laxative, emulsifying agent, filler in soft gelatin capsules, etc. in the pharmaceutical industry. The usual dosage forms for magnesium hydroxide as found on the US market include: oral liquids of 400 mg/5 mL, oral liquid concentrates of 800 mg/5 mL, and chewable tablets of 311 mg. [8] The adult dose for the antacid is 5-15 mL of liquid (2.5-7.5 mL for concentrate) or 2-4 tablets as needed up to 4 times/day. A dose of about 1 g by month is given, for a saline laxative as 30-60 mL/day of liquid (15-30 mL for concentrate) or 6-8 tablets before bedtime, or up to about 5 g by month. [1, 8]
2) Waste water treatment: to adjust the pH levels of "slurry" waste water in the extraction of minerals; to control levels of ammonia and hydrogen phosphorous; to replace toxic polymers and ferric chlorite used for dewatering and controlling odor in sewage treatment; to help remove metals from waste streams in the treatment of drinking water. [9]
3) As a flame retardant filler in the plastics industry, by releasing its 31% water when heated to above 325°C, which cools the product below its flash point to reduce fire occurrence. [9]
4) As a vulcanizing agent in the rubber industry where it can be used as a replacement for the traditionally-used magnesium oxide. [9]

5) As a replacement for caustic soda and magnesium sulfate in pulp bleaching in the paper industry. [9]
6) As an insecticide or organic pesticide which is effective against bed bugs, roaches, ants and termites. [9]
7) As an additive in the food industry. [1]
8) Other uses include sugar refining; dentifrices; as an emollient in skin creams; uranium processing; ink production, etc.. [8]

7.1.1.4 Physiological Properties

Magnesium hydroxide is an effective, non-systemic substance used in the short-term treatment of symptoms of hyperacidity, occasional constipation, and magnesium replacement therapy. As an antacid, magnesium hydroxide reacts with hydrochloric acid in the stomach to form magnesium chloride. As a saline laxative, any magnesium hydroxide remaining in the stomach after reacting is moved into the small intestine. It promotes bowel evacuation by causing osmotic retention of fluid which distends the colon with increased peristaltic activity; therefore, magnesium hydroxide is found under the category of osmotic laxatives. [10]

For patients with normal renal function, about 15-30% of the magnesium chloride is absorbed and rapidly excreted by the kidneys. If the renal function of the patient is damaged, it might result in hypermagnesaemia, symptoms of which include flushing of the skin, thirst, hypotension, blocking of neuromuscular transmission, loss of reflexes and respiratory depression. This problem can be treated by an IV injection of 10-20 mL of 10% calcium gluconate. [11]

7.1.2 Carboxymethyl Cellulose (CMC)

Carboxymethyl cellulose occurs as white granules; whose solubility in water depends on the degree of substitution (Figure 7.3). Water-soluble CMC is available in various viscosities (5-2000 centipoises as a 1% solution). The solubility is equally good in hot and cold water (which differs from methylcellulose). It is often used as its sodium salt, sodium carboxymethyl cellulose. The presence of metal salts has little effect on the viscosity. CMC solutions are stable between a pH 2 and 10. Below pH 2 precipitation of a solid occurs, above the pH the viscosity decreases rapidly. It is used in drilling muds, in detergents as a soil-suspending agent, in resin emulsion paints, adhesives, printing inks, textile sizing, as protective colloid in general, and in pharmacy for preparing suspensions. [2]

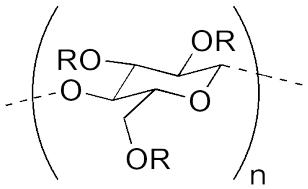

R = H or CH_2CO_2H

Figure 7.3 Chemical structure of CMC

Carboxymethyl cellulose, Sodium Med Viscosity 7MF (CMC) was obtained from Amend Drug & Chemical Co., Inc. Viscosity of 2% water solution is > 25CPS. CAS # 9004-32-4, NDC# 17317-0172-1, Lot # W42042G04.

CMC solution concentrations of 0.005%, 0.01% and 0.02% (w/v) were used as a suspending agent and protective colloid to provide a flocculated system for the magnesium hydroxide suspensions. The 0.02% (w/v) dispersion of CMC was the highest concentration required to keep the system flocculated, above this concentration, the system deflocculated.

7.2 Determination of Density and Viscosity

7.2.1 Determination of Density (Specific Gravity)

A 10 mL pycnometer was weighed and filled with water until it overflowed. It was then allowed to stand in a constant temperature bath at 25℃ for 30 minutes dried externally, and then weighed. The experiment was repeated for the 0.005%, 0.01% and 0.02% (w/v) CMC dispersions. The density for each medium was then obtained by standard calculations.

7.2.2 Determination of Viscosity

An Ostwald viscometer was used to determine the viscosity of the dispersion medium, as seen in Figure 7.4. The solution was raised by vacuum to a level above the upper mark; the time required for the solution to flow down from the upper mark to the lower mark is recorded using a stopwatch.

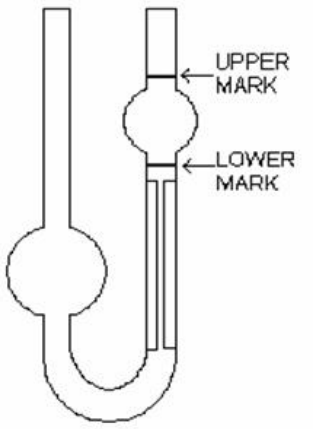

Figure 7.4 An Ostwald viscometer [12]

Purified Water USP with a known viscosity of 0.01 poise is used as the standard to calculate the viscosity of the other dispersion media using the following equation:

$$\frac{\eta_1}{\eta_2} = \frac{(\rho_1)(t_1)}{(\rho_2)(t_2)} \qquad \text{Eqn. 7.2}$$

where (η_1), (η_2) are viscosities of water and the medium respectively in poise ($g.cm^{-1}s^{-1}$); (ρ_1), (ρ_2) are densities of water and the medium respectively in g/mL; (t_1), (t_2) are time required for the solution to flow between the two marks in seconds.

7.3 Hindered Settling Experiments

Various quantities of dried powder magnesium hydroxide, namely 15, 20, 25, 30, 35, 40 and 45 Gm were weighed and added a 250 mL cylinder respectively, scaled with 200 mm graph paper from the 200 mL mark. The cylinder was filled with Purified Water USP, and dispersion medium to achieve a final concentration of 0.005%, 0.01% and 0.02% (w/v), respectively, to 200 mL mark. The mixture was stirred with a glass-stirring rod to insure full contact of the powder to the medium. It was then allowed to rest for 24 hours in order to wet (hydrate) the powder, and finally capped with Parafilm®.

After resting, the cylinder was shaken 20 times. The cylinder was then placed on the bench top and the height of the supernatant interface was recorded with respect to time. These samples were prepared for each weight of powder and the data collected. After 24 hours these same samples were again shaken and the data collected a record time. It was then repeated a third time. Hindered settling experiments for each quantity of powder were done in triplicate.

7.4 Determination of Particle Size

7.4.1 Hindered Settling Theory

A plot of the height of interface versus time was obtained and the slope of the linear

section was recorded as the rate of fall of the interface (Q-value). By incorporating this value into the three equations discussed in Chapter 2, Section 2.4, Stokes' velocity of fall for the particles in the suspensions was determined. By determining the viscosity and density of the dispersion medium, with the known Stokes' velocity of fall of the particles, the particle size of the dispersed phase was calculated using Stokes' law as discussed in Chapter 2 Section 2.2 (Eqn. 2.6):

$$r = \sqrt{\frac{9\eta V_S}{2g(\rho_s - \rho_l)}} \qquad \text{Eqn. 2.6}$$

7.4.2 Sieve Analysis

US Standard Sieve No. 20, 30, 40, 50, 60, 80, 100, and 120 were selected. They were assembled in descending order. A pan was placed under the bottom sieve to catch any powder which came through. An 80 Gm sample of magnesium hydroxide powder was accurately weighed and placed on the top sieve. A lid was placed to cover the top sieve and prevent dust from escaping. The sieves were shaken for approximately fifteen minutes until the powders were well distributed between the sieves. The powder retained on each sieve was collected and weighed. The data were noted and used to plot the size distribution curve.

7.4.3 Scanning Electron Microscopy (SEM)

SEM was used to examine the particle size, shape and porosity of the dispersed phase. The clear supernatant liquids and the sediments of the suspension were spread onto glass slab and dried under low temperature in an oven. The dried samples together with the dry powder magnesium hydroxide were mounted on a specimen stub and coated with ultra thin coating of gold layer of 20 nm by the low vacuum sputter coating method.

Photographs were then taken using a JSM-5200 Scanning Electron Microscope (Tokyo, Japan) operated at 1.00 kV.

7.4.4 Laser Diffraction (LD)

The Malvern Mastersizer 2000[e] was used to analyze the particle size and size distribution of dry powder magnesium hydroxide in various media suspensions. A specific suspension concentration at 20 g/200 mL was chosen. A sample was placed in a centrifuge tube and sonicated for dispersion and then added into the flow system. The size distribution and mean particle size was then obtained from the Malvern Mastersizer 2000[e] software.

7.5 Thermal Analysis

7.5.1 Differential Scanning Calorimetry (DSC)

The DSC 822[e] Mettler Toledo with a TS0801R0 Sample Robot and a TS0800GCI Gas Controller was used to measure the heat flow properties of dry powder magnesium hydroxide in various media suspensions as filtered sediments with dried sediments and liquid media. A specific suspension concentration at 20 g/200 mL was chosen. Samples (10 to 20 mg) were weighed into 100 µl aluminum pans, covered with aluminum lids, and sealed. The temperature program was as follows: cool from 25°C to -30°C at 10°C/min, hold at -30°C for 5min, heat from -30°C to 150°C at 10°C/min, from 150°C to 350°C at 50°C/min, and from 350°C to 500°C at 10°C/min. Mettler Toledo STAR[e] software (version 10.10b) was used to analyze the data.

7.5.2 Thermogravimetry (TG)

The TGA/SDTA 851[e] Mettler Toledo with a TS0801R0 Sample Robot and a TS0800GCI

Gas Controller was used to measure the water lose for the dry powder magnesium hydroxide in various suspensions media as filtered sediments. A specific suspension concentration at 20 g/200 mL was chosen. Samples (20 mg) were carefully weighed into 100 µl aluminum pans using a Mettler MT50 analytical balance, covered with aluminum lids, sealed and pinhole in the lid. The temperature program was to heat the samples from 25°C to 500°C at 10°C/min under nitrogen gas purge of 20 mL/min. Mettler Toledo STAR^e software (version 10.00b) was used to analyze the data.

7.6 X-Ray Powder Diffraction (PXRD)

PXRD was used to evaluate the dry powder magnesium hydroxide as well as the dried suspension sediment samples before and after high temperature heating. X-ray spectra were recorded with PANalytical X'Pert Pro MPD (PANalytical, Tokyo, Japan) using Cu X-ray source, a voltage of 45 kV, a current of 40 mA, with 0.04 rad Soller slits, 1/4° divergence slit, 10 mm mask, 1/2° anti-scattered slit, Nickel filter and X'Celerator detector. The instrument was operated in the continuous scanning speed of step size 0.04 and time/step 25 second over a 2θ range of 10° to 70°. The samples were ground using a Wedgwood mortar and pestle, placed into the cavity of an aluminum sample holder and packed smoothly using a glass slide. The results were evaluated using the X'Pert Data High Score Plus software.

Chapter 8

Results & Discussions

8.1 Particle Size Determination

8.1.1 Sieving Results for Dry Powder Magnesium Hydroxide

The particle size distribution for the dry powder magnesium hydroxide, determined by sieving as provided in Chapter 6 Section 6.4.2, are given in Figure 8.1and Tables 8.1, and 8.2.

Table 8.1 Particle size distribution for dry powder magnesium hydroxide determined by sieving

Sieve #	Size opening (µ m)	Particle size on sieve (µ m)	Mass on sieve (gm)	% Retained on sieve	% Cumulative Retained	% Cumulative Passing
20	841	841	2.8243	3.58	3.58	96.42
30	595	718	13.0417	16.51	20.09	79.91
40	420	507.5	13.0768	16.56	36.65	63.35
50	297	358.5	13.4178	16.99	53.64	46.36
60	250	273.5	11.1587	14.13	67.76	32.24
80	177	213.5	9.7628	12.36	80.12	19.88
100	149	163	7.5832	9.60	89.72	10.28
120	125	137	2.2001	2.79	92.51	7.49
Pan	-	62.5	5.9191	7.49	100.00	0.00
Total			78.9845	100.00		

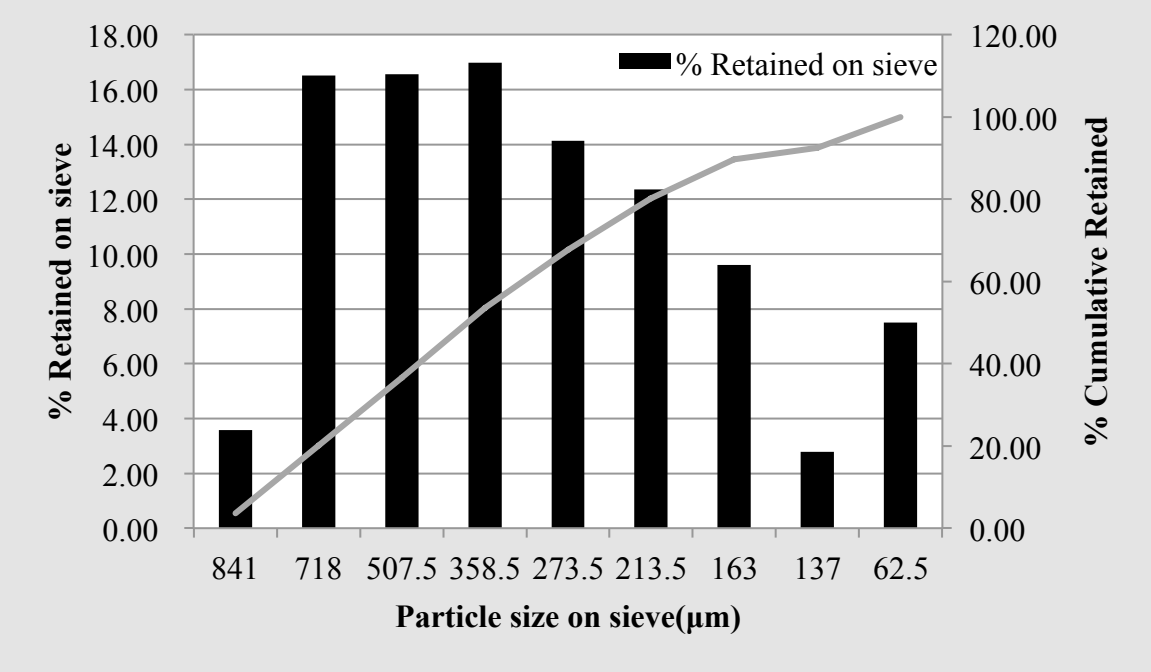

Figure 8.1 Distribution of the particle size for dry powder magnesium hydroxide determined by sieving

Table 8.2 Statistical data for the particle size distribution of dry powder magnesium hydroxide determined by sieving

Term	Size (µm)
Median	273.50
Mean	363.83
Mode	358.50
S.D.	255.42
Geo. Mean	274.86

The statistical data shown in Table 8.2 demonstrates how close the size results for both the mean and mode. This determination verified the correct choice of the Sieve numbers used in this experiment as well as the normality of the size distribution obtained from the sieve analysis. The results of sieving analysis were then compared with the results obtained from other types of particle size measurement methods, including hindered settling experiments, SEM and LD as found in later sections.

8.1.2 Hindered Settling Results

8.1.2.1 Specific Gravity and Viscosity of the Medium

According to Stokes' law as discussed in Chapter 2 Section 2.2, the specific gravity and viscosity for each the suspending media are required for the calculation of the particle size. Based on the method provided in Chapter 6 Sections 6.2.1 and 6.2.2, the values are shown in Table 8.3.

Table 8.3 Specific gravity and viscosity determination for suspending media

Suspending media	Specific gravity (g/mL)	Viscosity (poise, gcm-1sec-1)
Purified Water USP	0.98327	0.01000
0.005% (w/v) CMC	0.98942	0.01354
0.01% (w/v) CMC	0.99557	0.01646
0.02% (w/v) CMC	1.01386	0.02111

Carboxymethyl cellulose (CMC) solutions of various concentrations were used in this study as the suspending media for the magnesium hydroxide suspensions.

A CMC concentration of 0.1% (w/v) was attempted to be used, however, the system was deflocculated under such high polymer concentration, and a cloudy supernatant was obtained. No clear interface was observed in order for the hindered settling experiments to be performed. This may due to the nature of polymer. With high polymer concentrations, the system will be deflocculated, and only under certain concentrations will the protective colloid be a good flocculating agent as well as a wetting agent based on the discussion given in Chapter 3 Section 3. Thus, it was essential to determine the maximum concentration of CMC that should be used. It was then found that 0.02% (w/v) CMC provided a clear supernatant above the suspension. The actual viscous enhancement due to the addition of CMC was then determined as the upper-limit of addition. As the

results shown in Table 8.1, the viscosity of the solution was enhanced by about 35% at 0.005%(w/v), and about 100% at 0.02% (w/v) compared to the viscosity of water. Therefore, the viscosity enhancement by CMC was large enough to study the effect of viscosity on hindered settling and hence the particle size.

8.1.2.2 Sedimentation Curves

The results of the hindered settling experiments for various weights of dry powder magnesium hydroxide are shown in this section. The rate of fall of the interface (Q) for each amount of magnesium hydroxide in various media was then determined.

The experiments were carried out as provides in Chapter 6 Section 6.3. Various amounts of dry powder magnesium hydroxide, namely 15, 20, 25, 30, 35, 40 and 45 Gm were used to prepare the suspensions for a total volume of 200 mL. With each amount of dry powder, various media, namely Purified Water USP, 0.005% (w/v) CMC solution, 0.01% (w/v) CMC solution, 0.02% (w/v) CMC solution were used. For each quantity of dry powder and each media, a flocculated suspension was obtained with a clear supernatant and interface.

Three main tendencies were observed for the plots of interface against time for various quantities of powder using each media. Typical examples are given in Figures 8.2 to 8.4.

For all the suspensions at low concentrations, such as 0.075 g/mL or 7.5% (w/v), that is 15 Gm of dry powder in a total of 200 mL suspensions, the sedimentation curves show the same tendency (I) as seen in Figure 8.2. These suspensions have cloudy supernatant liquids during the process of hindered settling. This makes the interface difficult to be observed. The linear regions were also difficult to be distinguished from the compressive region. This was probably due to the low concentration of dry powder. The number of

particles present was not large enough to produce the collisions between the particles to undergo flocculation.

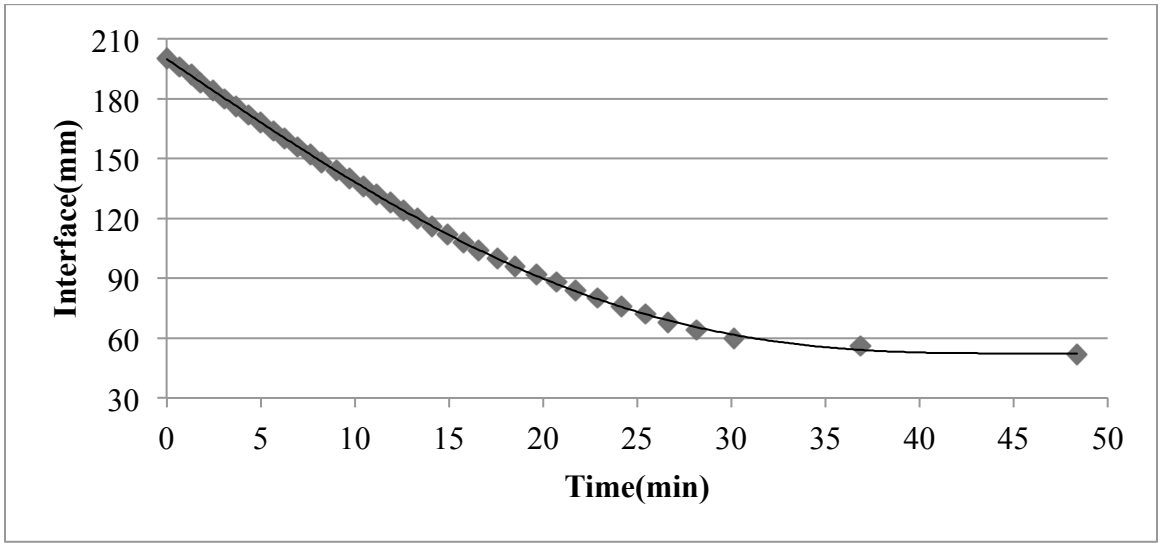

Figure 8.2 Tendency (I): sedimentation curve for 15 Gm dry powder magnesium hydroxide suspension in Purified Water USP

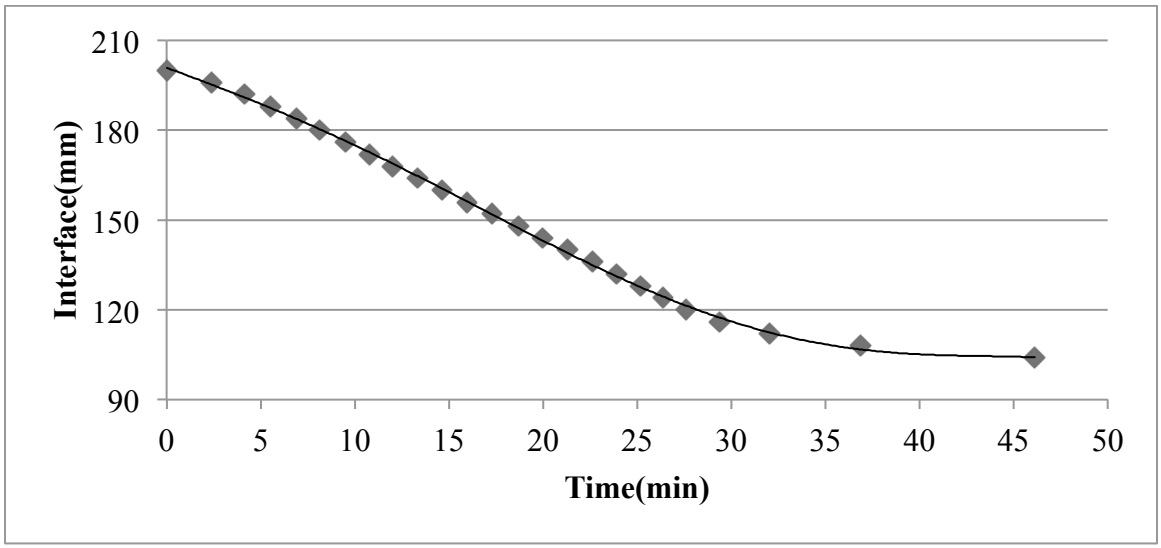

Figure 8.3 Tendency (II): sedimentation curve for 30 Gm dry powder magnesium hydroxide suspension in 0.01% (w/v) CMC

For suspensions with concentrations from 0.01 to 0.02 g/mL or 10% (w/v) to 20% (w/v), that is 20 Gm to 40 Gm of dry powder in a total of 200 mL of suspension, the

sedimentation curves show tendency (II) as seen in Figure 8.3. All these suspensions show a similar settling pattern and were used in the determination of the (Q) values.

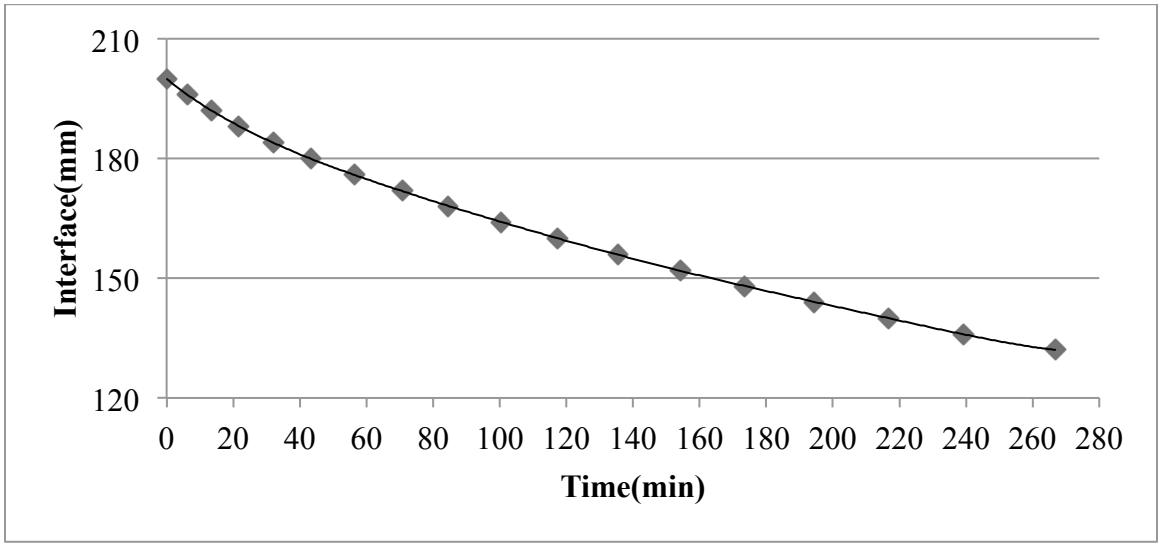

Figure 8.4 Tendency (III): sedimentation curve for 45 Gm dry powder magnesium hydroxide suspension in 0.005% (w/v) CMC

For suspensions at high concentrations, such as 0.225 g/mL or 22.5% (w/v), that is 45 Gm of dry powder in a total of 200 mL of suspension, the sedimentation curves show tendency (III) as seen in Figure 8.4. These suspensions show quite different settling pattern compared to the other two cases in a way that fall of the interface were faster in the initial region, then slowed down as the interface fell. The linearity of the curve also showed a small regression coefficient. This was especially true for suspensions using CMC solutions.

The sedimentation curves for the various amounts (20 to 40 Gm) of dry powder in each media are given in Figures 8.5 to 8.8, and linear region are re-plotted in Figures 8.9 to 8.28 to obtain the Q values from the slope of the linear regression. The sedimentation parameters from the linear plots are given in Tables 8.4 to 8.7.

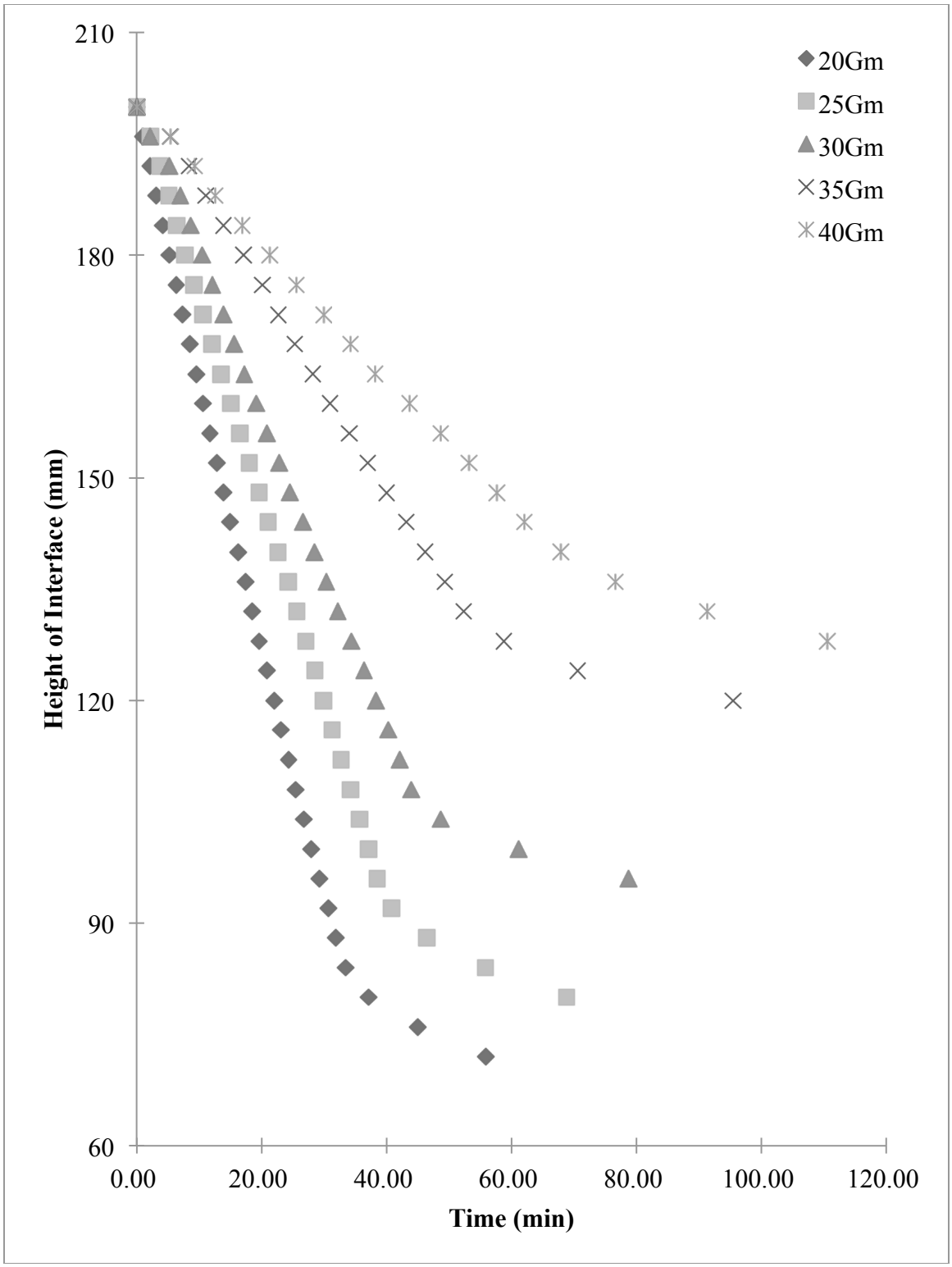

Figure 8.5 Sedimentation curves for the various amounts of dry powder magnesium hydroxide suspensions in Purified Water USP

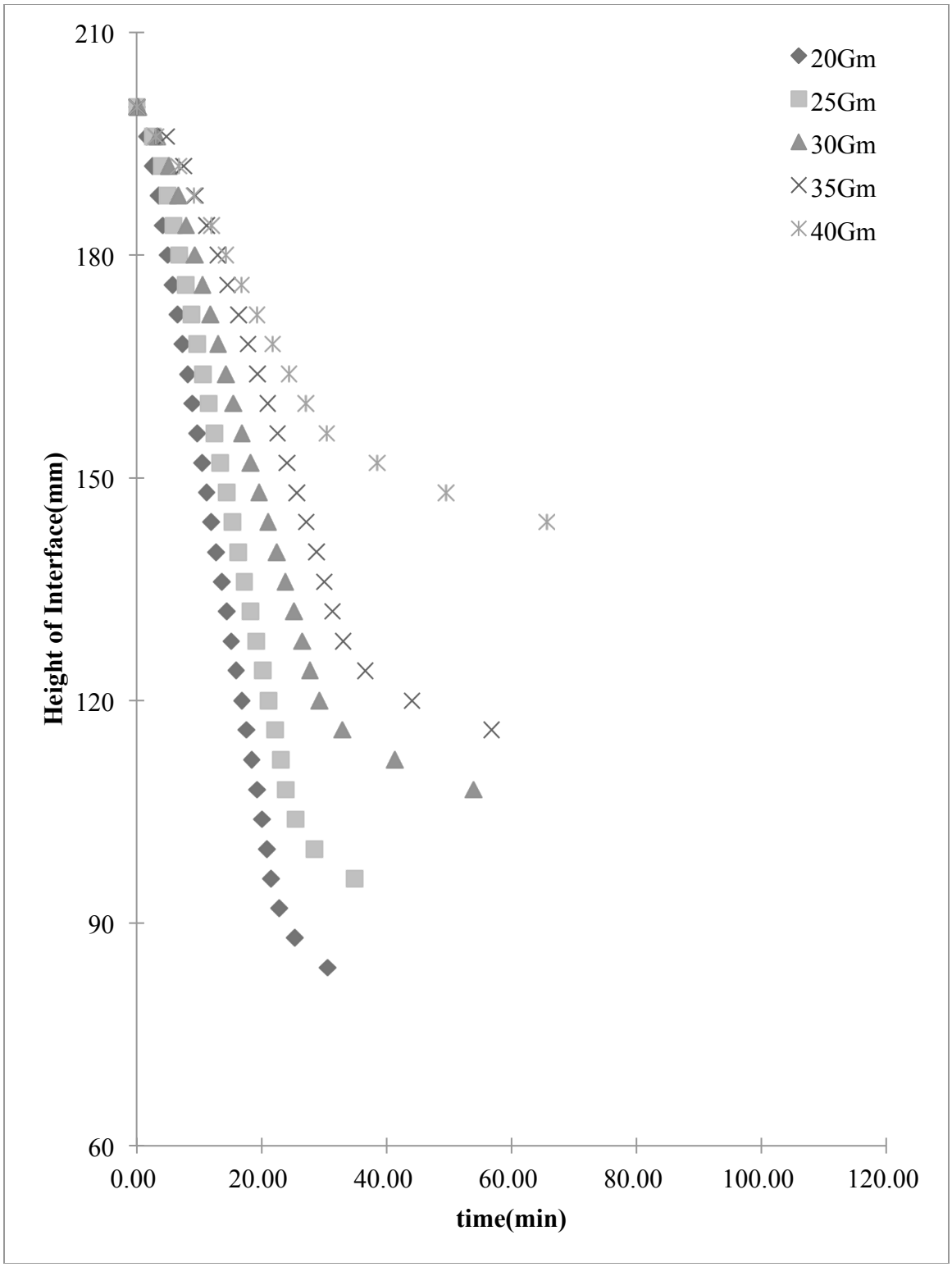

Figure 8.6 Sedimentation curves for the various amounts of dry powder magnesium hydroxide suspensions in 0.005% (w/v) CMC

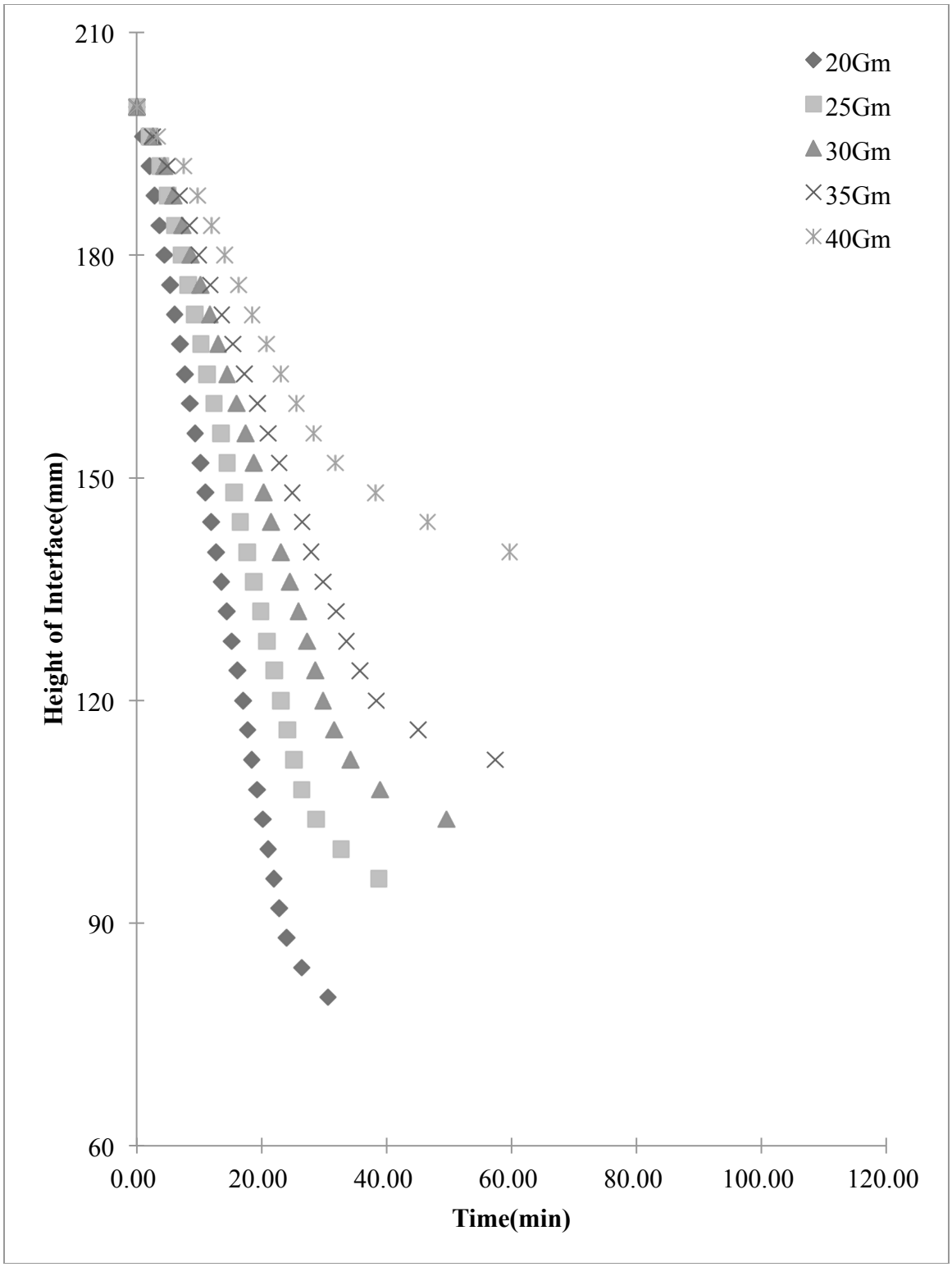

Figure 8.7 Sedimentation curves for the various amounts of dry powder magnesium hydroxide suspensions in 0.01% (w/v) CMC

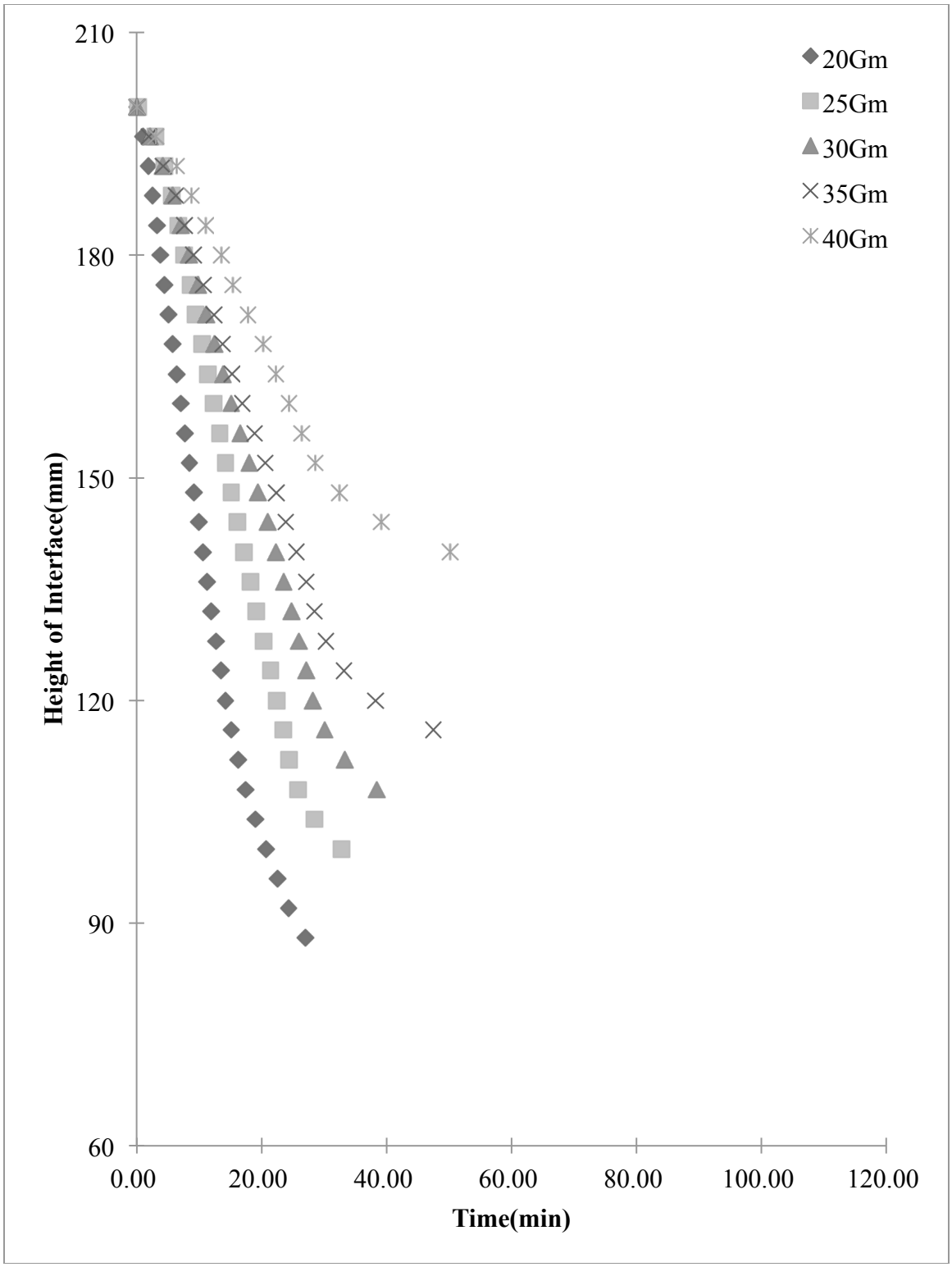

Figure 8.8 Sedimentation curves for the various amounts of dry powder magnesium hydroxide suspensions in 0.02% (w/v) CMC

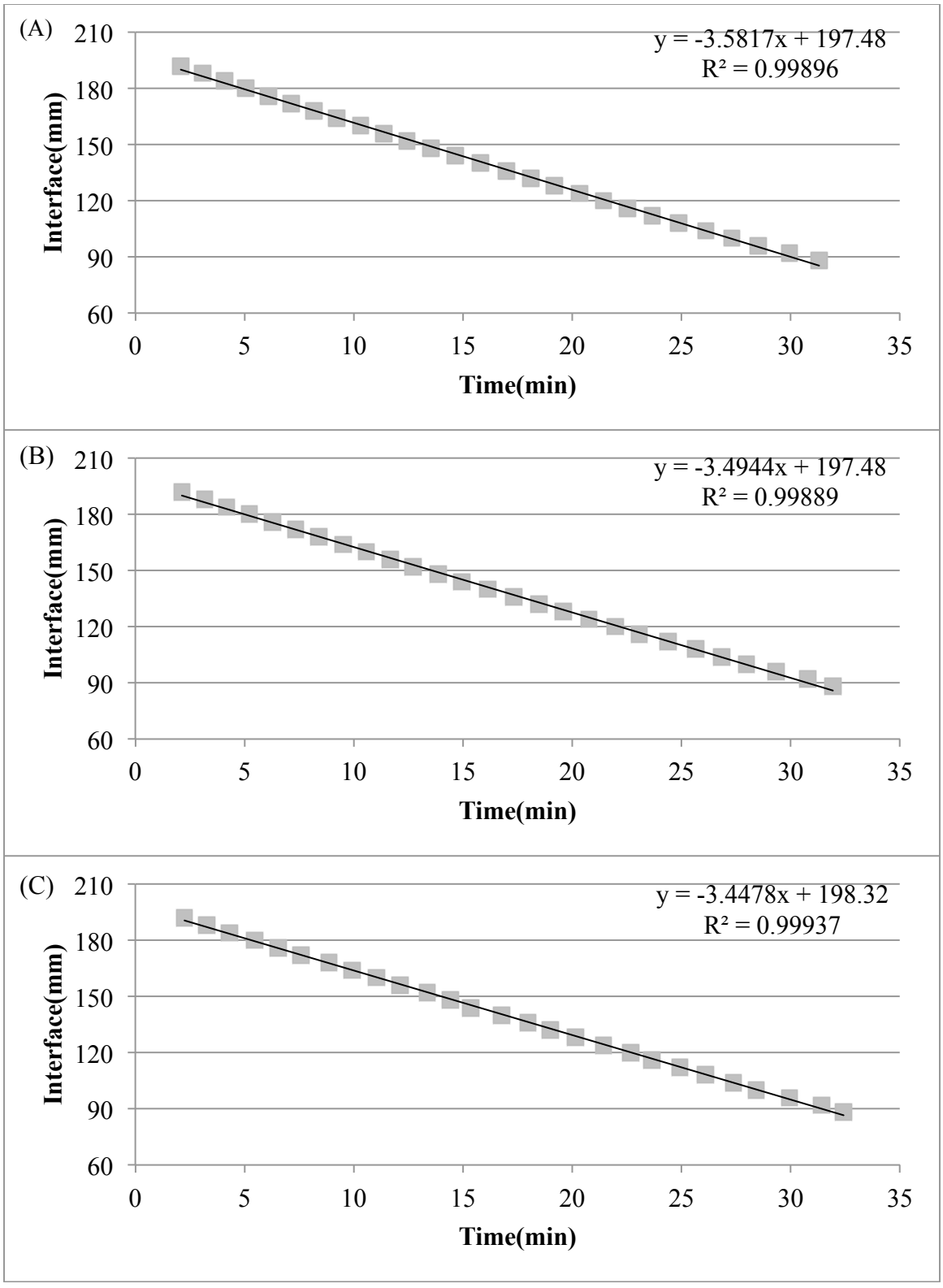

Figure 8.9 Linear plot for the fall of the interface against time for 20 Gm dry powder magnesium hydroxide suspensions in Purified Water USP.
(Experiment in triplicate A, B and C)

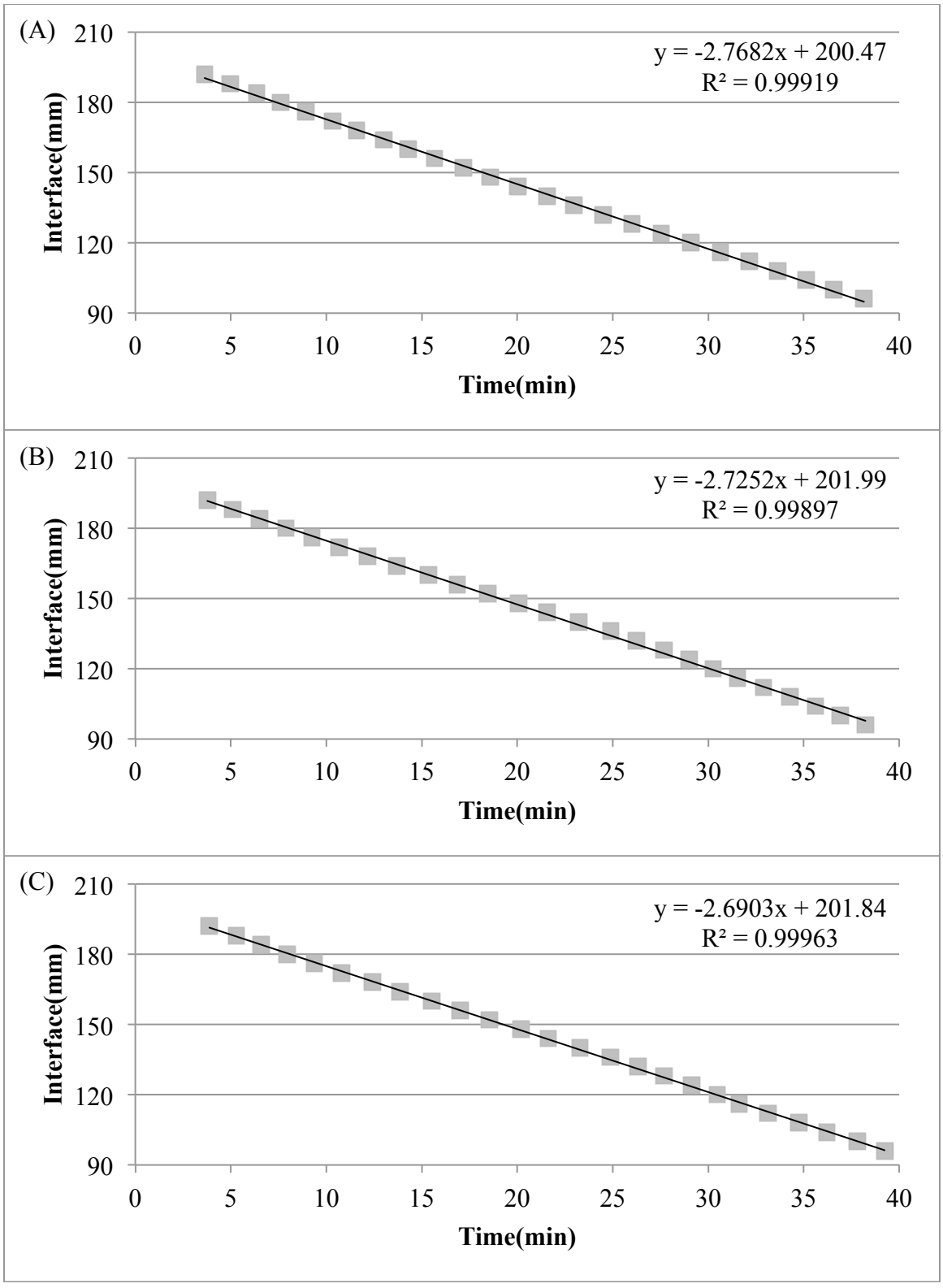

Figure 8.10 Linear plot for the fall of the interface against time for 25 Gm dry powder magnesium hydroxide suspensions in Purified Water USP.
(Experiment in triplicate A, B and C)

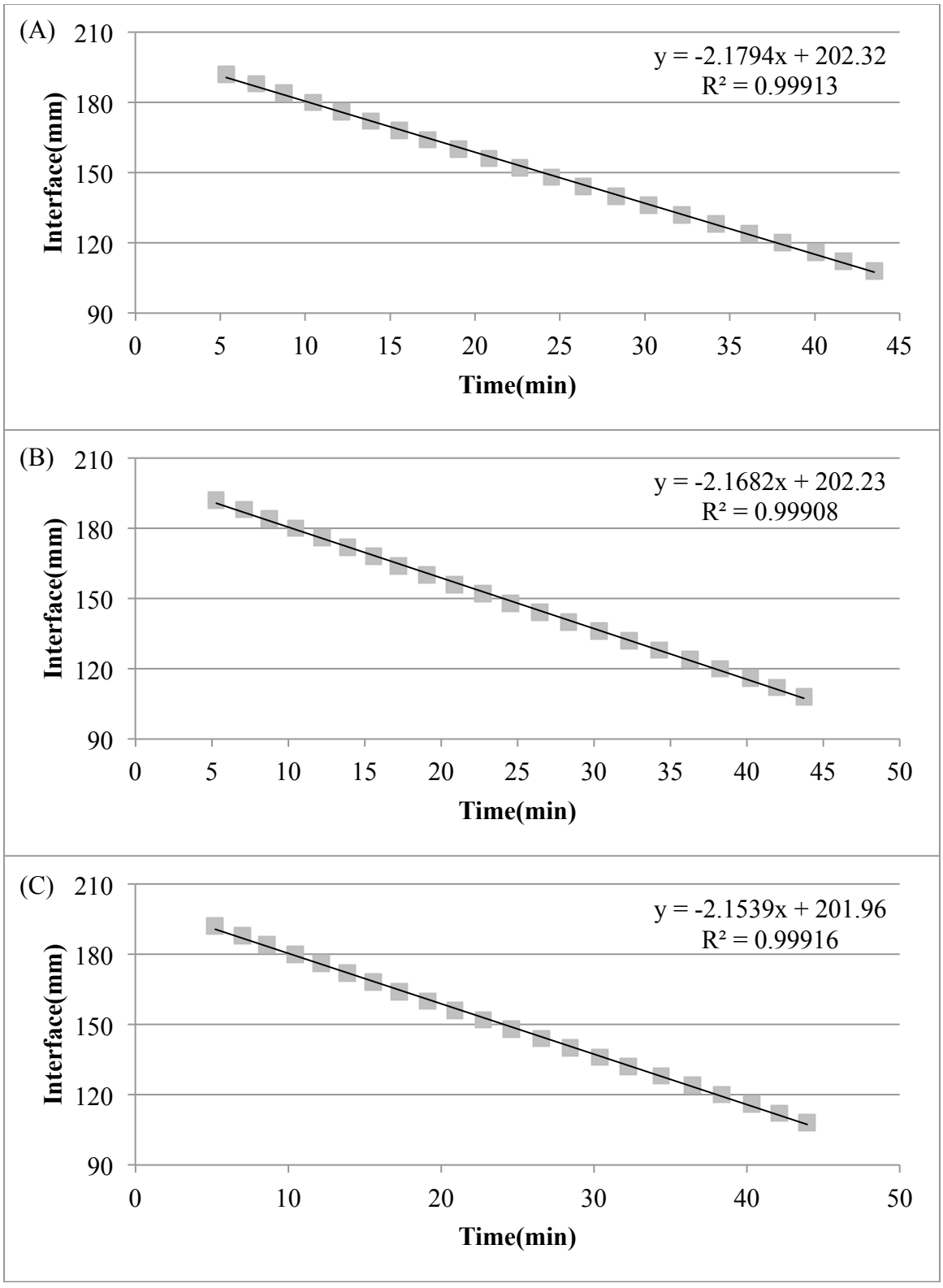

Figure 8.11 Linear plot for the fall of the interface against time for 30 Gm dry powder magnesium hydroxide suspensions in Purified Water USP.
(Experiment in triplicate A, B and C)

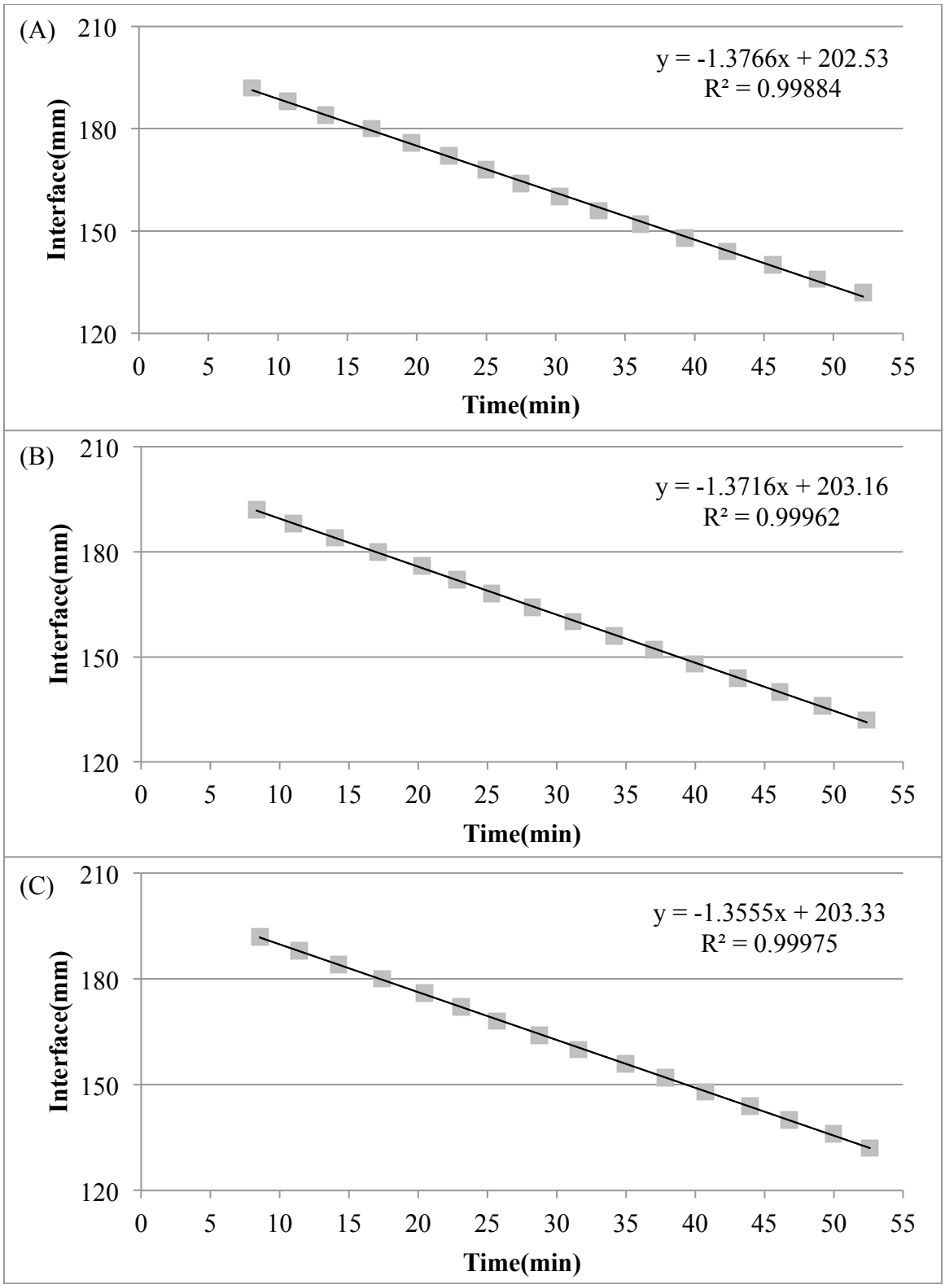

Figure 8.12 Linear plot for the fall of the interface against time for 35 Gm dry powder magnesium hydroxide suspensions in Purified Water USP.
(Experiment in triplicate A, B and C)

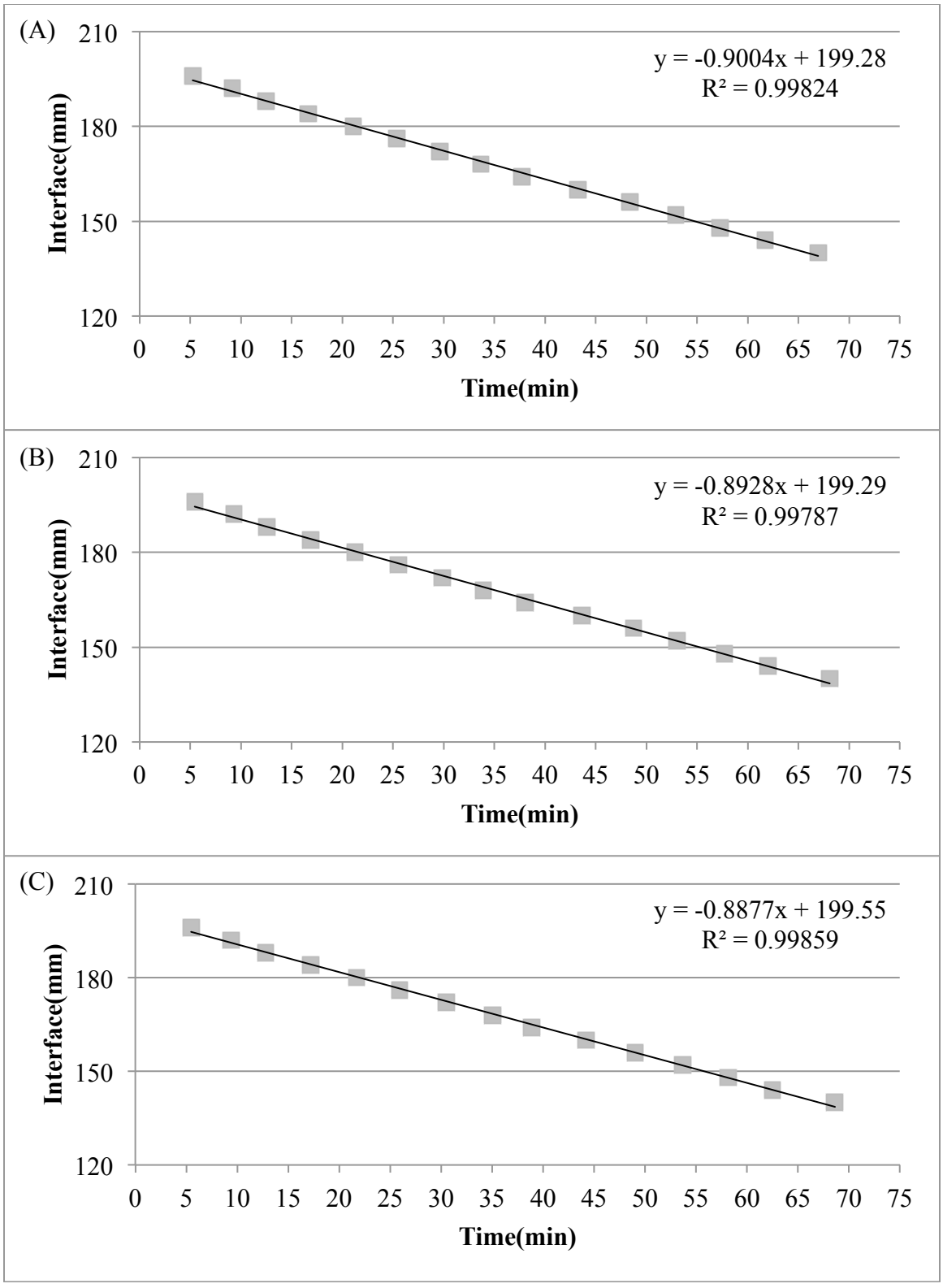

Figure 8.13 Linear plot for the fall of the interface against time for 40 Gm dry powder magnesium hydroxide suspensions in Purified Water USP.
(Experiment in triplicate A, B and C)

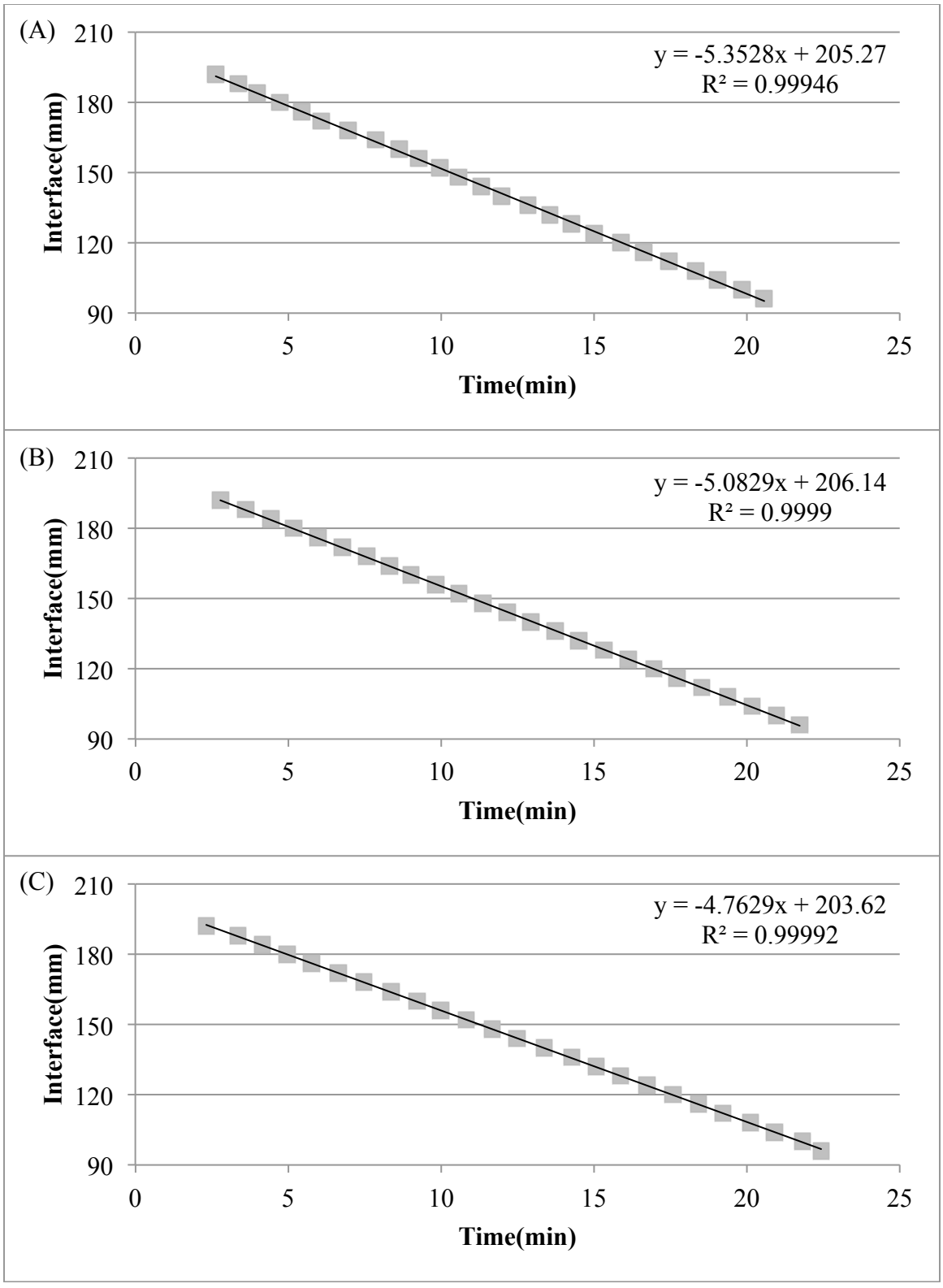

Figure 8.14 Linear plot for the fall of the interface against time for 20 Gm dry powder magnesium hydroxide suspensions in 0.005% (w/v) CMC. (Experiment in triplicate A, B and C)

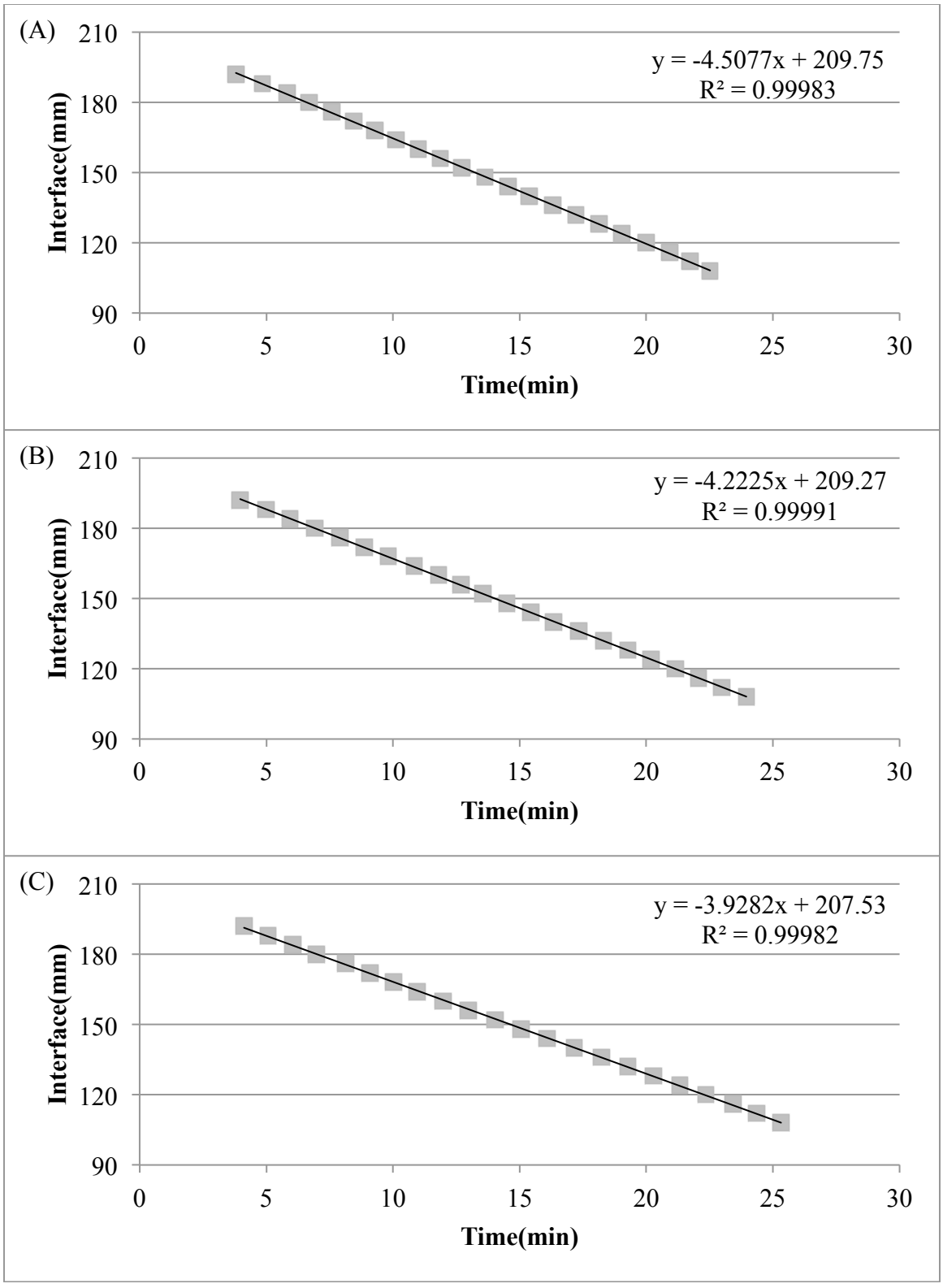

Figure 8.15 Linear plot for the fall of the interface against time for 25 Gm dry powder magnesium hydroxide suspensions in 0.005% (w/v) CMC.
(Experiment in triplicate A, B and C)

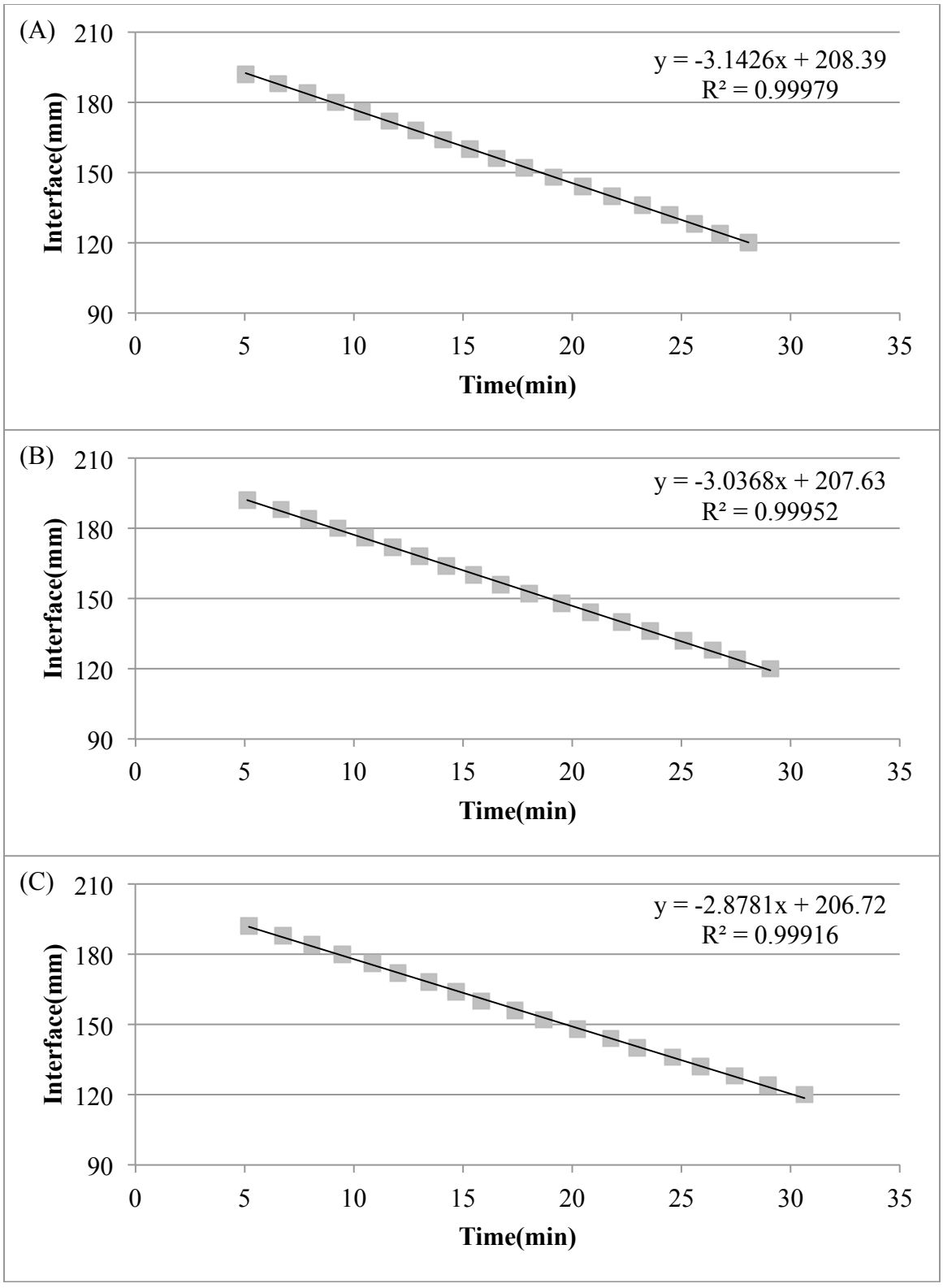

Figure 8.16 Linear plots for the fall of the interface against time for 30 Gm dry powder magnesium hydroxide suspensions in 0.005% (w/v) CMC.
(Experiment in triplicate A, B and C)

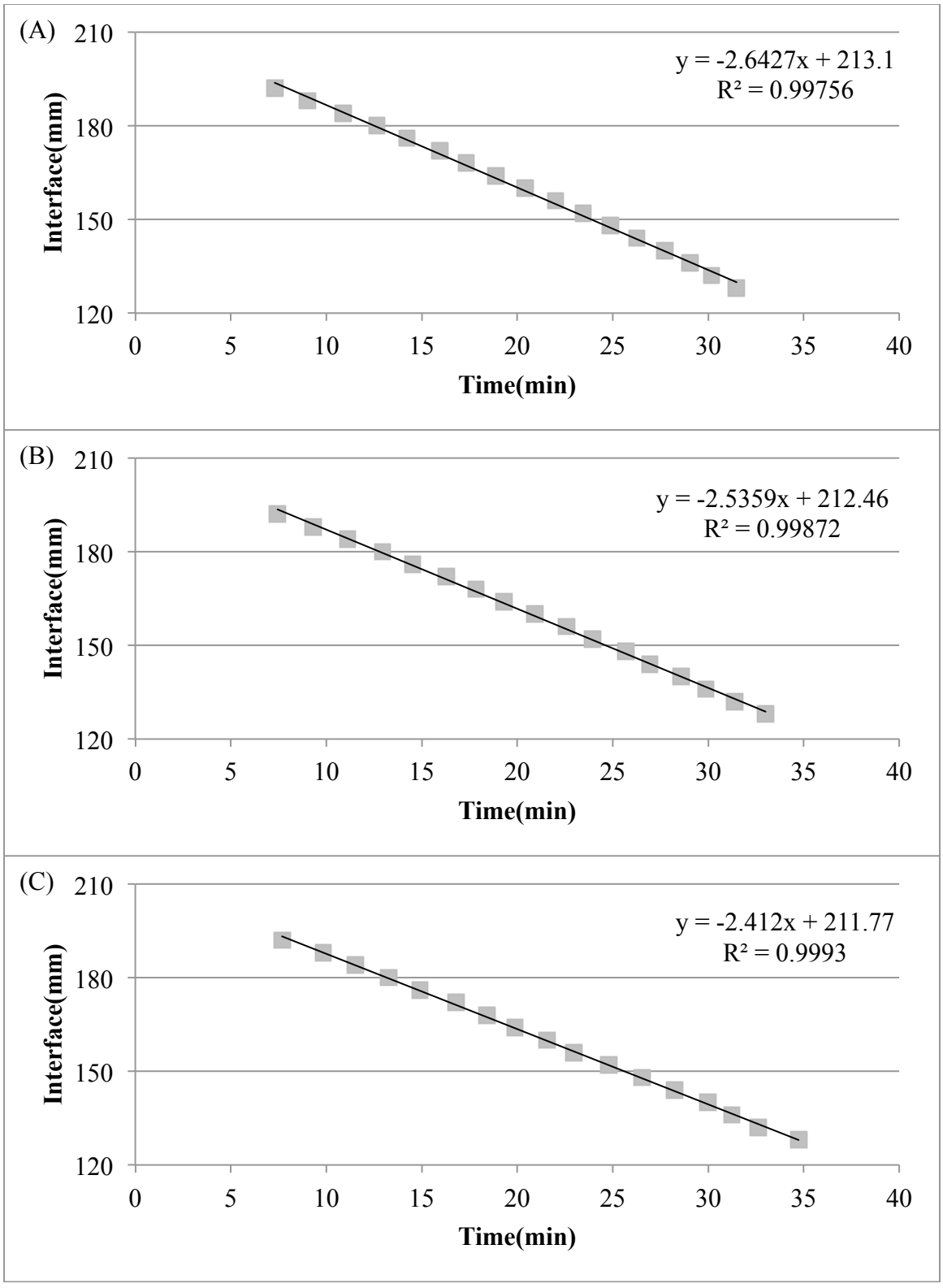

Figure 8.17 Linear plot for the fall of the interface against time for 35 Gm dry powder magnesium hydroxide suspensions in 0.005% (w/v) CMC. (Experiment in triplicate A, B and C)

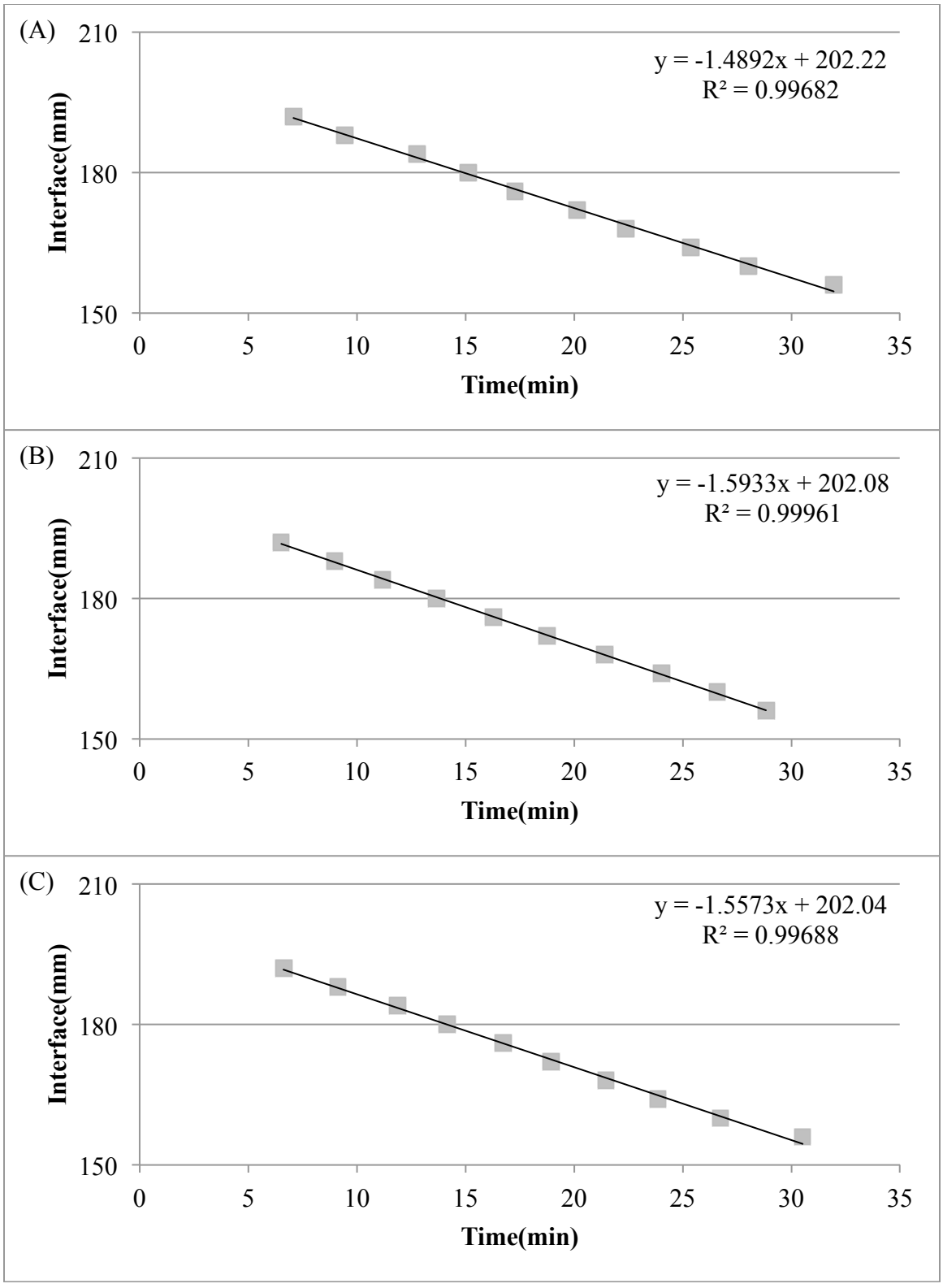

Figure 8.18 Linear plot for the fall of the interface against time for 40 Gm dry powder magnesium hydroxide suspensions in 0.005% (w/v) CMC.
(Experiment in triplicate A, B and C)

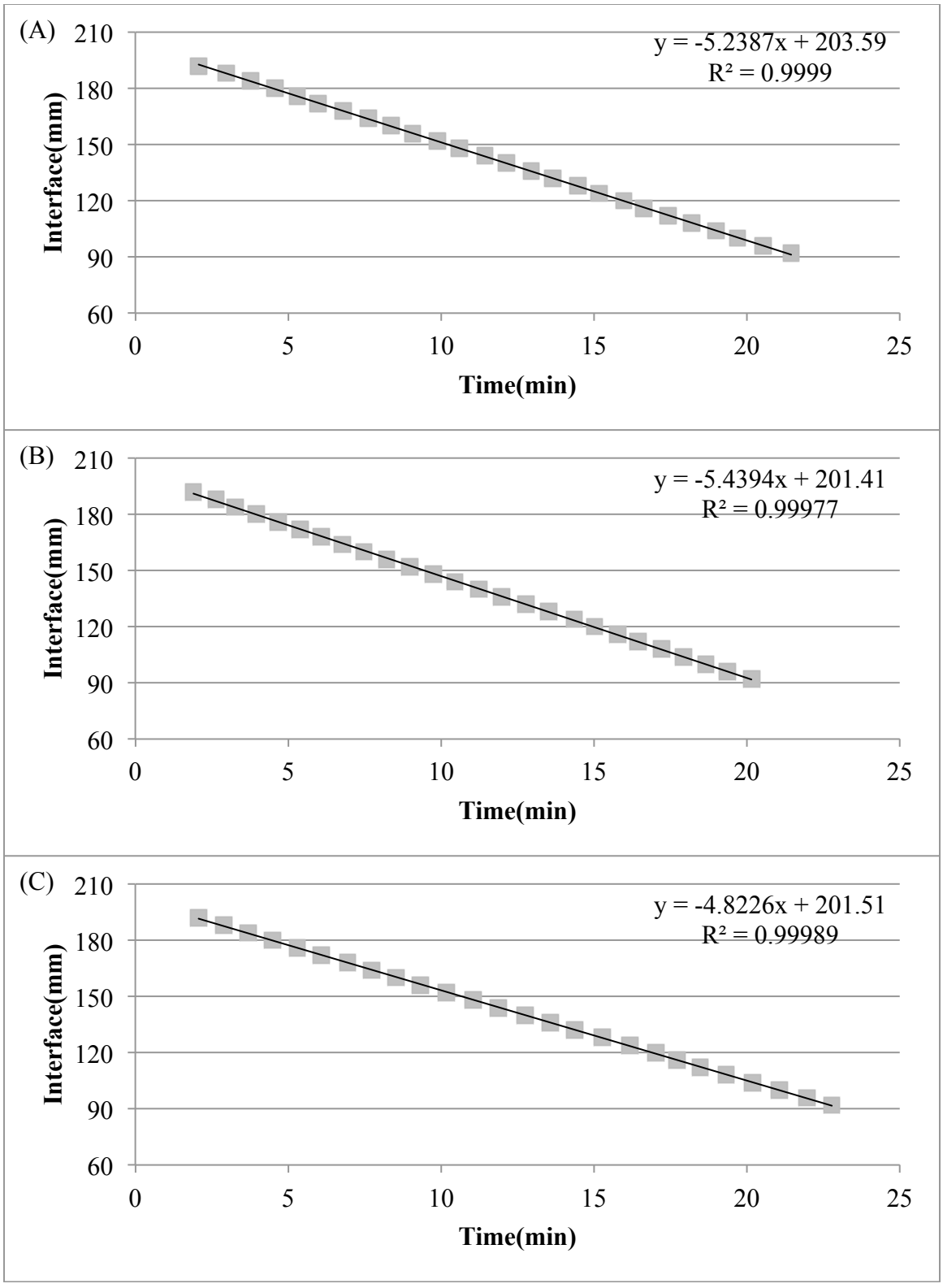

Figure 8.19 Linear plot for the fall of the interface against time for 20 Gm dry powder magnesium hydroxide suspensions in 0.01% (w/v) CMC.
(Experiment in triplicate A, B and C)

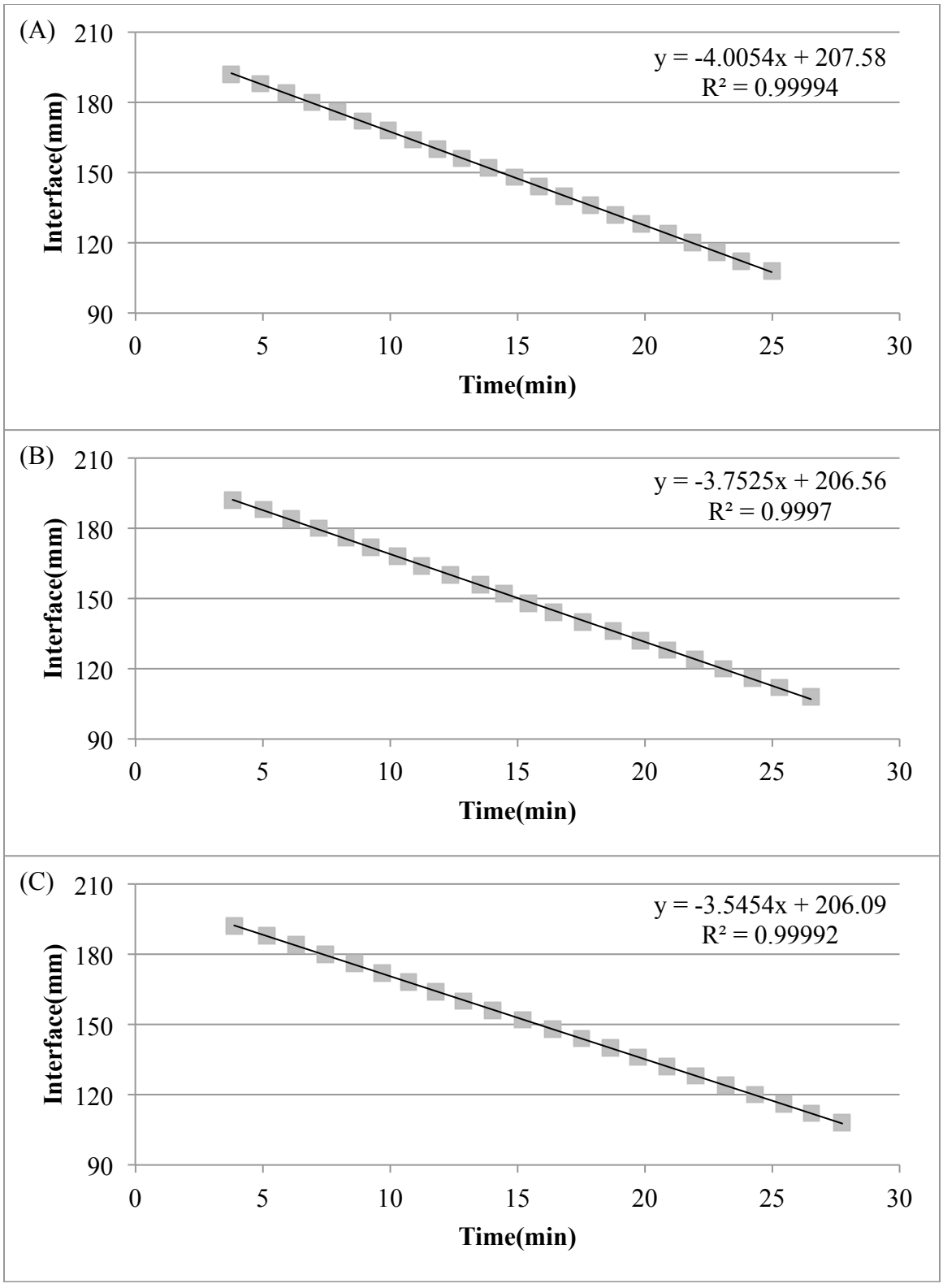

Figure 8.20 Linear plot for the fall of the interface against time for 25 Gm dry powder magnesium hydroxide suspensions in 0.01% (w/v) CMC.
(Experiment in triplicate A, B and C)

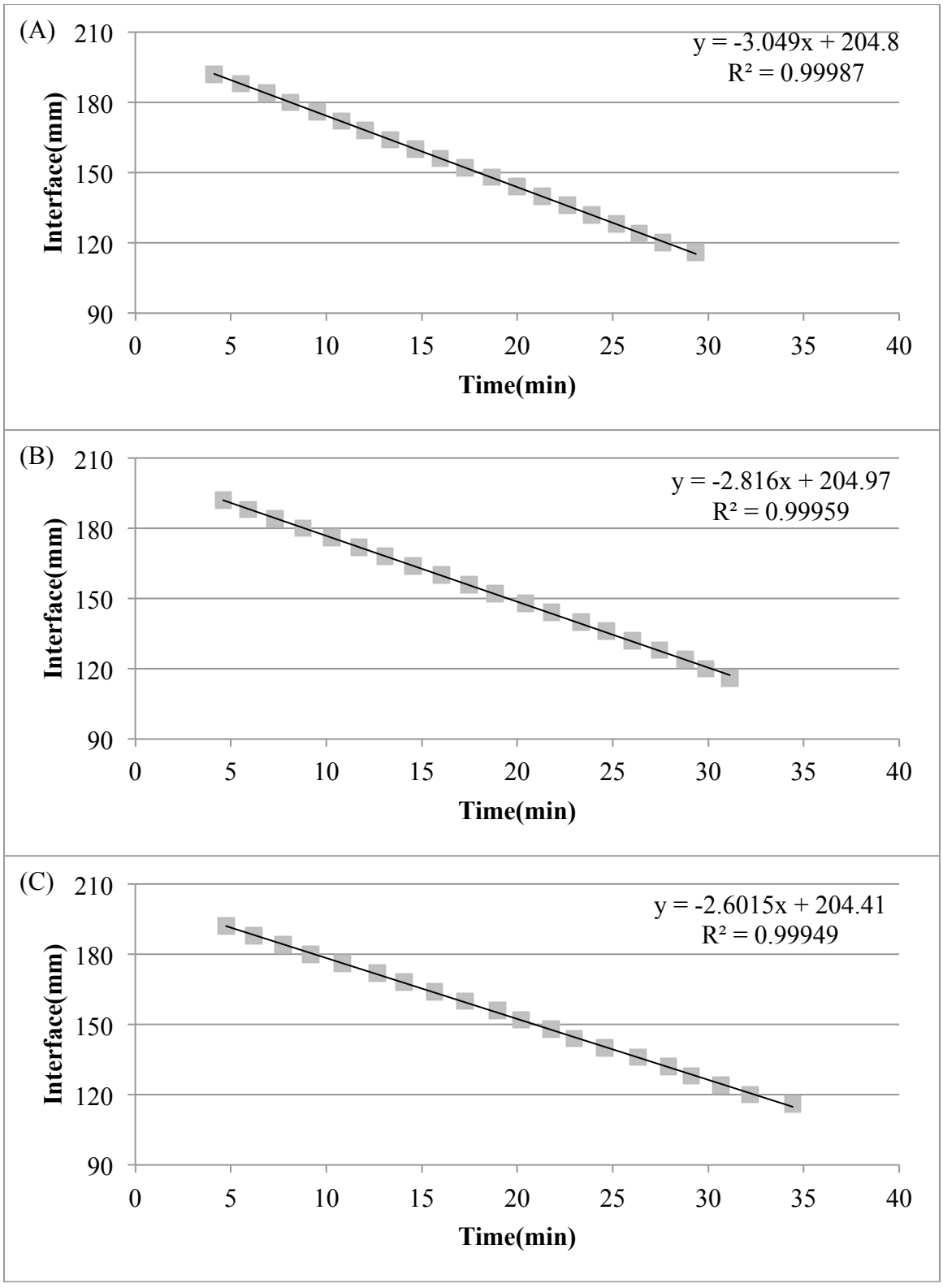

Figure 8.21 Linear plots for the fall of the interface against time for 30 Gm dry powder magnesium hydroxide suspensions in 0.01% (w/v) CMC.
(Experiment in triplicate A, B and C)

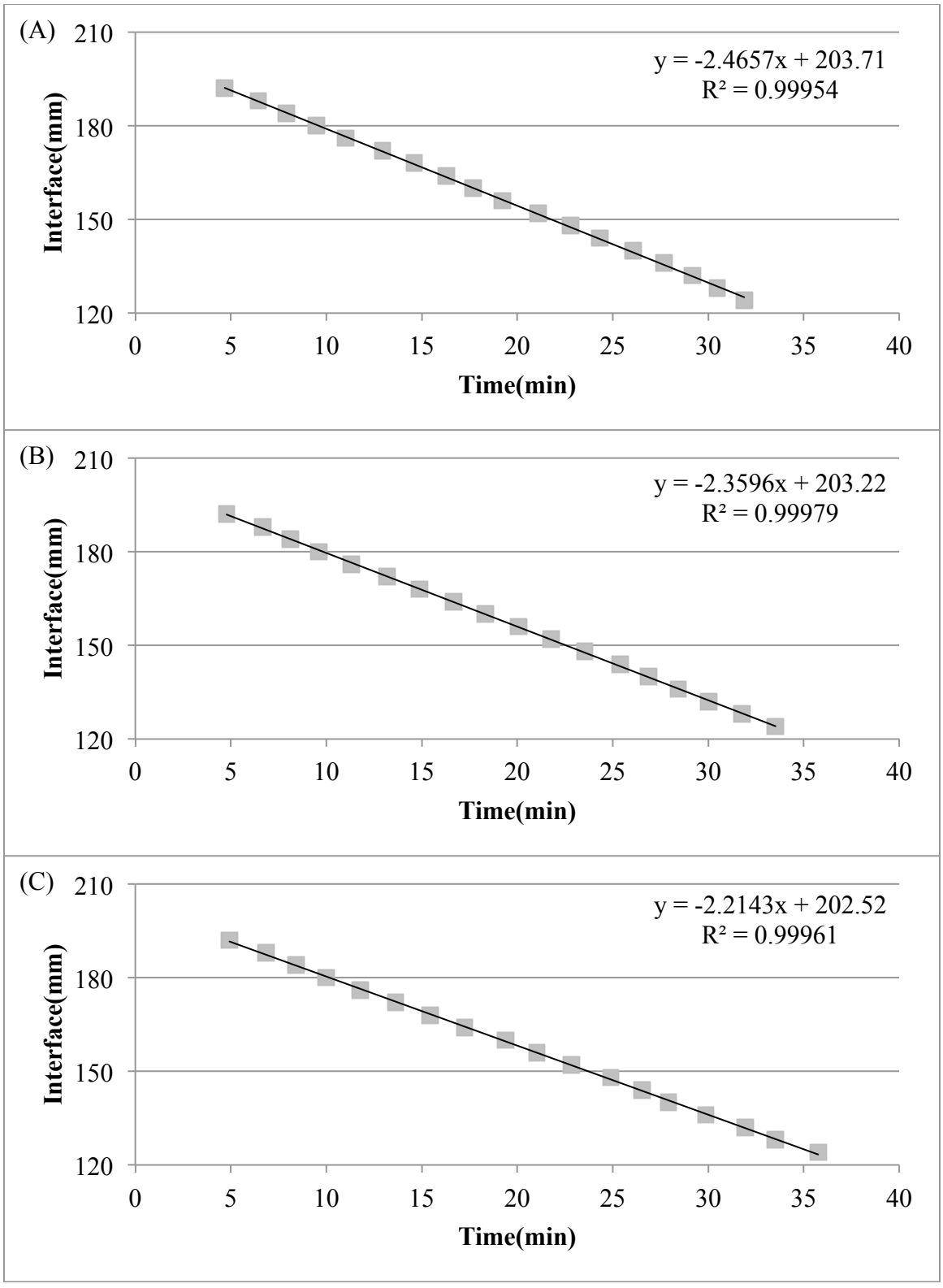

Figure 8.22 Linear plot for the fall of the interface against time for 35 Gm dry powder magnesium hydroxide suspensions in 0.01% (w/v) CMC.
(Experiment in triplicate A, B and C)

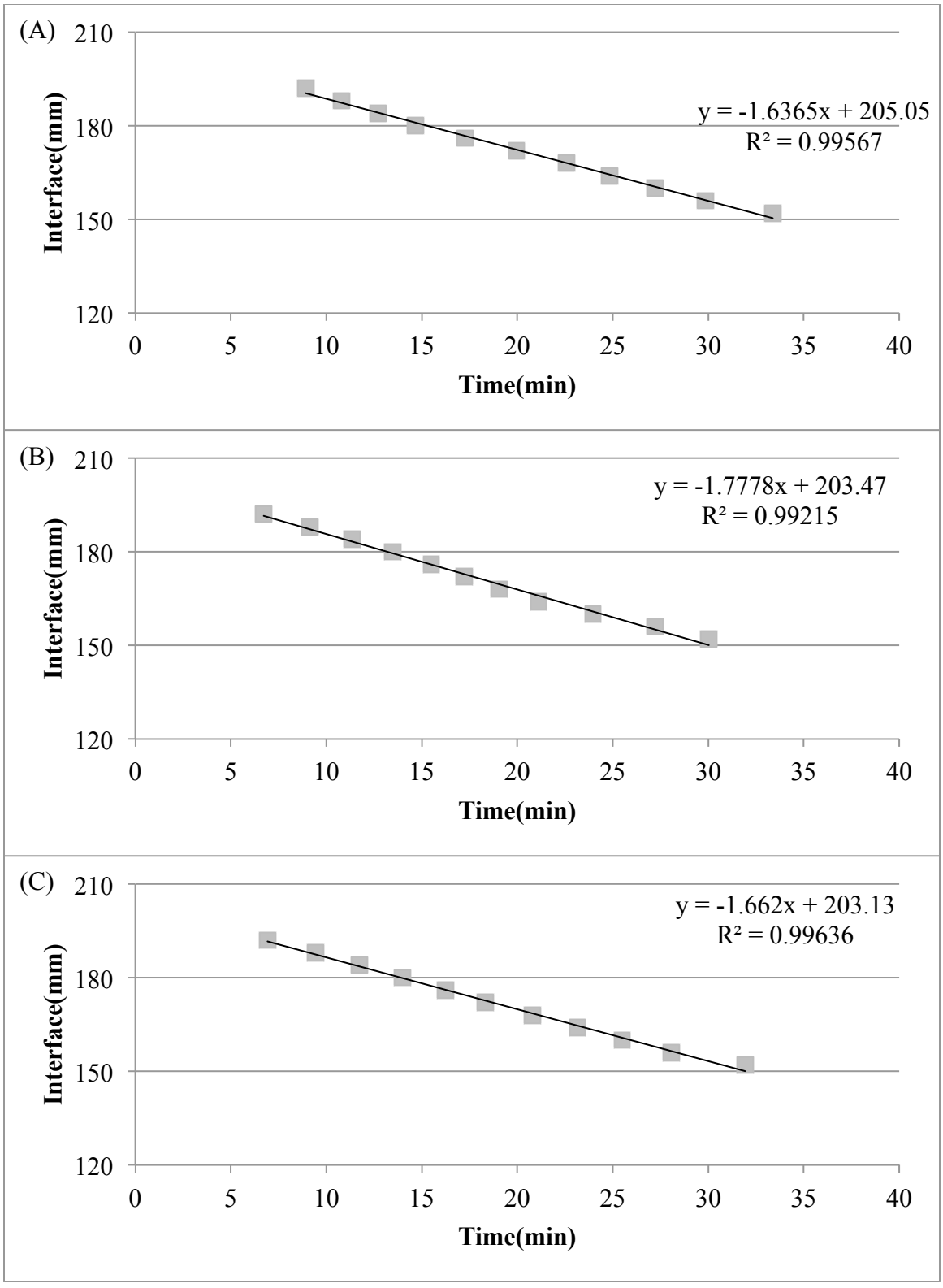

Figure 8.23 Linear plot for the fall of the interface against time for 40 Gm dry powder magnesium hydroxide suspensions in 0.01% (w/v) CMC.
(Experiment in triplicate A, B and C)

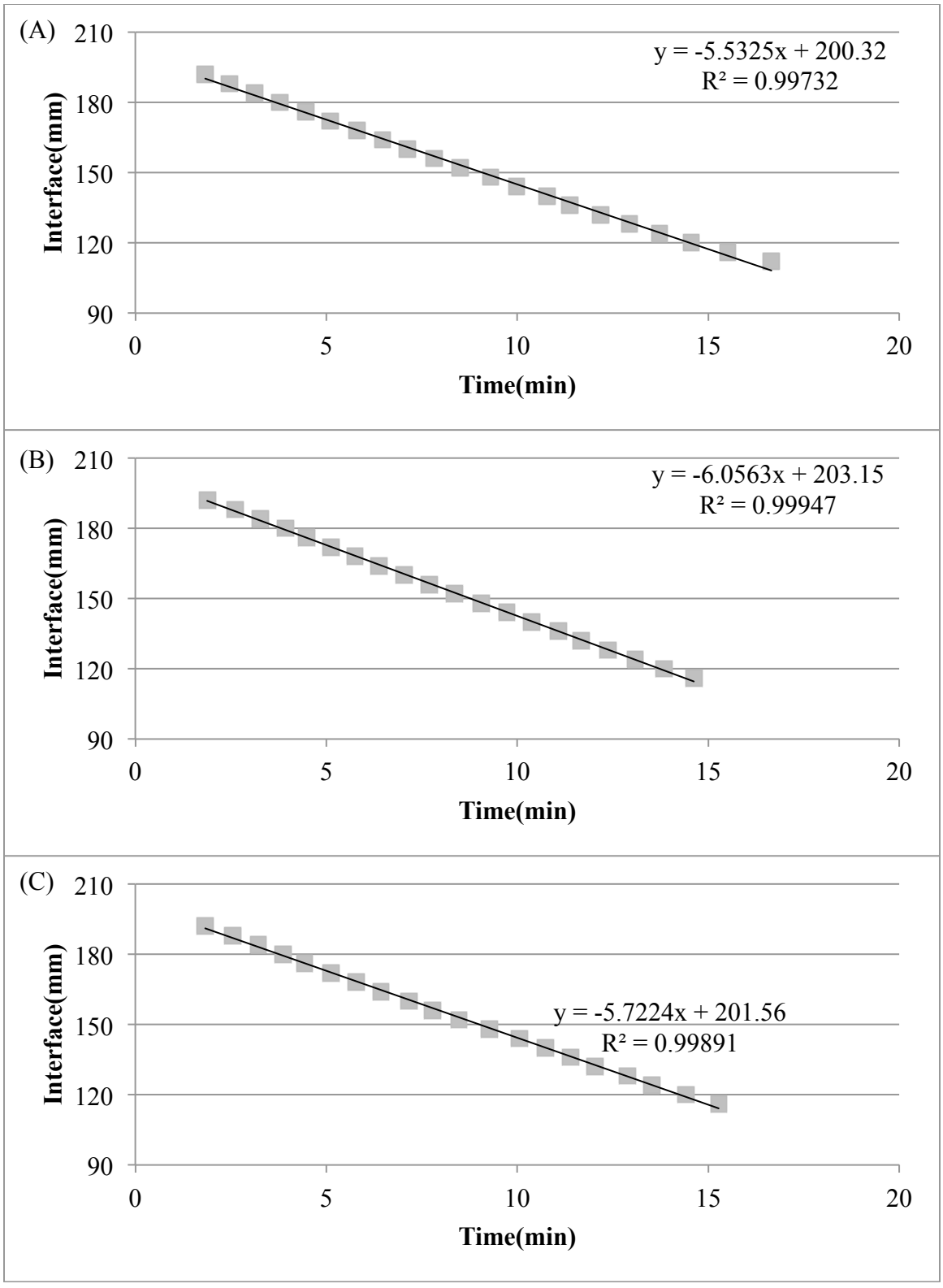

Figure 8.24 Linear plot for the fall of the interface against time for 20 Gm dry powder magnesium hydroxide suspensions in 0.02% (w/v) CMC.
(Experiment in triplicate A, B and C)

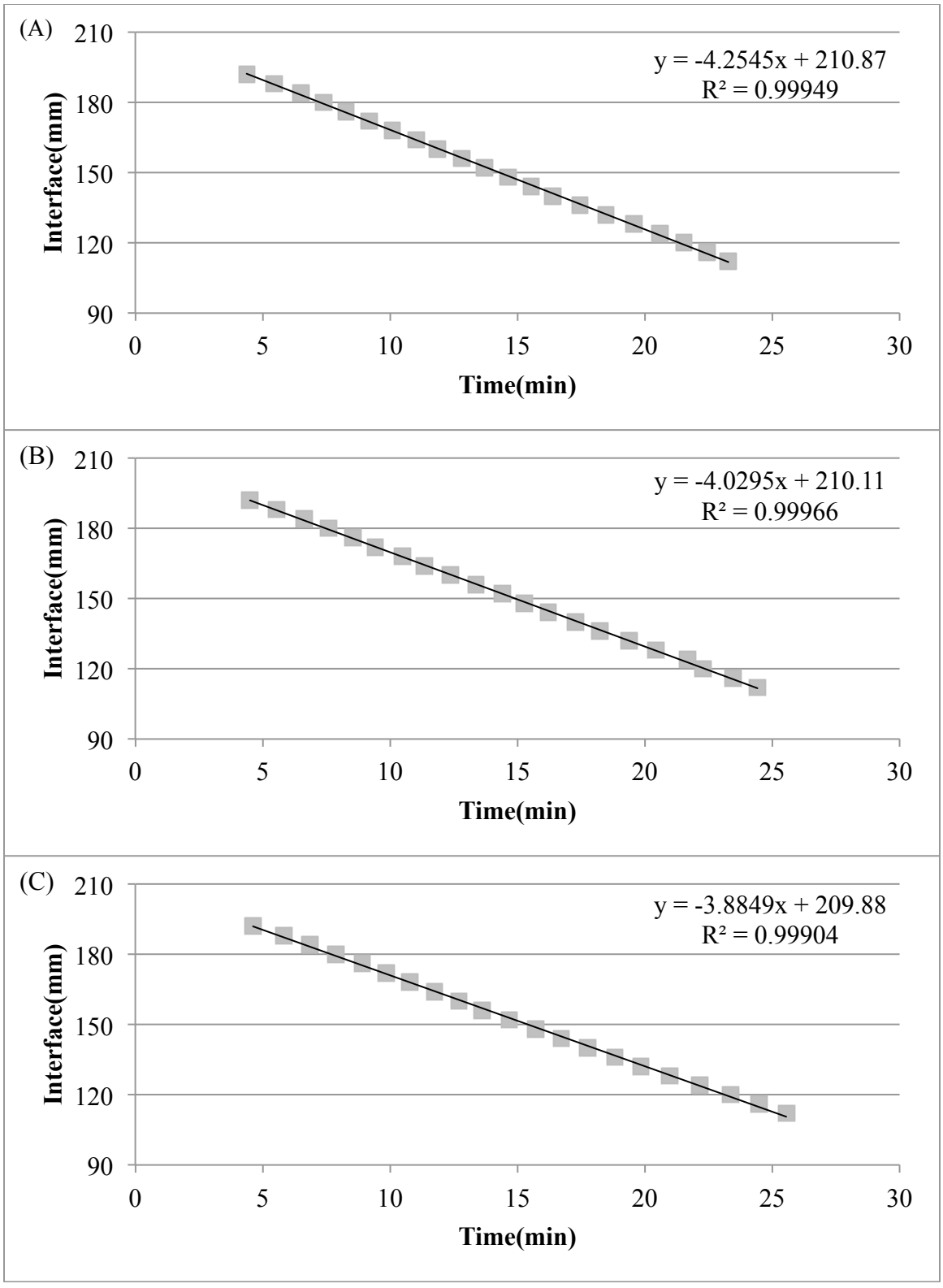

Figure 8.25 Linear plot for the fall of the interface against time for 25 Gm dry powder magnesium hydroxide suspensions in 0.02% (w/v) CMC.
(Experiment in triplicate A, B and C)

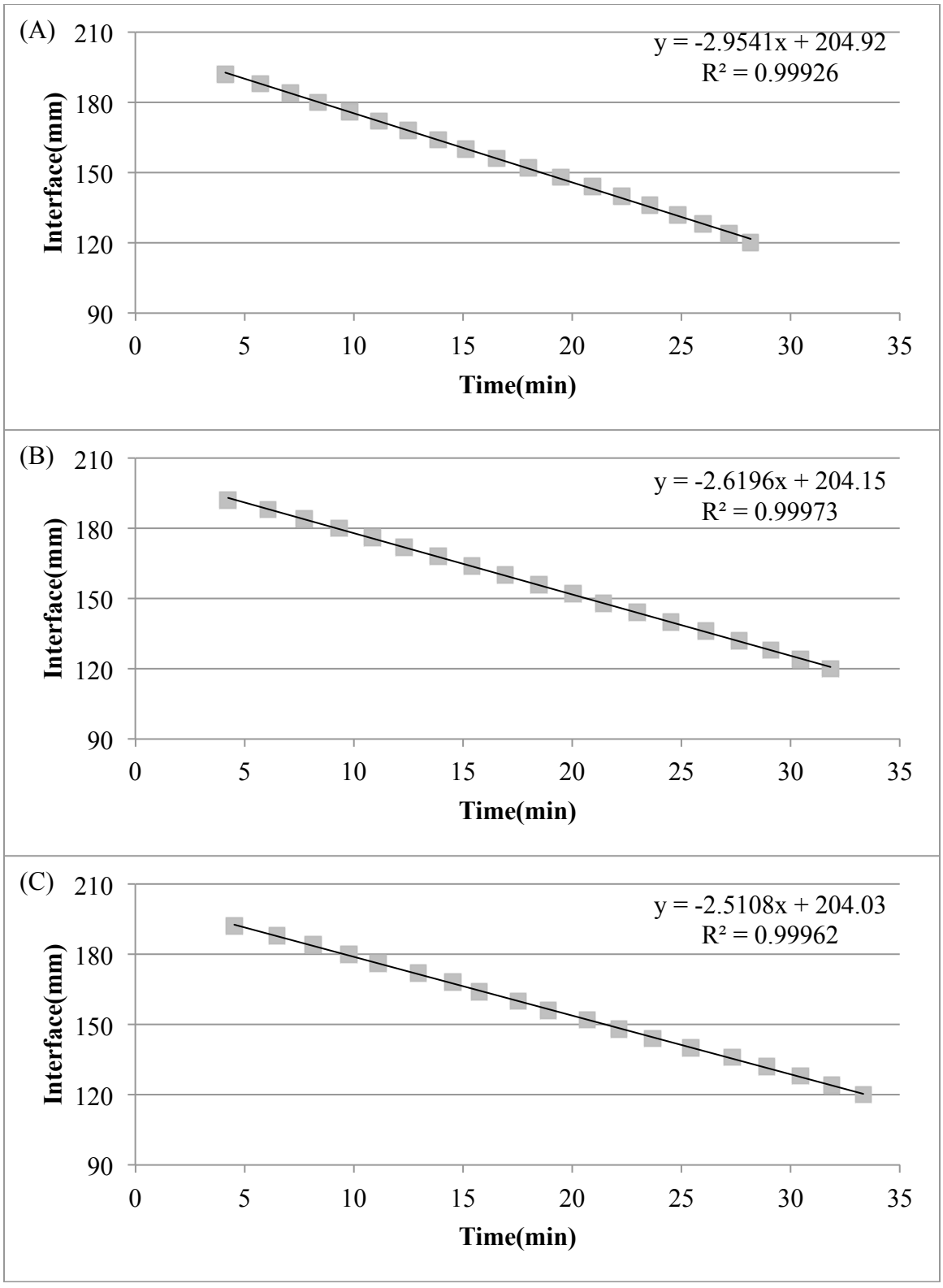

Figure 8.26 Linear plot for the fall of the interface against time for 30 Gm dry powder magnesium hydroxide suspensions in 0.02% (w/v) CMC.
(Experiment in triplicate A, B and C)

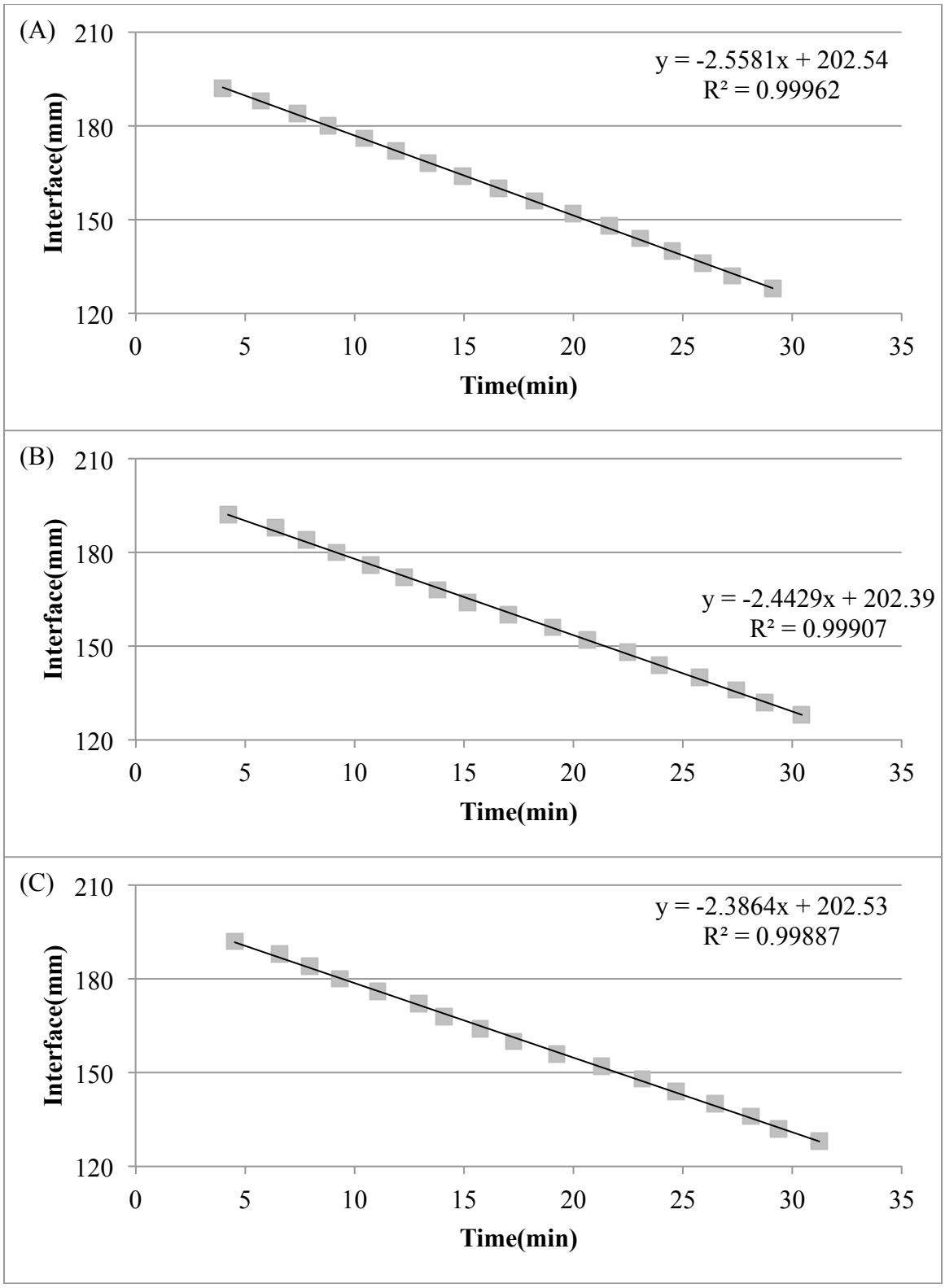

Figure 8.27 Linear plot for the fall of the interface against time for 35 Gm dry powder magnesium hydroxide suspensions in 0.02% (w/v) CMC.
(Experiment in triplicate A, B and C)

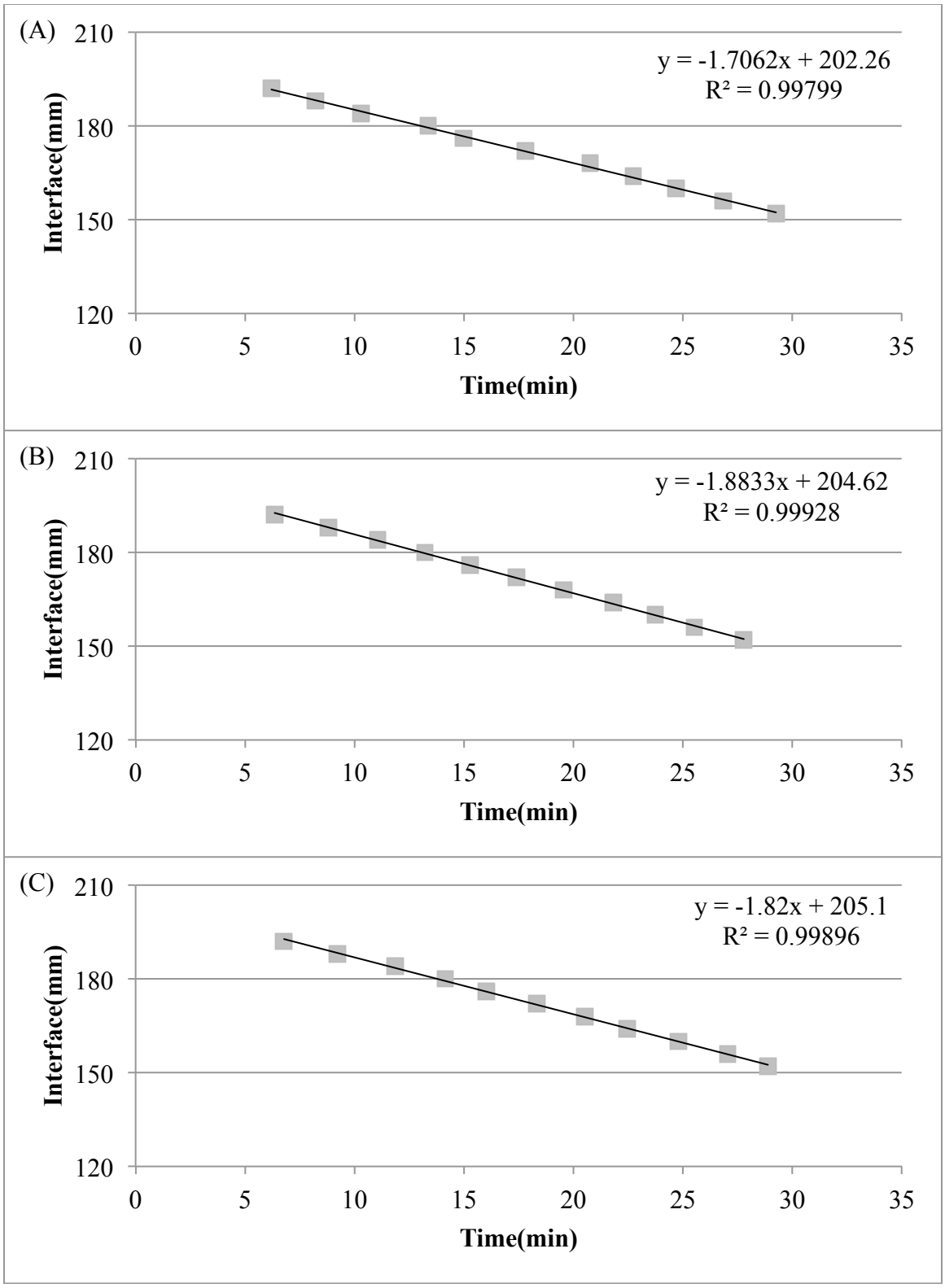

Figure 8.28 Linear plot for the fall of the interface against time for 40 Gm dry powder magnesium hydroxide suspensions in 0.02% (w/v) CMC.
(Experiment in triplicate A, B and C)

Table 8.4 Sedimentation parameters for the various quantities of magnesium hydroxide suspensions in Purified Water USP

Weight (g)	C (g/mL)	Q_1 (mm/min)	Q_2 (mm/min)	Q_3 (mm/min)	Q_{ave} (mm/min)	SD	$\varepsilon = 1 - C/\rho_S$
20	0.100	3.5817	3.4944	3.4478	3.5080	0.0555	0.9573
25	0.125	2.7682	2.7252	2.6903	2.7279	0.0319	0.9467
30	0.150	2.1794	2.1682	2.1539	2.1672	0.0104	0.9360
35	0.175	1.3766	1.3617	1.3555	1.3646	0.0089	0.9254
40	0.200	0.9004	0.8928	0.8877	0.8936	0.0052	0.9147

Table 8.5 Sedimentation parameters for the various quantities of magnesium hydroxide suspensions in 0.005% (w/v) CMC

Weight (g)	C (g/mL)	Q_1 (mm/min)	Q_2 (mm/min)	Q_3 (mm/min)	Q_{ave} (mm/min)	SD	$\varepsilon = 1 - C/\rho_S$
20	0.100	5.3528	5.0829	4.7629	5.0662	0.2411	0.9573
25	0.125	4.5077	4.2225	3.9282	4.2195	0.2366	0.9467
30	0.150	3.1426	3.0368	2.8781	3.0192	0.1087	0.9360
35	0.175	2.6427	2.5359	2.4120	2.5302	0.0943	0.9254
40	0.200	1.4892	1.5933	1.5573	1.5466	0.0432	0.9147

Table 8.6 Sedimentation parameters for the various quantities of magnesium hydroxide suspensions in 0.01% (w/v) CMC

Weight (g)	C (g/mL)	Q_1 (mm/min)	Q_2 (mm/min)	Q_3 (mm/min)	Q_{ave} (mm/min)	SD	$\varepsilon = 1 - C/\rho_S$
20	0.100	5.2387	5.4394	4.8226	5.1669	0.2569	0.9573
25	0.125	4.0054	3.7525	3.5454	3.7678	0.1881	0.9467
30	0.150	3.0490	2.8160	2.6015	2.8222	0.1827	0.9360
35	0.175	2.4657	2.3596	2.2143	2.3465	0.1030	0.9254
40	0.200	1.5802	1.7778	1.6620	1.6733	0.0811	0.9147

Table 8.7 Sedimentation parameters for the various quantities of magnesium hydroxide suspensions in 0.02% (w/v) CMC

Weight (g)	C (g/mL)	Q_1 (mm/min)	Q_2 (mm/min)	Q_3 (mm/min)	Q_{ave} (mm/min)	SD	$\varepsilon = 1 - C/\rho_S$
20	0.100	5.5325	6.0563	5.7224	5.7704	0.2165	0.9573
25	0.125	4.2545	4.0295	3.8849	4.0563	0.1521	0.9467
30	0.150	2.9541	2.6196	2.5108	2.6948	0.1886	0.9360
35	0.175	2.5581	2.4429	2.3864	2.4625	0.0714	0.9254
40	0.200	1.7062	1.8833	1.8200	1.8032	0.0733	0.9147

The results from the hindered settling experiments showed that with increasing in amount of dry powder, or an increase in the concentration, a slower rate of fall of the interface was observed. This was true for all four media. This was due to the inherent nature of hindered settling, where as increase in the concentration made the hindrance by the particles on the falling path more severe.

It was obvious that for a given concentration of solid, the addition of CMC increased the rate of fall of the interface ((Q) value). This may be explained by the flocculating effect of the CMC polymer. The degree of flocculation was increased with increasing polymer concentration, which made the rate of settling more rapid.

The triplicate experiments, after 24 hours, showed a slight decrease in the rate of fall of the interface ((Q) value). This phenomenon may be explained by the wetting process of the magnesium hydroxide dry powder. After 24 hours of initial wetting without any disturbance, the powder was wetted to some extent, however, after the settling experiments, when the powder was left to be contact with the media for an extended time, it made a further and deeper wetting possible, and the hindered settling results were affected to some extent.

However, for the 20% (w/v), or 40 Gm/ 200 mL, magnesium hydroxide suspensions in a

media of CMC solutions, this may not be totally correct. The initial wetting process took longer time to obtain an interpretable linearity compared to that in Purified Water USP, namely 48 hours instead of 24 hours. There was an increased (Q) value 24 hours after the first reading, and a decreased (Q) value 24 hours after the second reading. This may due to the addition of the polymers.

The flocculating and binding effects of CMC made the wetting process more difficult to be completely uniform under such a high solids concentration. A possible explanation could be as follows: the naturally flocculated suspensions were undisturbed during this wetting process; the high concentration of solid caused the wetting of all solids to be only partially completed before the first settling reading; the wetting then processed during the first reading caused all solids was wetted to a similar extent; therefore only the second and the third readings showed the same phenomenon as the other concentrations.

8.1.2.3 Determination of the Particle Size Using Steinour's, Richardson and Zaki's, and Dollimore and McBride's Equations

As discussed in Chapter 2 Section 2.4, there are three modified equations which can be used to correlate the observed rate of fall of the interface ((Q) value) with the Stokes' law limiting velocity (V_s). The later was then used to determine the particle size by Stokes' law.

These three equations can be summarized as follows:

1) Steinour's equation:

$$Log\left(\frac{Q}{\varepsilon^2}\right) = A\epsilon - (LogV_s - A) \qquad \text{Eqn. 2.21}$$

A plot of $\left[Log\left(\frac{Q}{\varepsilon^2}\right)\right]$ against (ε) should be linear and provide data for (V_s) from the slope and intercept.

2) Richardson and Zaki's equation:

$$LogQ = nLog\varepsilon + LogV_s \qquad \text{Eqn. 2.24}$$

A plot of $[LogQ]$ against $[Log\varepsilon]$ should be linear and provide data for (V_s) from the intercept.

3) Dollimore and McBride's equation:

$$LogQ = LogV_s - b\rho_s(1-\varepsilon) \qquad \text{Eqn. 2.42}$$

A plot of $[LogQ]$ against (1-ε) should be linear and provide data for (V_s) from the intercept.

The average (Q) and (ε) values from the linear plots in Section 8.1.2.2 were then used to calculate the parameters, as see in Tables 8.8 to 8.11. The linear plots the equations are given in Figures 8.29 to 8.40.

Table 8.8 The parameters for plotting the equations for the various concentrations of magnesium hydroxide suspensions in Purified Water USP

C (g/mL)	Q_{ave} (mm/min)	ε	1-ε	logε	logQ	$\log(Q/\varepsilon^2)$
0.100	3.5080	0.95735	0.04265	-0.01893	0.54506	0.58292
0.125	2.7279	0.94669	0.05331	-0.02379	0.43583	0.48342
0.150	2.1672	0.93602	0.06398	-0.02871	0.33589	0.39332
0.175	1.3646	0.92536	0.07464	-0.03369	0.13501	0.20238
0.200	0.8936	0.91470	0.08530	-0.03872	-0.04884	0.02860

Table 8.9 The parameters for plotting the equations for the various concentrations of magnesium hydroxide suspensions in 0.005% (w/v) CMC

C (g/mL)	Q_{ave} (mm/min)	ε	1-ε	logε	logQ	$\log(Q/\varepsilon^2)$
0.100	5.0662	0.95735	0.04265	-0.01893	0.70468	0.74254
0.125	4.2195	0.94669	0.05331	-0.02379	0.62526	0.67285
0.150	3.0192	0.93602	0.06398	-0.02871	0.47989	0.53731
0.175	2.5302	0.92536	0.07464	-0.03369	0.40315	0.47053
0.200	1.5466	0.91470	0.08530	-0.03872	0.18938	0.26682

Table 8.10 The parameters for plotting the equations of the various concentrations of magnesium hydroxide suspensions in 0.01% (w/v) CMC

C (g/mL)	Q_{ave} (mm/min)	ε	1-ε	logε	logQ	log(Q/ε^2)
0.100	5.1669	0.95735	0.04265	-0.01893	0.71323	0.75109
0.125	3.7678	0.94669	0.05331	-0.02379	0.57608	0.62367
0.150	2.8222	0.93602	0.06398	-0.02871	0.45058	0.50801
0.175	2.3465	0.92536	0.07464	-0.03369	0.37043	0.43780
0.200	1.6733	0.91470	0.08530	-0.03872	0.22358	0.30103

Table 8.11 The parameters for plotting the equations of the various concentrations of magnesium hydroxide suspensions in 0.02% (w/v) CMC

C (g/mL)	Q_{ave} (mm/min)	ε	1-ε	logε	logQ	log(Q/ε^2)
0.100	5.7704	0.95735	0.04265	-0.01893	0.76121	0.79907
0.125	4.0563	0.94669	0.05331	-0.02379	0.60813	0.65572
0.150	2.6948	0.93602	0.06398	-0.02871	0.43053	0.48796
0.175	2.4625	0.92536	0.07464	-0.03369	0.39137	0.45875
0.200	1.8032	0.91470	0.08530	-0.03872	0.25604	0.33348

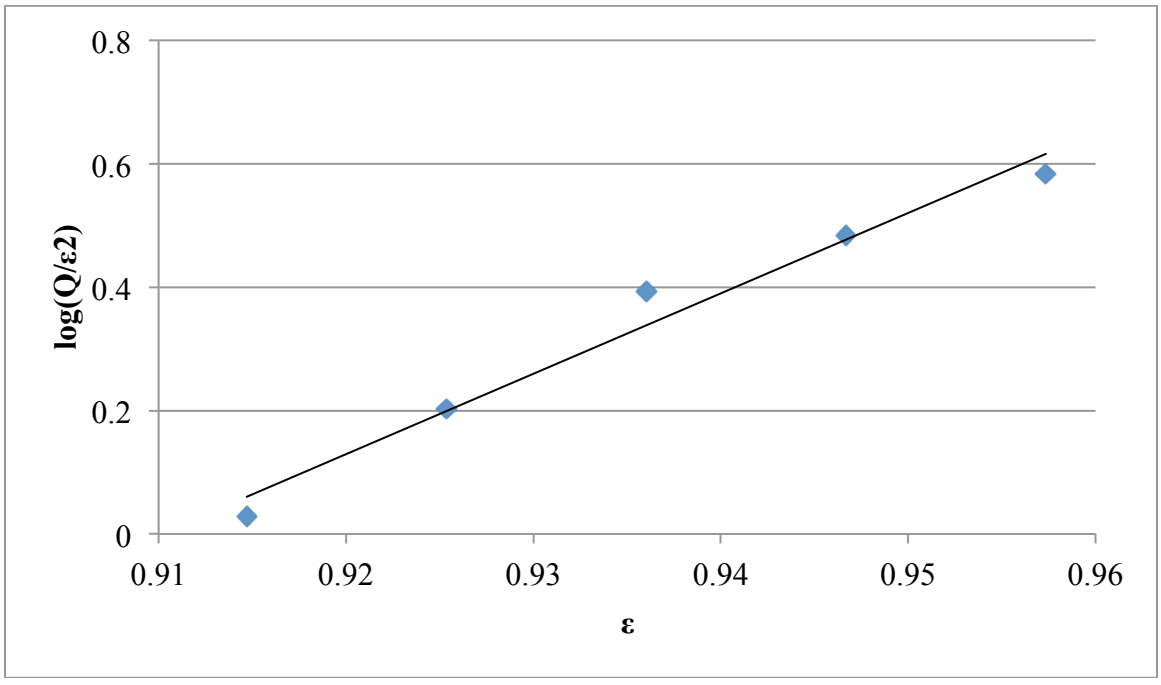

Figure 8.29 The linear plot for Steinour's equation for the suspensions in Purified Water USP where the slope = 13.033 and R^2 = 0.97381.

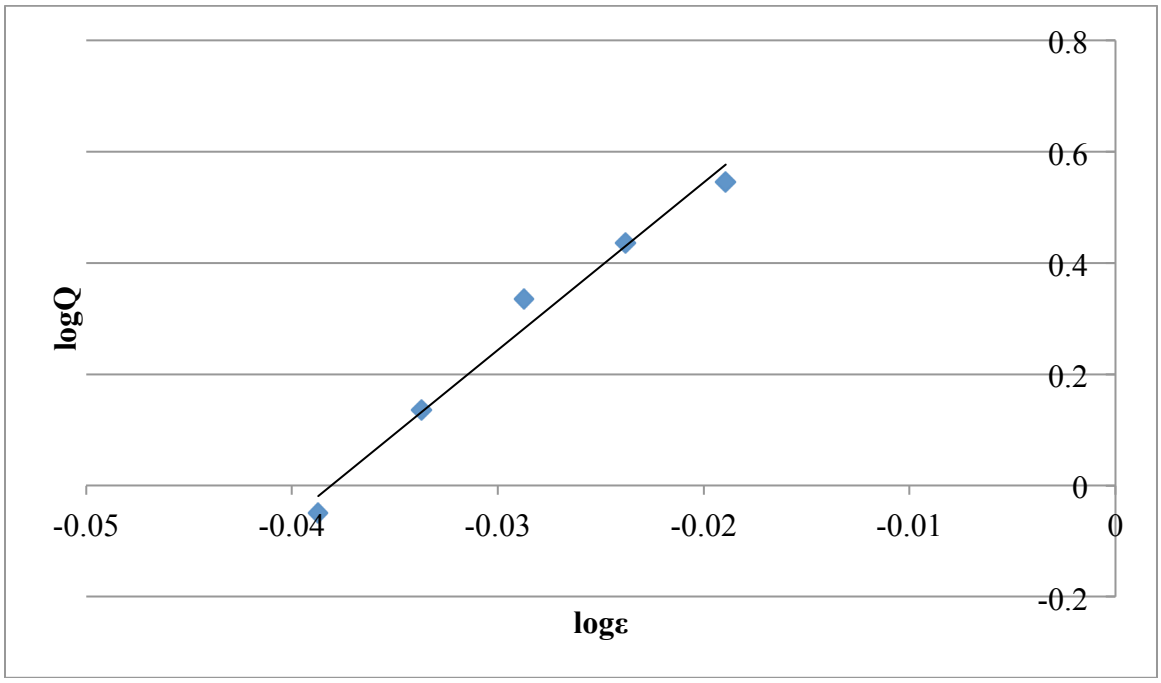

Figure 8.30 The linear plot for Richardson and Zaki's equation for the suspensions in Purified Water USP where slope = 30.112 and R^2 = 0.97881.

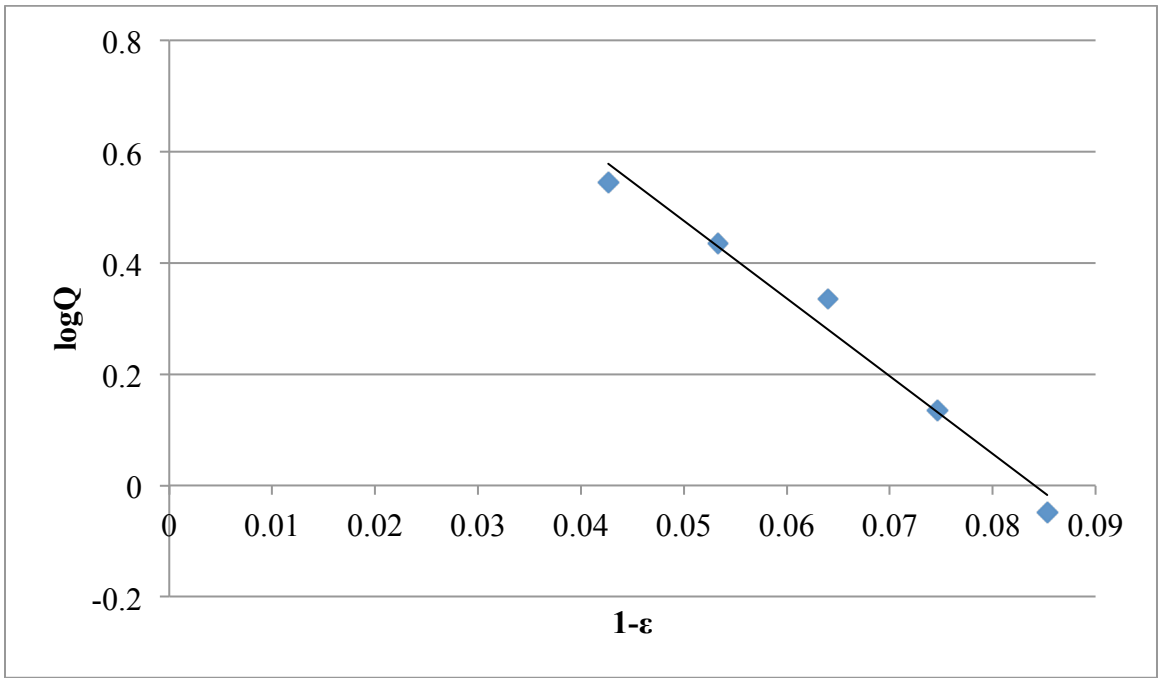

Figure 8.31 The linear plot for Dollimore and McBride's equation for the suspensions in Purified Water USP where slope = -13.961 and R^2 = 0.97698.

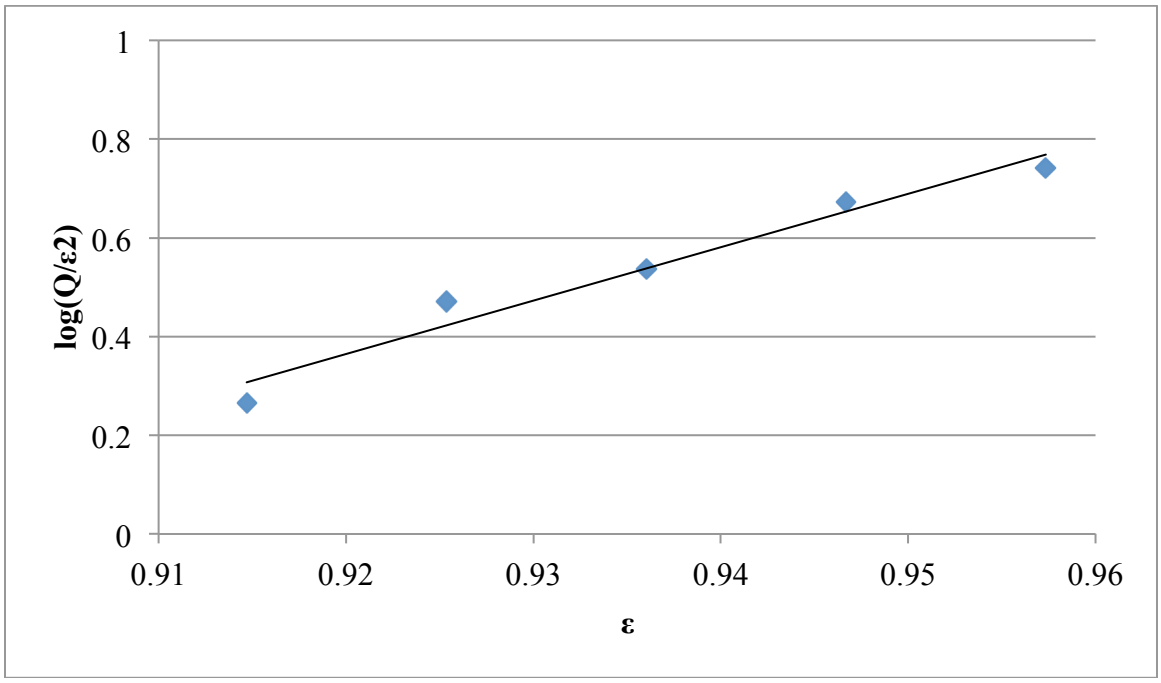

Figure 8.32 The linear plot for the Steinour's equation for the suspensions in 0.005% (w/v) CMC where slope = 10.82 and R^2 = 0.96383.

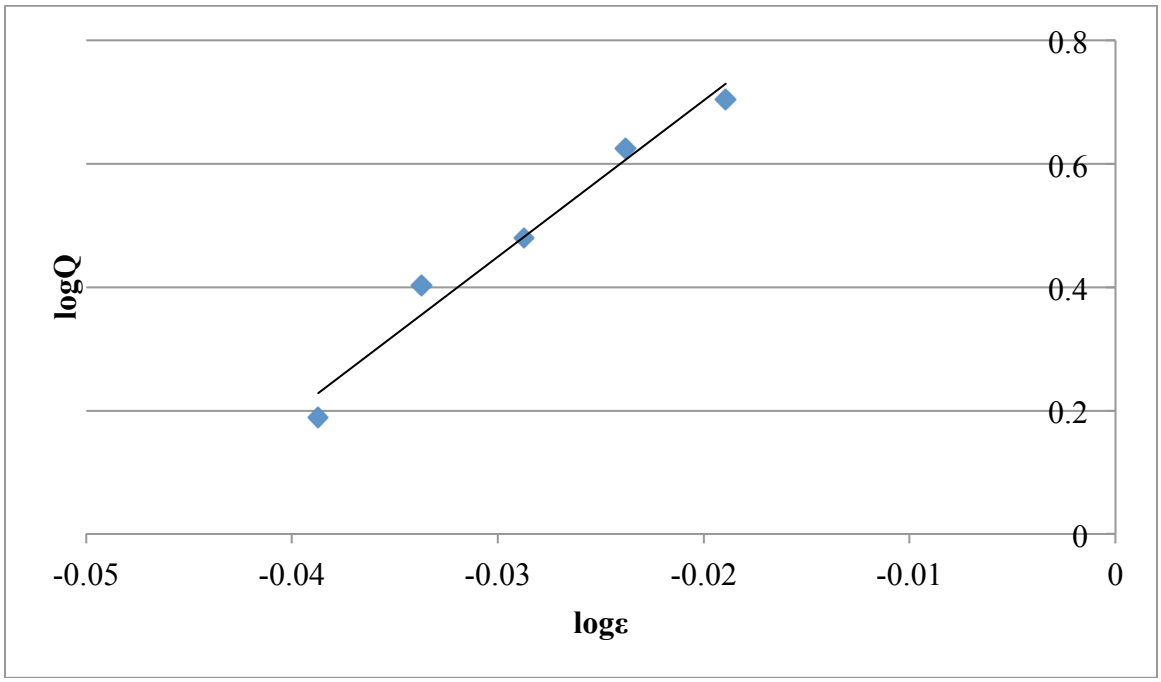

Figure 8.33 The linear plot for Richardson and Zaki's equation for the suspensions in 0.005% (w/v) CMC where slope = 25.339 and R^2 = 0.97074.

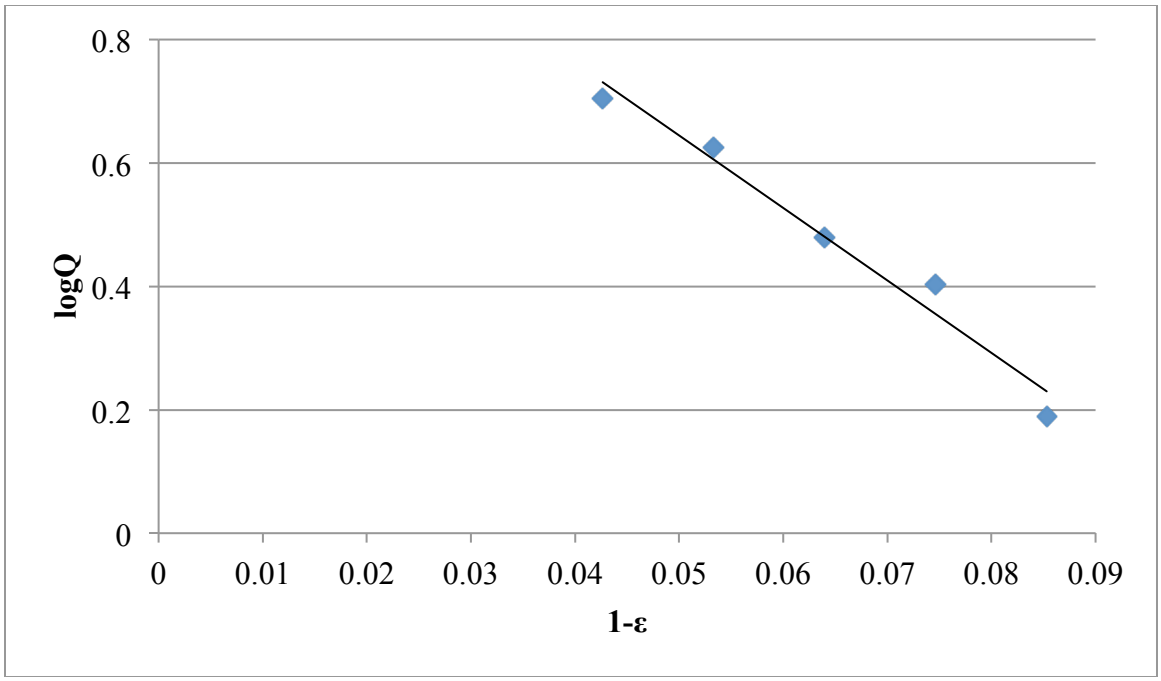

Figure 8.34 The linear plot for Dollimore and McBride's equation of suspensions in 0.005% (w/v) CMC where slope = -11.748 and R^2 = 0.96901.

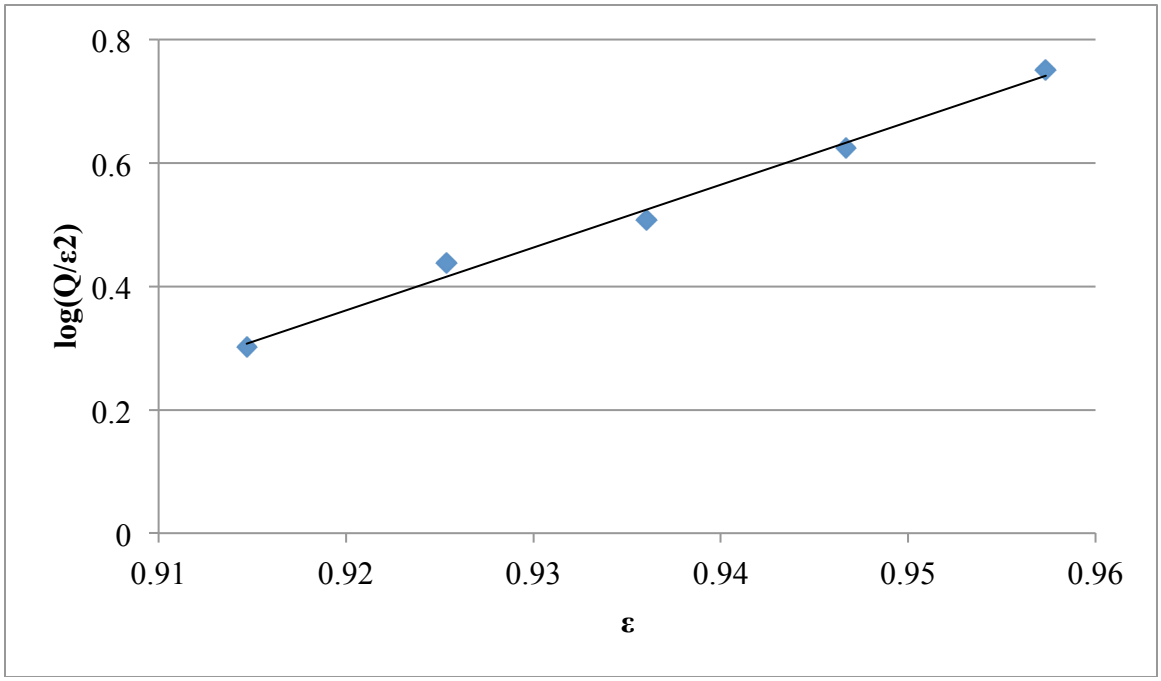

Figure 8.35 The linear plot for Steinour's equation of suspensions in 0.01% (w/v) CMC where slope = 10.185 and R^2 = 0.99186.

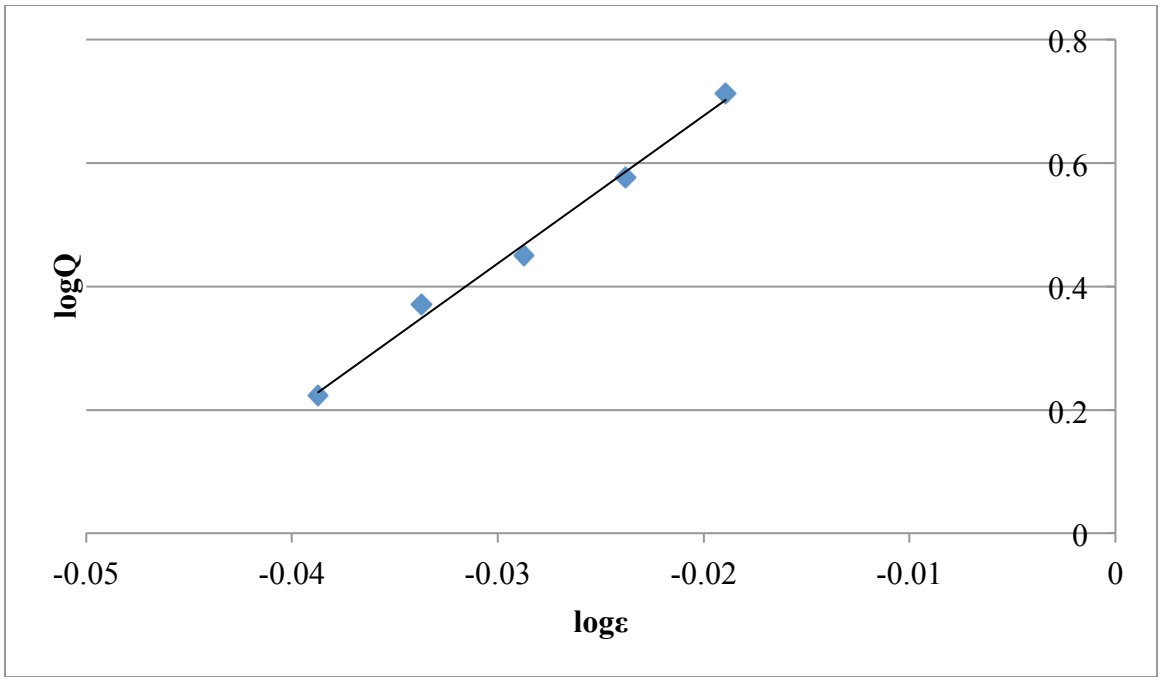

Figure 8.36 The linear plot for Richardson and Zaki's equation of suspensions in 0.01% (w/v) CMC where slope = 23.944 and R^2 = 0.99289.

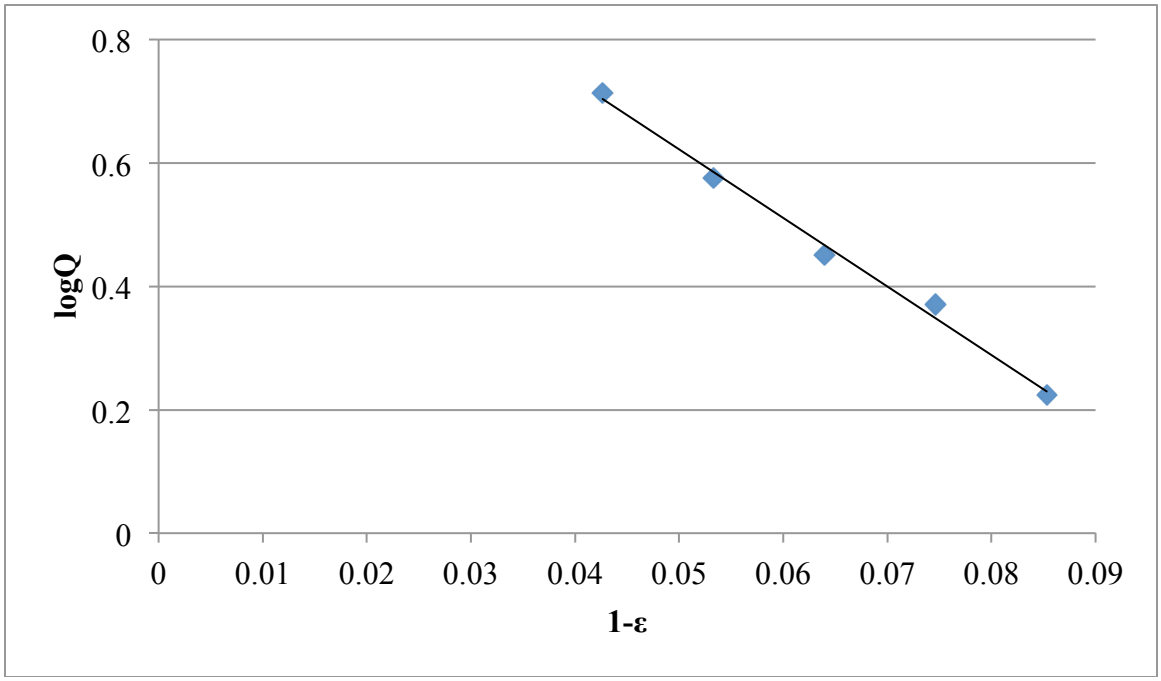

Figure 8.37 The linear plot for Dollimore and McBride's equation of suspensions in 0.01% (w/v) CMC where slope = -11.113 and R^2 = 0.99317.

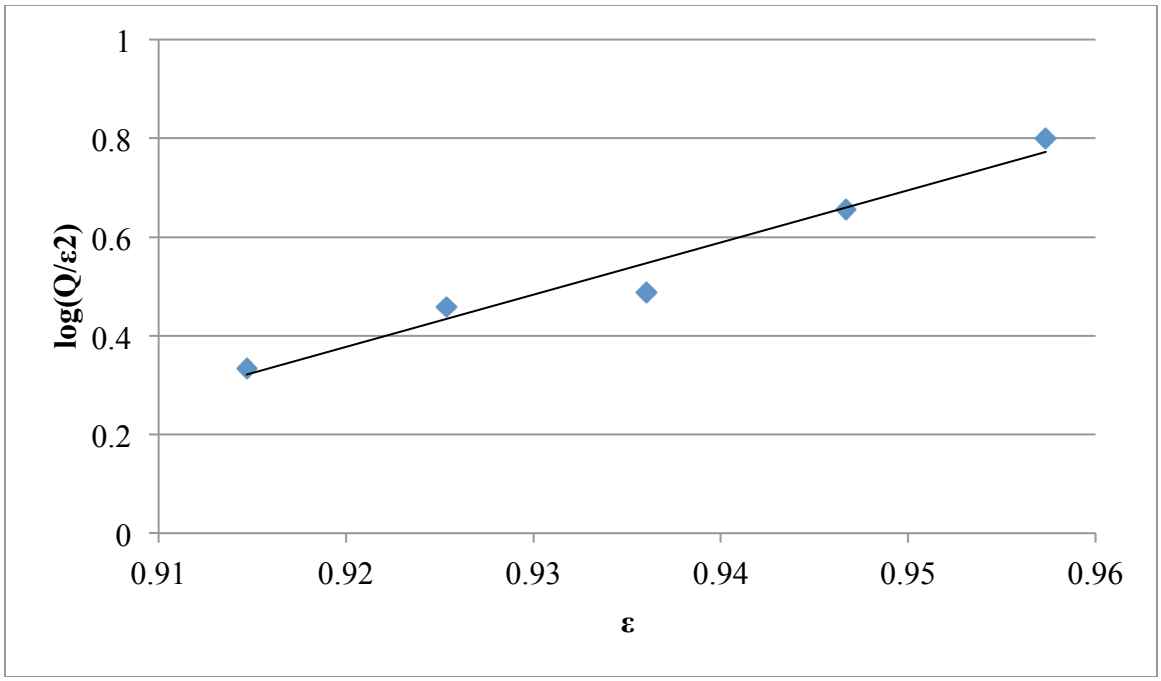

Figure 8.38 The linear plot for Steinour's equation of suspensions in 0.005% (w/v) CMC where slope = 10.58 and R^2 = 0.96255.

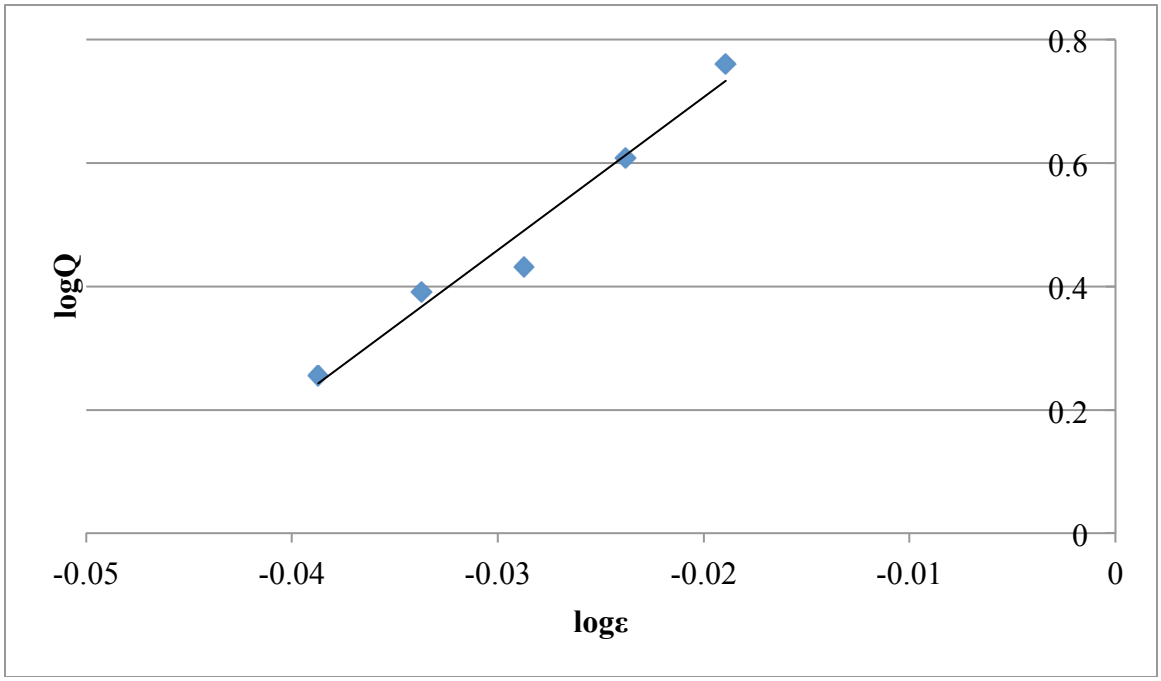

Figure 8.39 The linear plot for Richardson and Zaki's equation of suspensions in 0.02% (w/v) CMC where slope = 24.779 and R^2 = 0.96668.

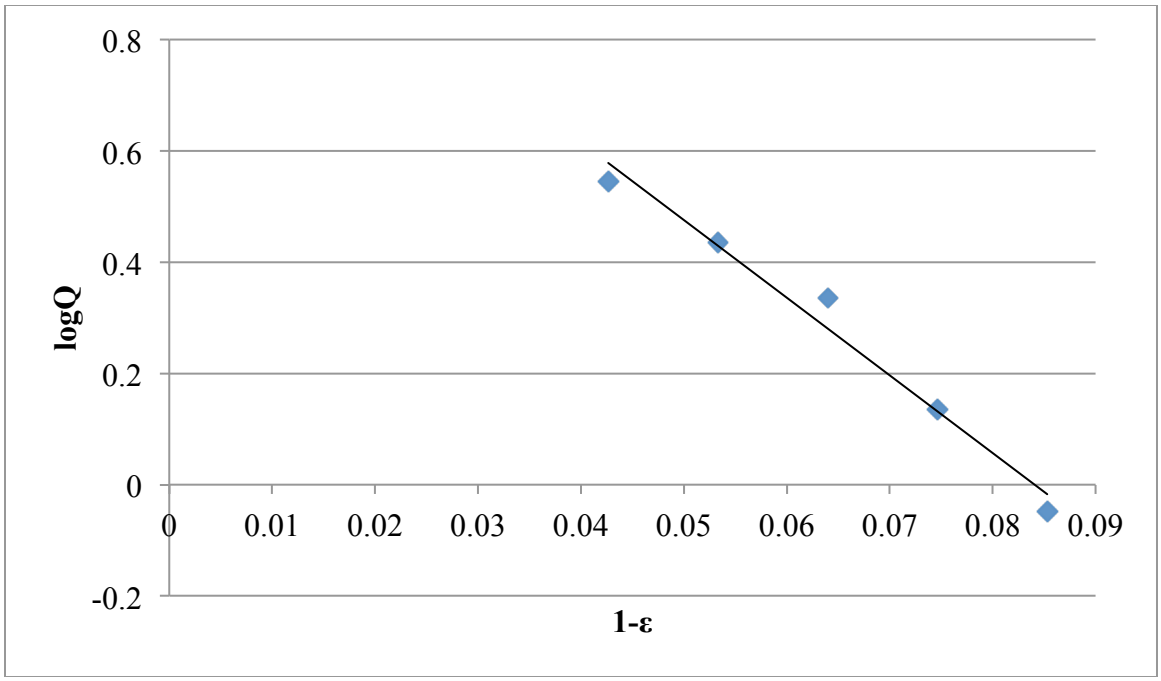

Figure 8.40 The linear plot of Dollimore and McBride's equation of suspensions in 0.02% (w/v) CMC where slope = -13.961 and R^2 = 0.97698.

The parameters obtained from the linear plots are summarized in Table 8.12, and the parameters for the equations in each media are given in Table 8.13. It was obvious from Table 8.12 that the plots all showed good linearity.

Table 8.12 The parameters summarized from linear plots in each media

Equations		Water	0.005% CMC	0.01% CMC	0.02% CMC
Steinour	Slope	13.022	10.82	10.185	10.58
	Intercept	-11.861	-9.5901	-9.0089	-9.3563
	R^2	0.97381	0.96383	0.99186	0.96255
Richardson & Zaki	Slope	30.112	25.339	23.944	24.779
	Intercept	1.1469	1.2095	1.1556	1.2023
	R^2	0.97881	0.97074	0.99289	0.96668
Dollimore & McBride	Slope	-13.961	-11.748	-11.113	-13.961
	Intercept	1.1738	1.2321	1.1778	1.1738
	R^2	0.97698	0.96901	0.99317	0.97698

Table 8.13 The parameters obtained from the linear plots for the equations in each media

Equation	Parameter	Water	0.005%CMC	0.01%CMC	0.02%CMC
Steinour	A	13.033	10.82	10.185	10.58
	Log V_s -A	-11.861	-9.5901	-9.0089	-9.3563
	Log V_s	1.172	1.2299	1.1761	1.2237
	V_s (mm/min)	14.8594	16.9785	15.0003	16.7379
Richardson & Zaki	n	30.112	25.339	23.944	24.779
	Log V_s	1.1469	1.2095	1.1556	1.2023
	V_s (mm/min)	14.0249	16.1994	14.3087	15.9331
Dollimore & McBride	Log V_s	1.1738	1.2321	1.1778	1.2257
	V_s (mm/min)	14.9211	17.0647	15.0591	16.8151

The particle size was then calculated by Stokes' law as discussed in Chapter 2 Section 2.2 using the density and viscosity results from Section 8.1.2:

$$r = \sqrt{\frac{9\eta V_S}{2g(\rho_s - \rho_l)}} \qquad \text{Eqn. 2.6}$$

The results of particle size (r) determination for the dry powder magnesium hydroxide suspensions in each media are given in Tables 8.14 to 8.17.

Table 8.14 The mean particle size (r) for dry powder magnesium hydroxide suspensions in Purified Water USP

Equation	V_s (mm/min)	V_s (cm/s)	r (μm)
Steniour	14.8594	0.02477	9.135
Richardson & Zaki	14.0249	0.02337	8.875
Dollimore & McBride	14.9211	0.02487	9.154
Average	14.6018	0.02434	9.055

Table 8.15 The mean particle size (r) for dry powder magnesium hydroxide suspensions in 0.005% (w/v) CMC

Equation	V_s (mm/min)	V_s (cm/s)	r (μm)
Steniour	16.9785	0.02830	11.388
Richardson & Zaki	16.1994	0.02700	11.124
Dollimore & McBride	17.0647	0.02844	11.417
Average	16.7475	0.02791	11.310

Table 8.16 The mean particle size (r) for dry powder magnesium hydroxide suspensions in 0.01% (w/v) CMC

Equation	V_s (mm/min)	V_s (cm/s)	r (μm)
Steniour	15.0003	0.02500	11.829
Richardson & Zaki	14.3087	0.02385	11.553
Dollimore & McBride	15.0591	0.02510	11.852
Average	14.7894	0.02465	11.745

Table 8.17 The mean particle size (r) for dry powder magnesium hydroxide suspensions in 0.02% (w/v) CMC

Equation	V_s (mm/min)	V_s (cm/s)	r (μm)
Steniour	16.7379	0.02790	14.248
Richardson & Zaki	15.9331	0.02656	13.901
Dollimore & McBride	16.8151	0.02803	14.280
Average	16.4954	0.02749	14.143

Comparing the particle size for the dry powder magnesium hydroxide in different media, it was observed that the addition of CMC increased the particle size (r) to some extent. It was more than 25% even with a 0.005% (w/v) CMC solution. This may be explained by the flocculating mechanism effect of the polymer. The soluble polymeric material absorbed onto more than one solid particle surface because of the repeating nature of the basic monomeric unit in the polymer structure and which has a high molecular weight. This bridging effect of the polymer resulted in the formation of a loosely connected floc.

Considering the regression coefficients from the linear plots of the three equations, the linearity was quite good. It was quite obvious that the particle size obtained form Steinour's equation was more close to that from Dollimore and McBride's equation, while Richardson and Zaki's equation gave a slightly smaller value.

The "two-compartment" model was attempted to be utilized for the calculation of particle size; however, this model requires a large amount of (Q) value points, at least 10, to

obtain a precise estimation of the linearity of the two compartments, which in this case was impossible due to the change in the sedimentation tendency as discussed in Section 8.1.2.2.

The calculated particle size from the above equations was smaller compared to the sieving results of dry powder from Section 8.1.1, which was 363.83 μm for the mean particle size (radius). This was about 40 times that of the calculated particle size (r) for the suspension in Purified Water USP, and at least 25 times that in CMC solutions. The inconsistency of particle sizes would be further discussed in later sections.

8.1.3 Scanning Electron Microscopy (SEM) Results

SEM was preformed using the method provided in Chapter 7 Section 7.4.3. Both the dry powder magnesium hydroxide and dried suspensions in various media were imaged by SEM, as seen in Figures 8.41 to 8.45.

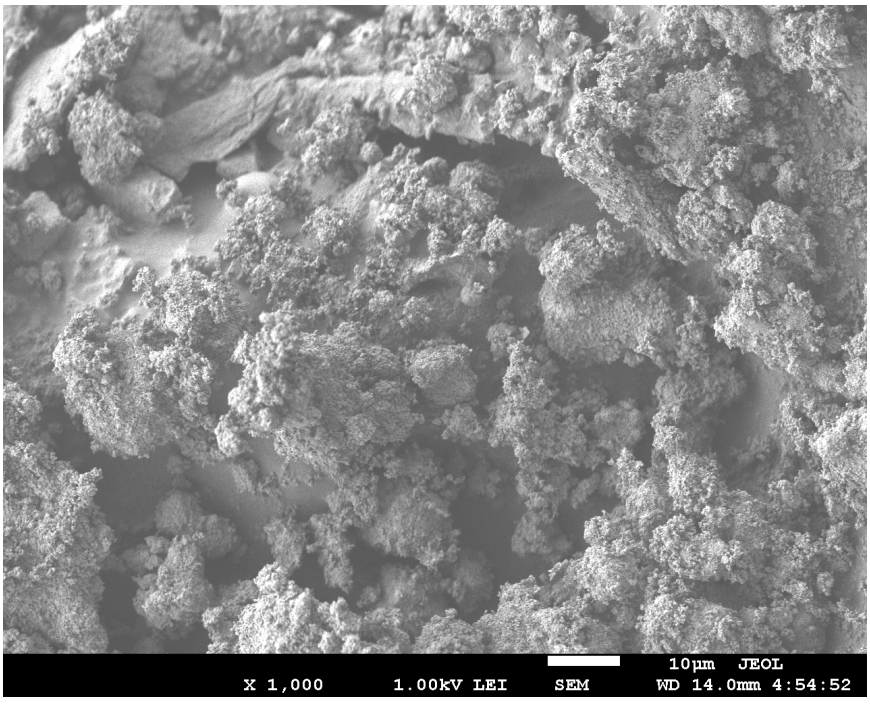

Figure 8.41 SEM image for dry powder magnesium hydroxide

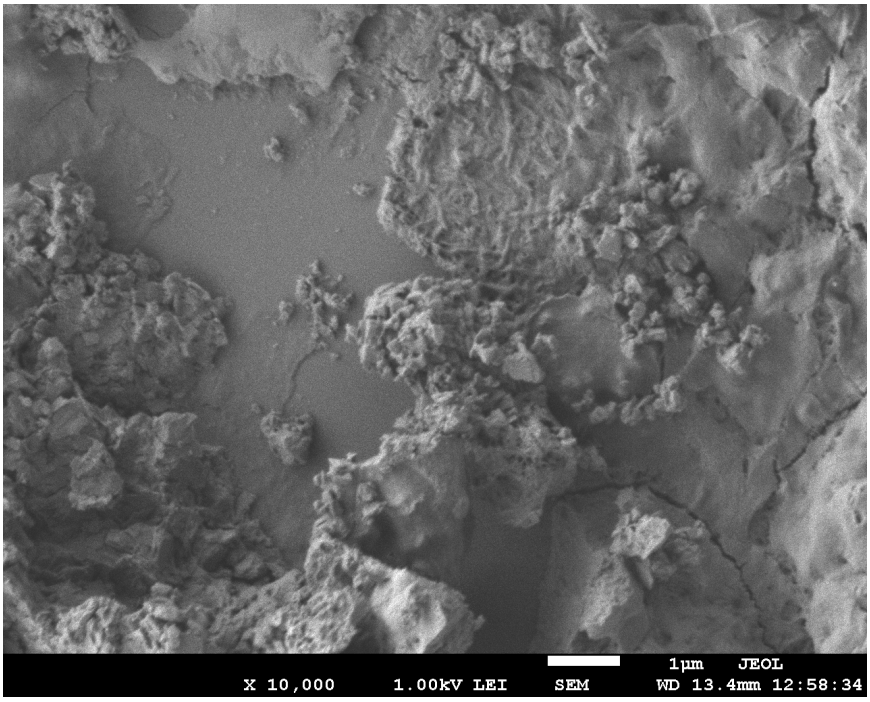

Figure 8.42 SEM image for dried suspension in Purified Water USP

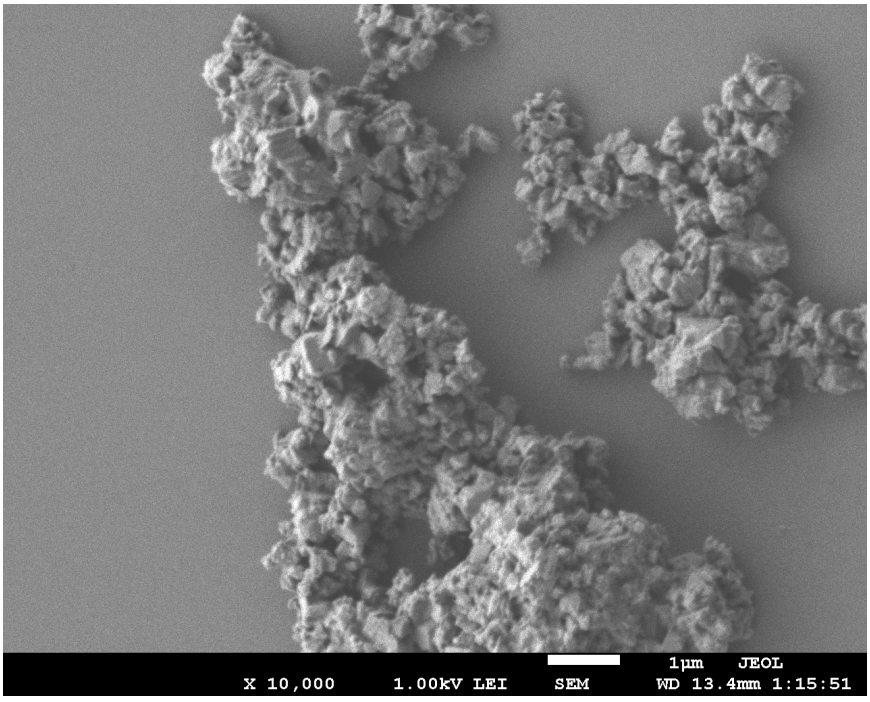

Figure 8.43 SEM image for dried suspension in 0.005% (w/v) CMC

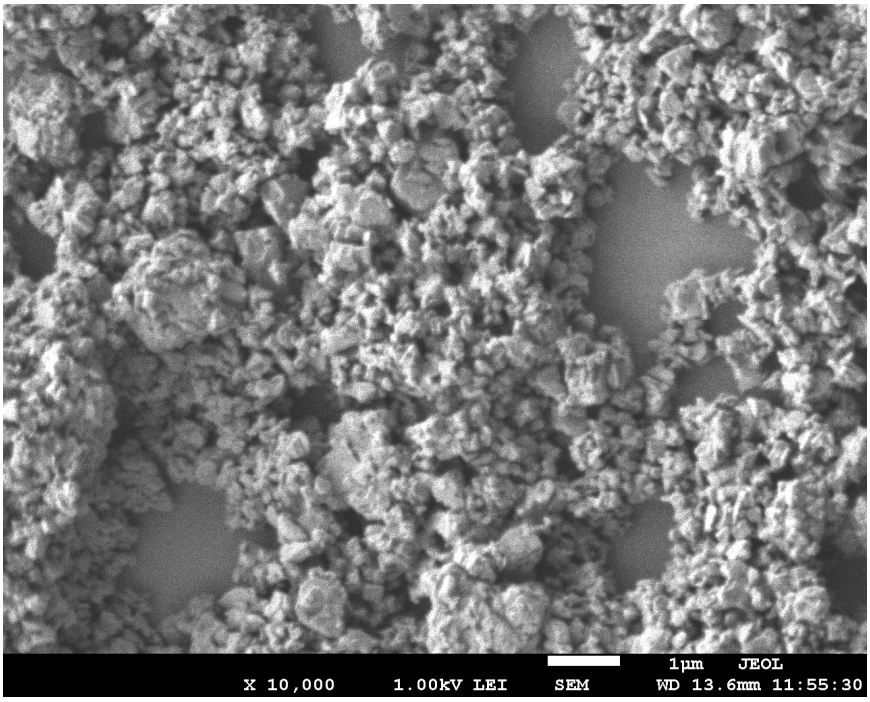

Figure 8.44 SEM image for dried suspension in 0.01% (w/v) CMC

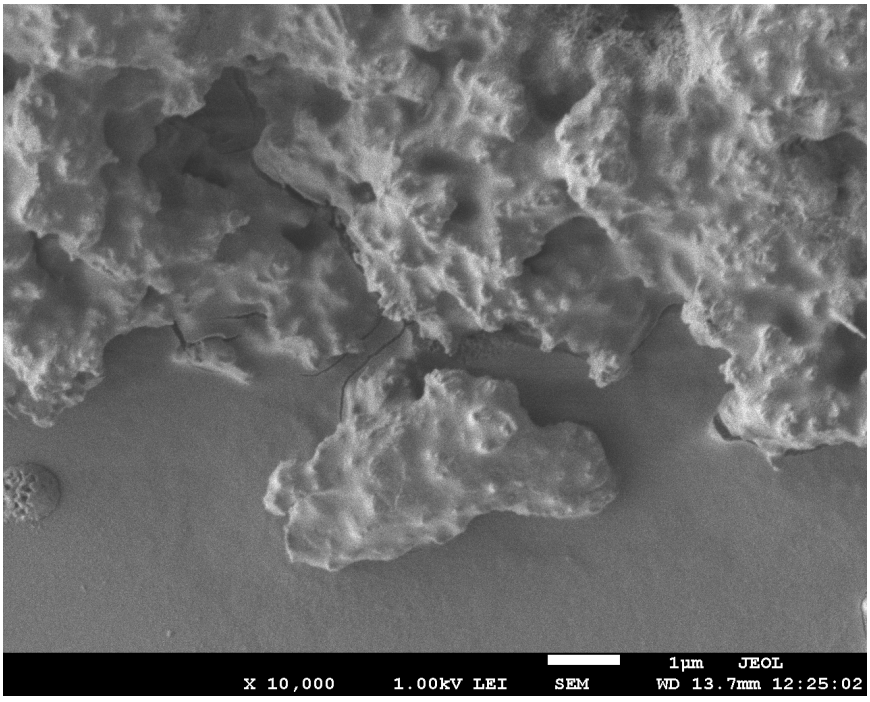

Figure 8.45 SEM image for dried suspension in 0.02% (w/v) CMC

It was quite obvious from Figure 8.41 that the dry powder magnesium hydroxide existed

in clusters. This may be the reason of the large particle size obtained from the sieving experiment. The force used to sieve the powder was not great enough to break the clusters into small particles, therefore the clusters was determined instead of single particles, which made the size and size distribution results from the sieving experiment inconsistent with the hindered settling calculations. The clusters were assumed to be broken during the preparation of suspensions, which made the floc size in the sediment, seen in Figures 8.42 to 8.45, considerably smaller compared to the dry powder.

The images for the dried suspension indicate that the floc size was quite difficult to be exactly determined by the imaging method due to the wide size range of the imaged flocs. The preparation method for SEM imaging also affected the precision of size determination. The heating of the suspension under low temperature in an oven may still change the particle size to some extent. The sampling method also can be modified for better imaging such as using double-sided tape to pick up dried sediments.

Considering the assumptions of spherical particles for the hindered settling theory, dry powder magnesium hydroxide would not fit the theory perfectly due to its rough, porous, clustered nature. However, the floc size could possibly be estimated to be from 1 to 15 μm, which would not be too far away from the hindered settling method. This will be further discussed in later sections.

8.1.4 Laser Diffraction (LD) Results

LD (Malvern Mastersizer 2000^{e}) was performed as the method provided in Chapter 7 Section 7.4.4. The distribution of particle size of dry powder magnesium hydroxide suspensions in various media are given in Figures 8.46 to 8.49. The mean particle sizes are summarized in Table 8.18.

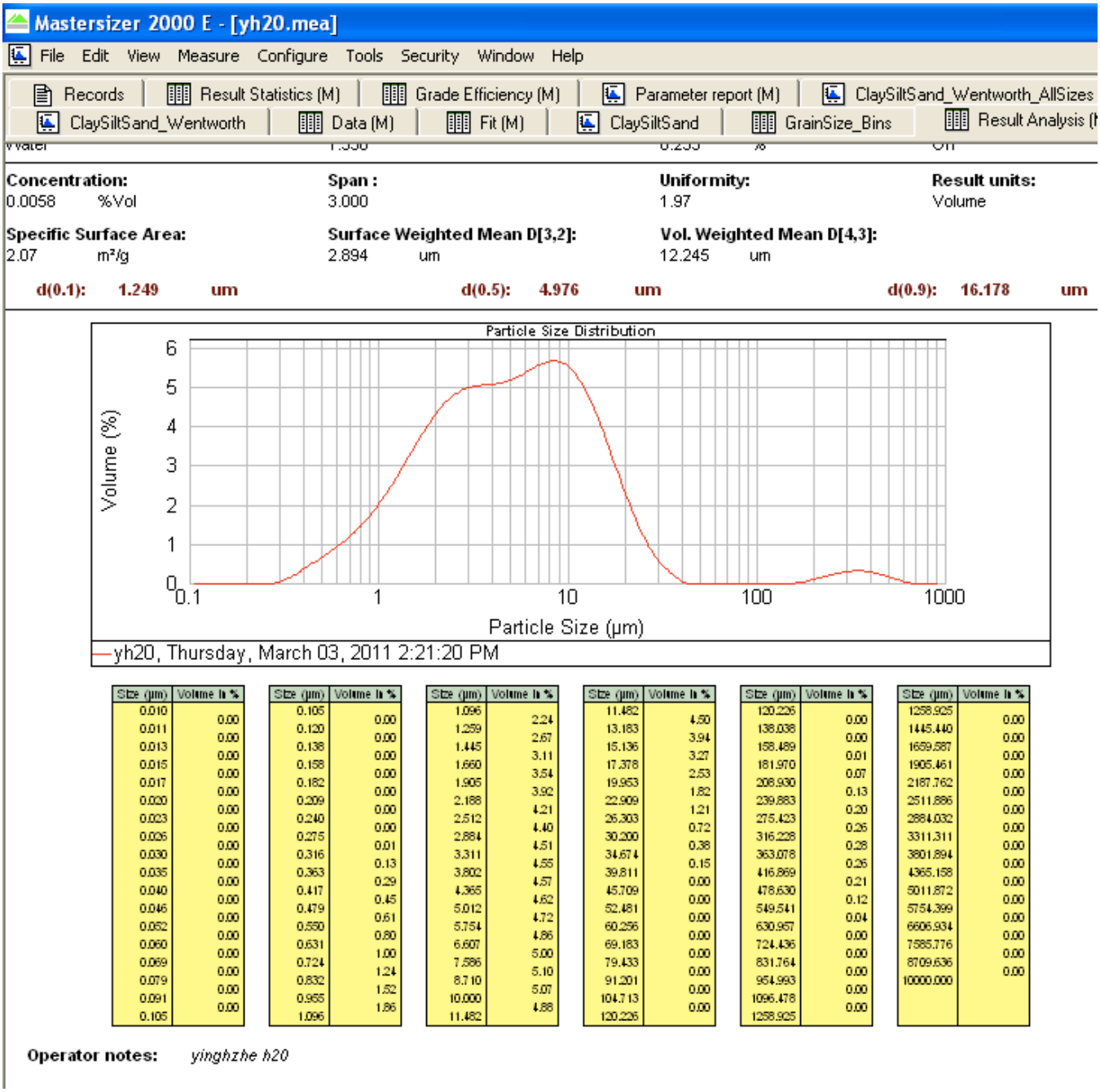

Figure 8.46 LD results for the dry powder magnesium hydroxide suspension in Purified Water USP at a concentration 20 g/200 mL

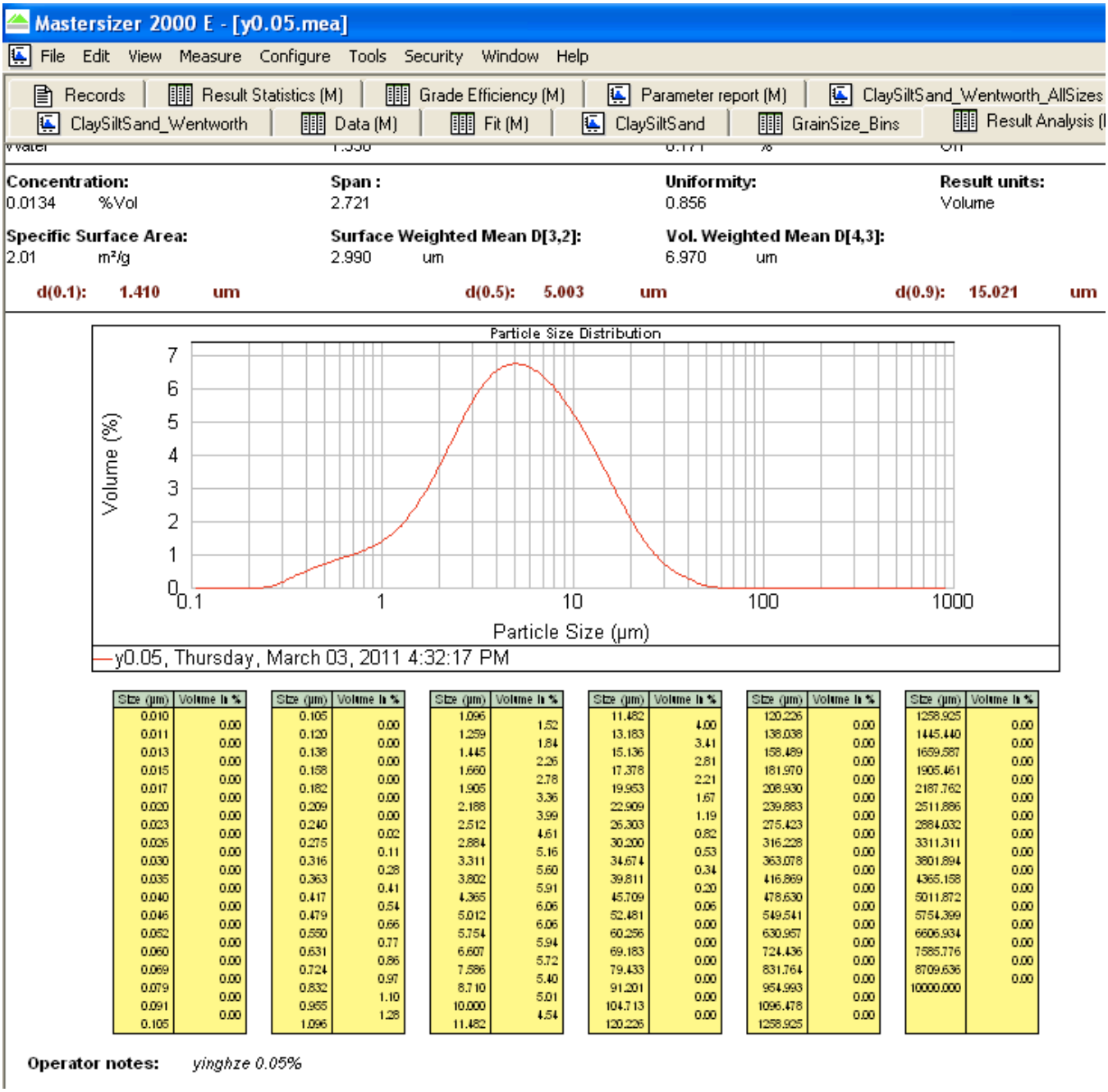

Figure 8.47 LD results for the dry powder magnesium hydroxide suspension in 0.005% (w/v) CMC at a concentration 20 g/200 mL

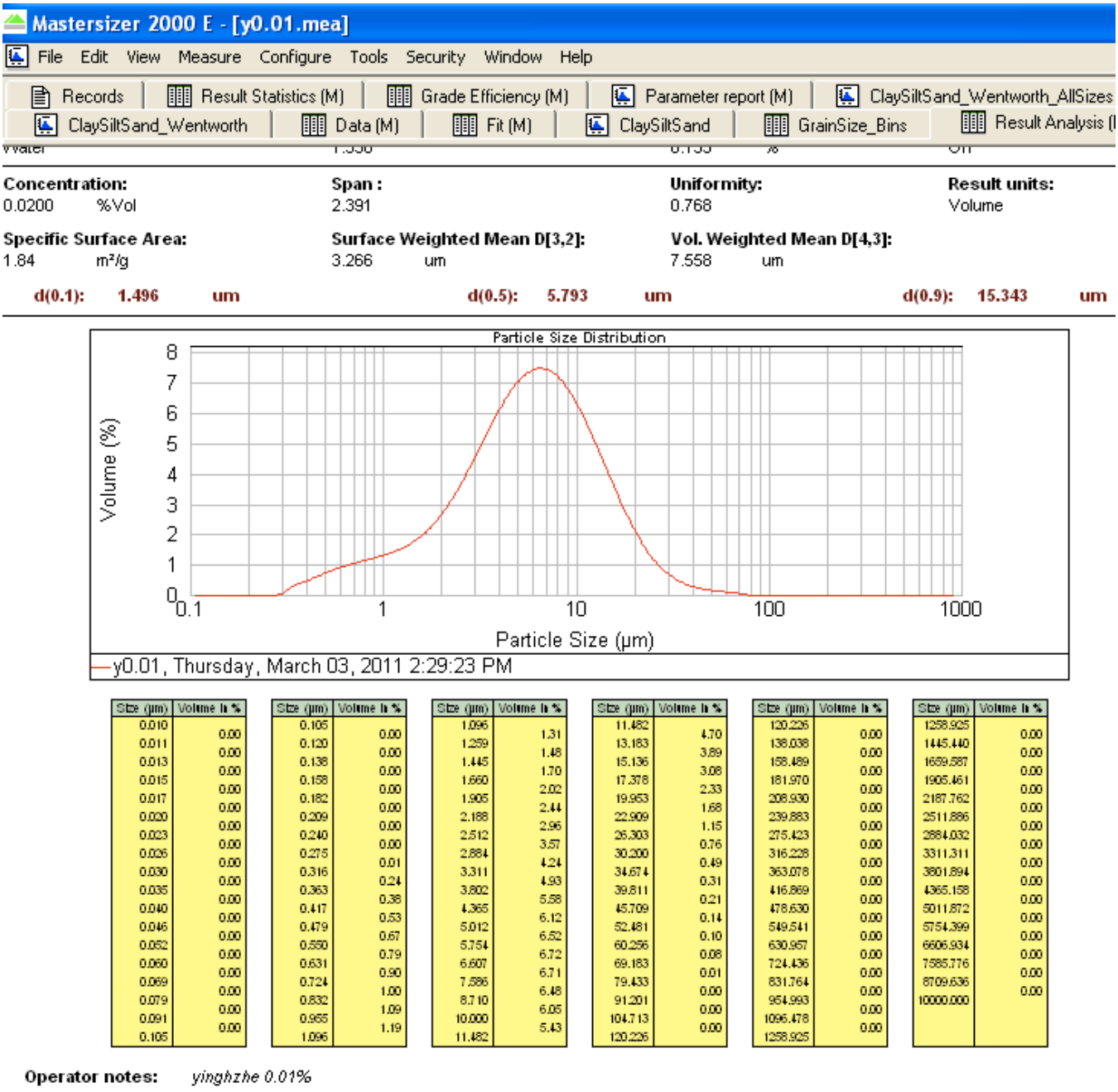

Figure 8.48 LD results for the dry powder magnesium hydroxide suspension in 0.01% (w/v) CMC at a concentration 20 g/200 mL

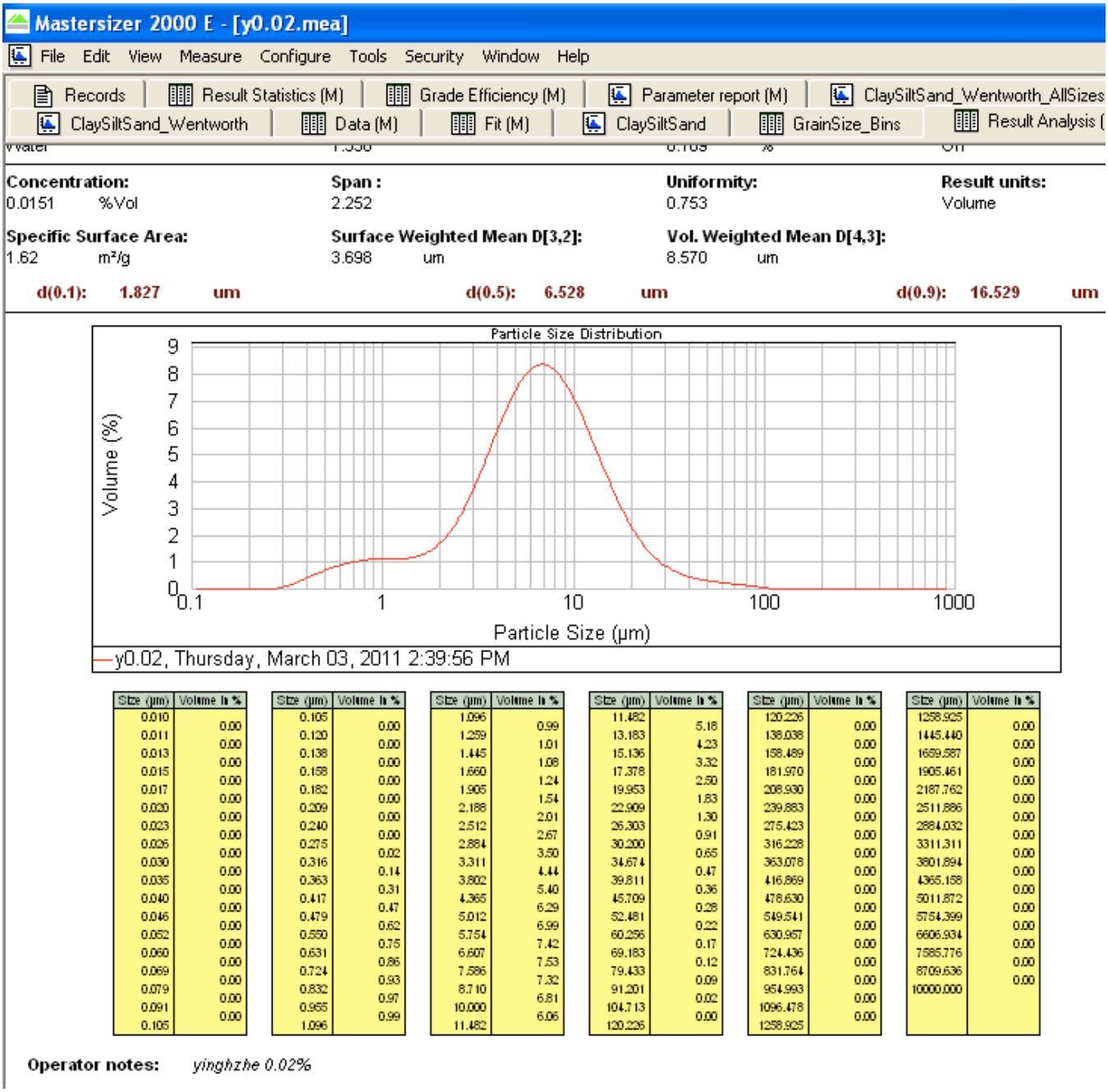

Figure 8.49 LD results for the dry powder magnesium hydroxide suspension in 0.02% (w/v) CMC at a concentration 20 g/200 mL

Table 8.18 Summarized LD results for particle sizes

Terms	Water	0.005% CMC	0.01% CMC	0.02% CMC
Surface Weighted Mean D [3,2] (μm)	2.894	2.990	3.266	3.698
Vol. Weighted Mean D [4,3] (μm)	12.245	6.970	7.558	8.570
d (0.1) (μm)	1.249	1.410	1.496	1.827
d (0.5) (μm)	4.976	5.003	5.793	6.528
d (0.9) (μm)	16.178	15.021	15.343	16.527

The size distributions of the suspensions in CMC solutions showed good normal distribution tendency. However, in Purified Water USP, the size distribution showed a bi-normal distribution, which caused the mean particle size to be askew. This demonstrated that the addition of CMC into the dispersion medium narrowed the particle size distribution to some extent. The particle sizes were slightly enlarged by the addition of CMC, according to the surface weighted mean d, (d (0.1)) and (d (0.5)). One problem with the LD method was that the suspensions were placed in a centrifuge tube, sonicated for dispersion and added into the flow system. These results were much more consistent with the hindered settling results compared to the sieving if not exactly the same.

8.2 Thermal Analyses

8.2.1 Differential Scanning Calorimetry (DSC) Results

The DSC experiments were performed using the method provide in Chapter 7 Section 7.5.1. The samples were prepared using various methods available. However, only filtering gave interpretable thermograms: Pipetting the final settled sediment gave board peaks making it difficult to accurately measure heat flow. Using drops of re-dispersed

suspension resulted in leakage of the suspension from the sample pan at temperatures higher than 100 °C. The DSC thermograms for the filtered sediments are given in Figures 8.50 to 8.53. All showed distinctive peaks for water of crystallization, fusion, vaporization, and magnesium hydroxide decomposition. The decomposition process is given in Eqn. 8.1

$$Mg(OH)_{2\,(solid)} \rightarrow MgO_{(solid)} + H_2O_{(vapor)} \qquad \text{Eqn. 8.1}$$

Each dispersion media and dried sediments as references are given in Figure 8.54 to 8.57. Data obtained from the thermograms are summarized in Table 8.19 as the heat of crystallization (ΔH_c) at crystallization temperature (T_c); the heat of fusion (ΔH_f) at melting temperature (T_m); the heat of vaporization (ΔH_v) at vaporization temperature (T_v); as well as the heat of decomposition (ΔH_d) at decomposition temperature (T_d).

Table 8.19 Data summarized from the TG thermograms (ΔH (J/g), T (°C), F = filtered sediment, R = references)

		ΔH_c	T_c	ΔH_f	T_m	ΔH_v	T_v	ΔH_d	T_d
Water	F	144.34	-6.95	-155.97	4.03	-1014.77	102.80	-710.09	423.51
	R	330.82	-11.65	-385.71	4.44	-2419.95	100.99	-1407.64	427.96
0.005%	F	160.93	-4.83	-165.80	3.93	-998.29	102.71	-668.28	420.89
CMC	R	312.71	-9.72	-371.85	3.84	-2268.46	100.00	-1366.34	424.60
0.01%	F	169.86	-5.81	-182.68	4.16	-1122.50	100.12	-591.22	421.29
CMC	R	333.39	-9.94	-382.58	4.04	-2229.59	100.32	-1462.46	420.37
0.02%	F	153.64	-6.47	-162.13	5.17	-1042.44	101.93	-615.15	423.26
CMC	R	327.21	-10.28	-375.16	4.10	-2406.51	101.23	-1470.35	425.39

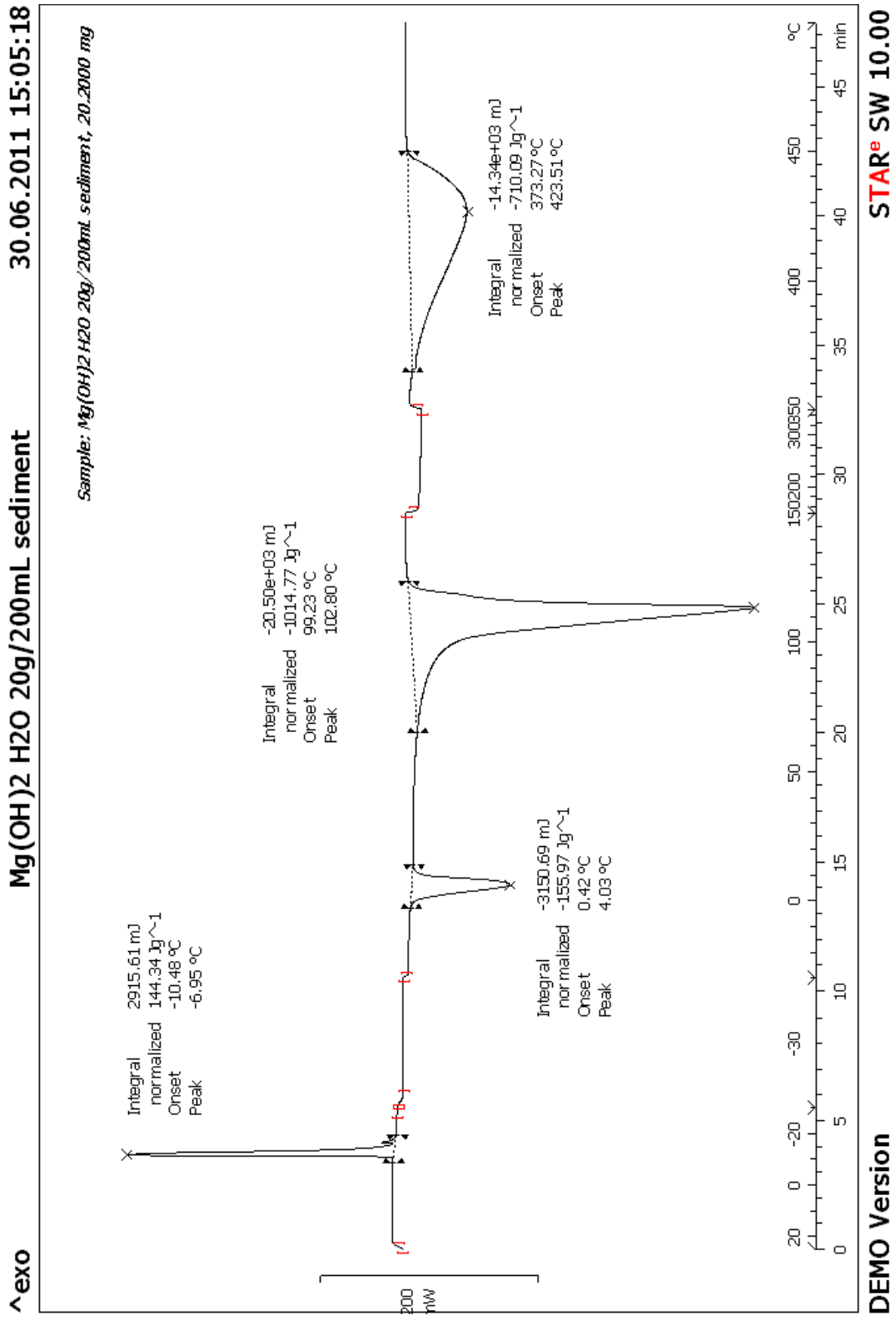

Figure 8.50 DSC thermogram for filtered sediment of dry powder magnesium hydroxide suspension in Purified Water USP at a concentration 20 g/200 mL

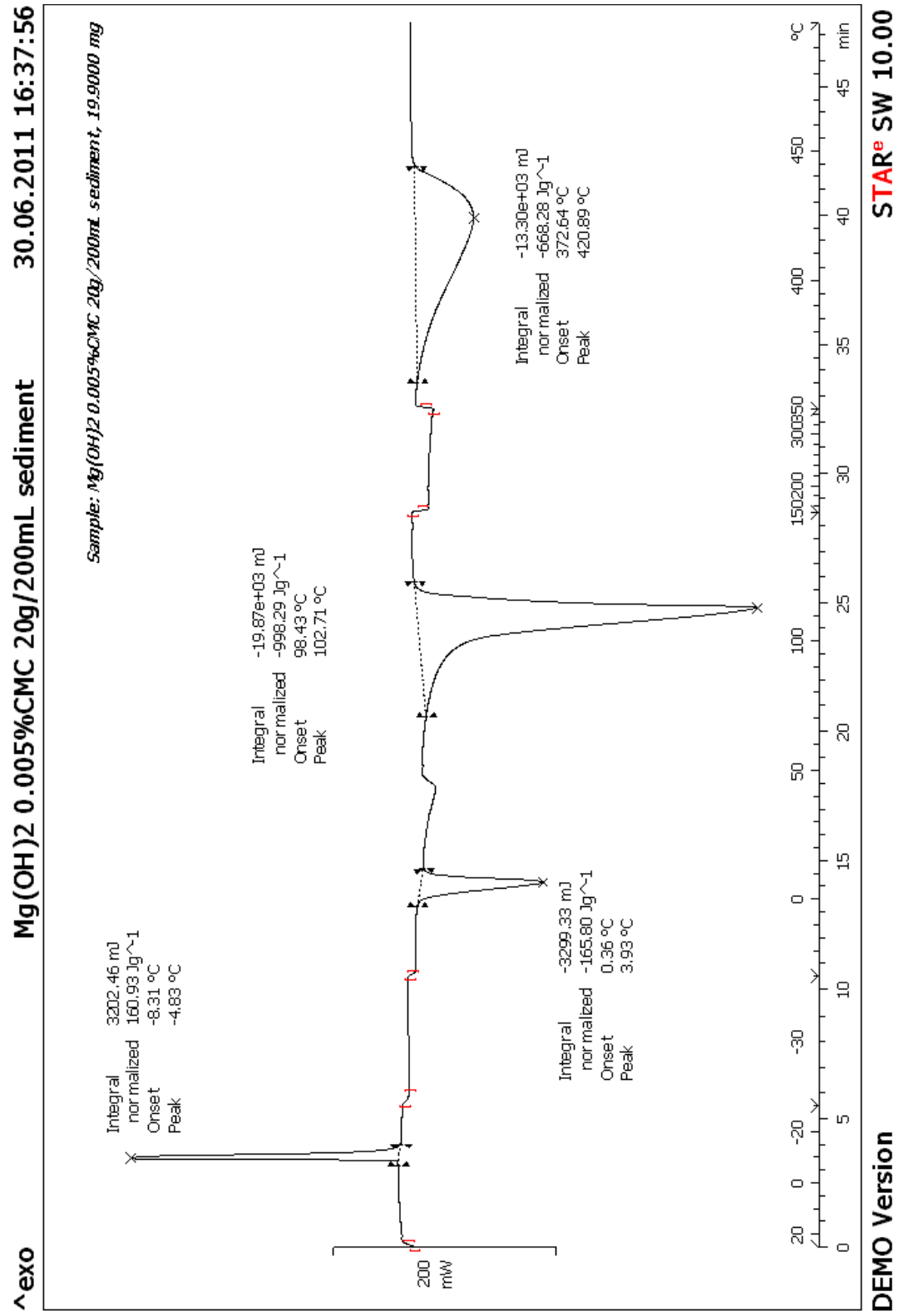

Figure 8.51 DSC thermogram for filtered sediment of dry powder magnesium hydroxide suspension in 0.005% (w/v) CMC at a concentration 20 g/200 mL

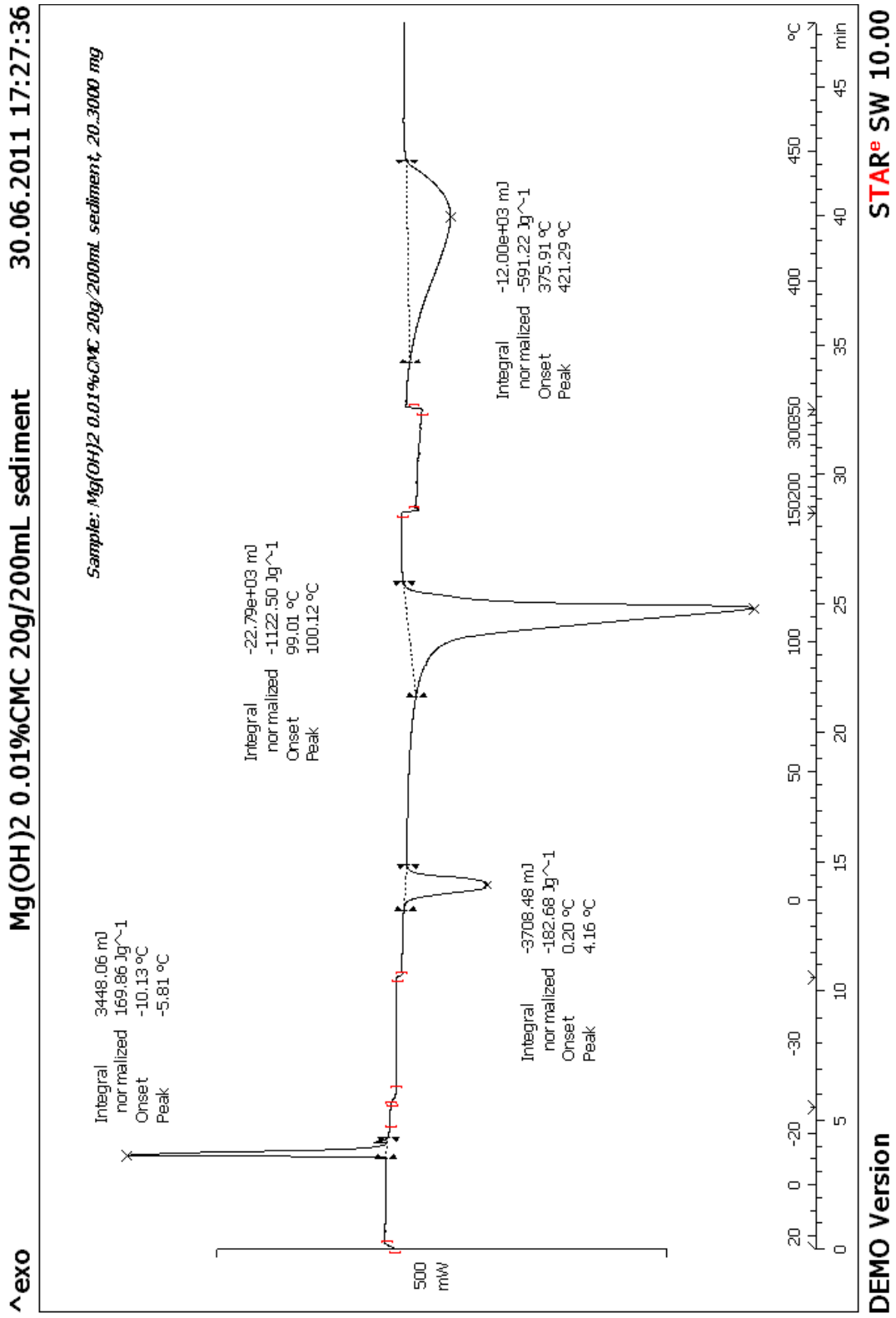

Figure 8.52 DSC thermogram for of filtered sediment dry powder magnesium hydroxide suspension in 0.01% (w/v) CMC at a concentration 20 g/200 mL

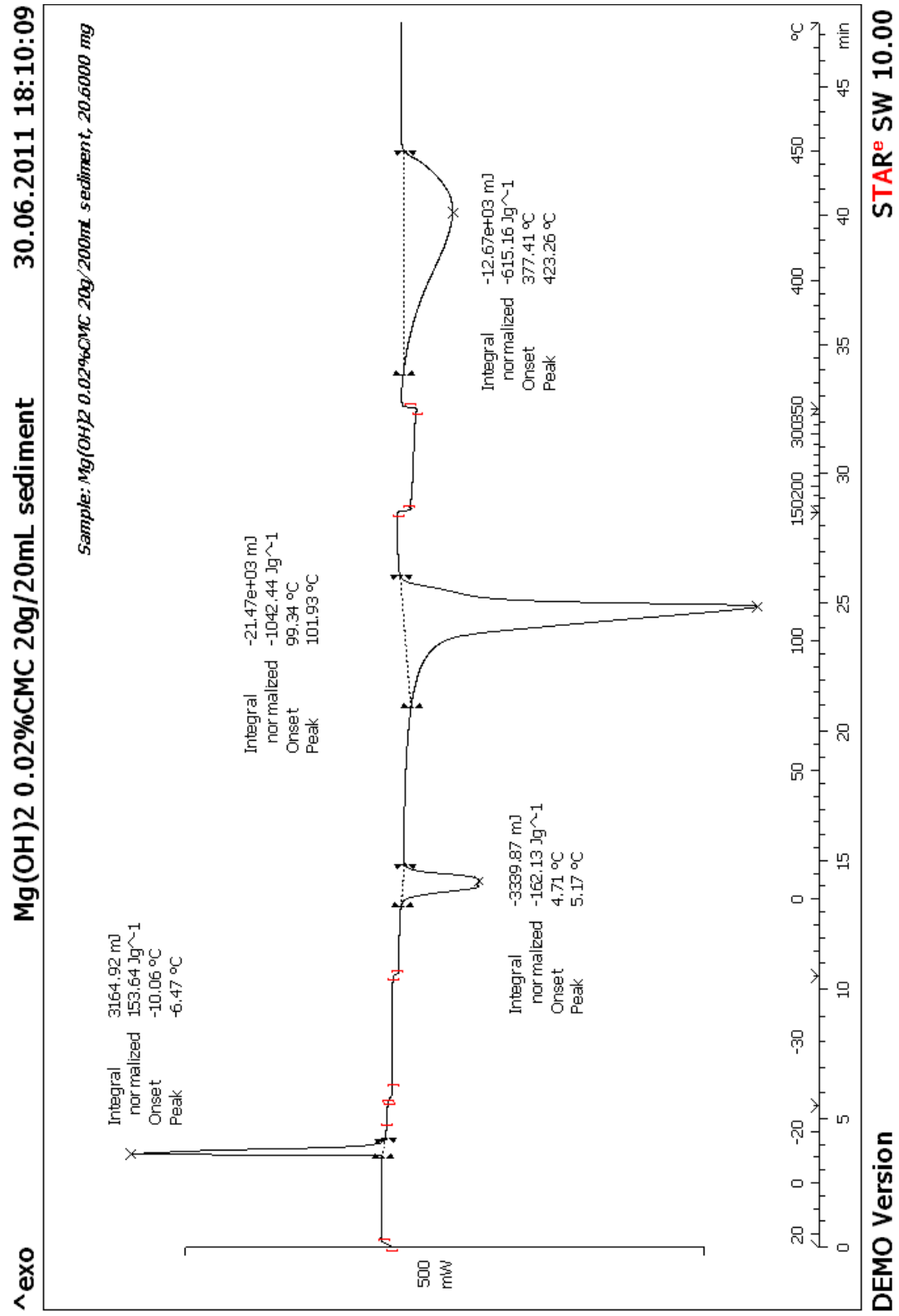

Figure 8.53 DSC thermogram for filtered sediment of dry powder magnesium hydroxide in 0.02% (w/v) CMC suspension at concentration 20g/200mL

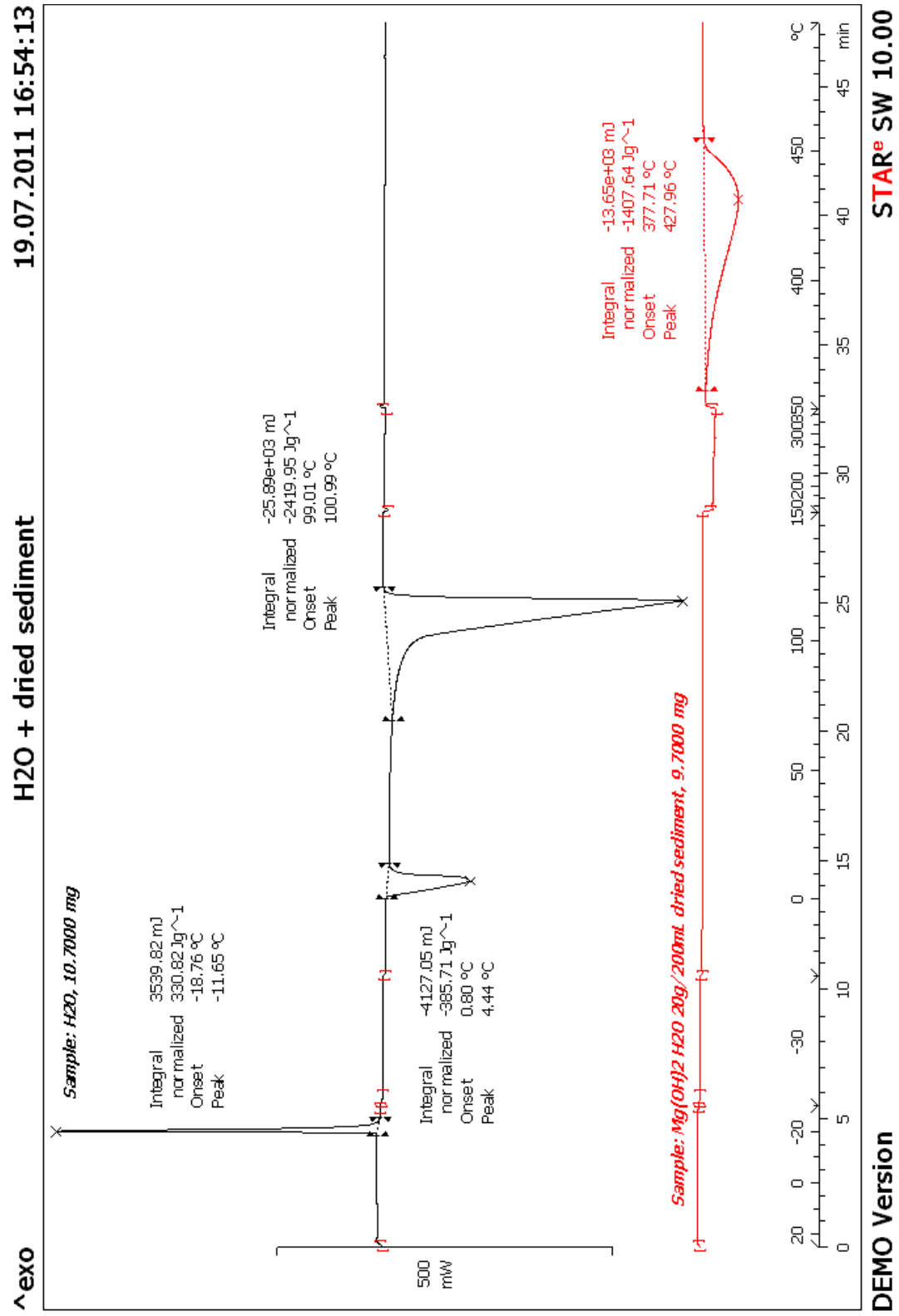

Figure 8.54 DSC thermogram for Purified Water USP and the same suspension sediment dried in a 50°C oven over night as the reference

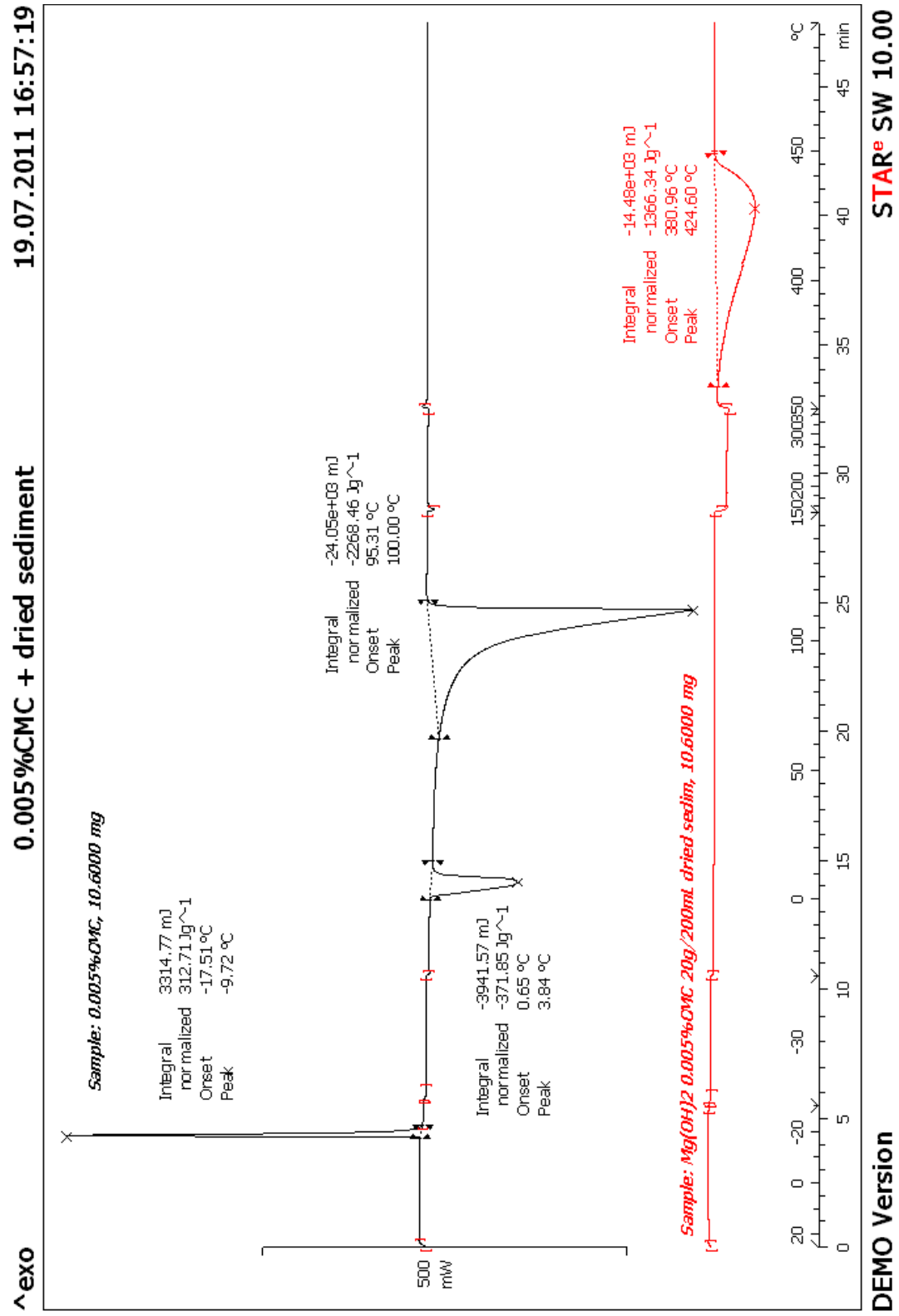

Figure 8.55 DSC thermogram for 0.005% (w/v) CMC and the same suspension sediment dried in a 50°C oven over night as the reference

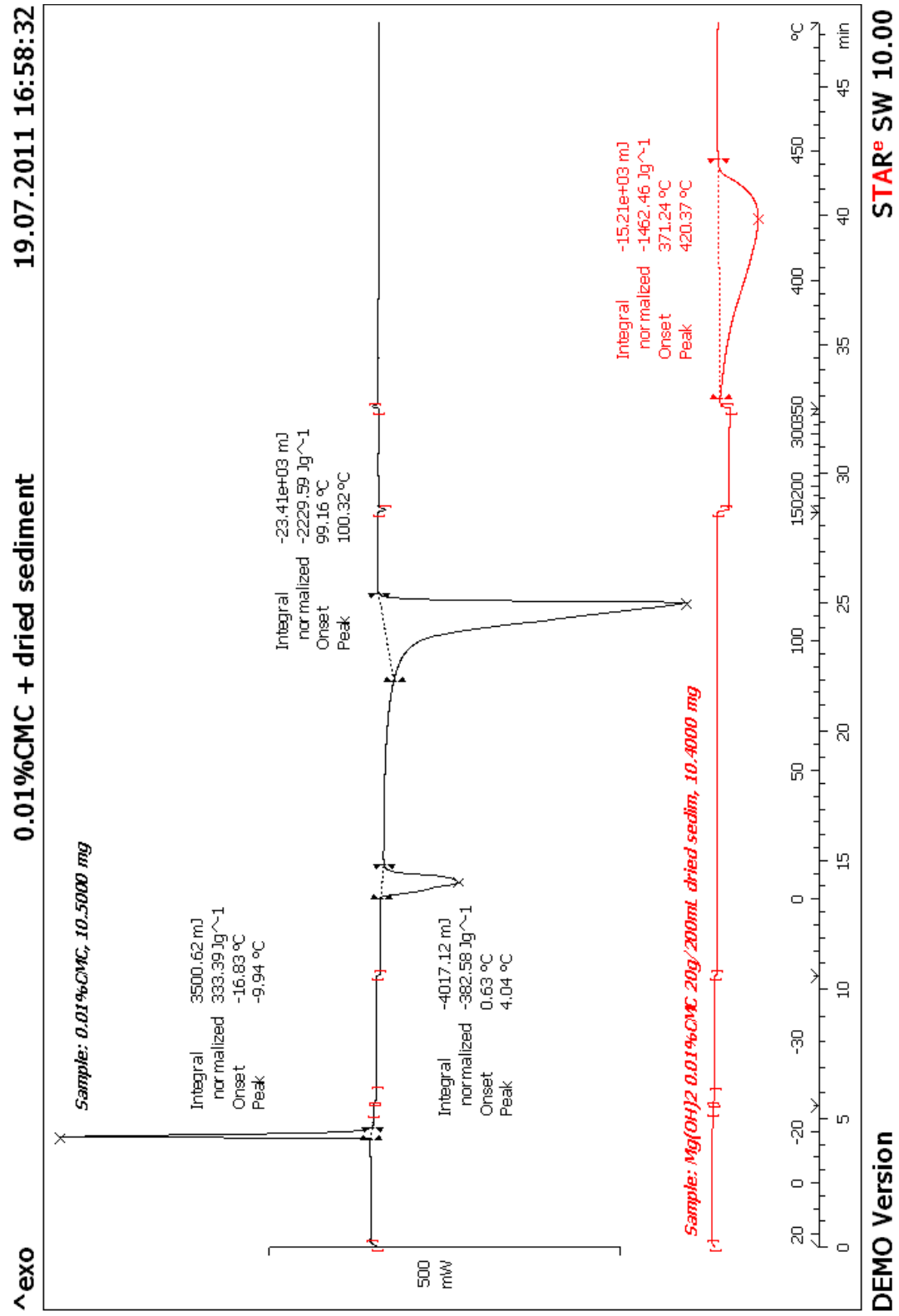

Figure 8.56 DSC thermogram for 0.01% (w/v) CMC and the same suspension sediment dried in a 50°C oven over night as the reference

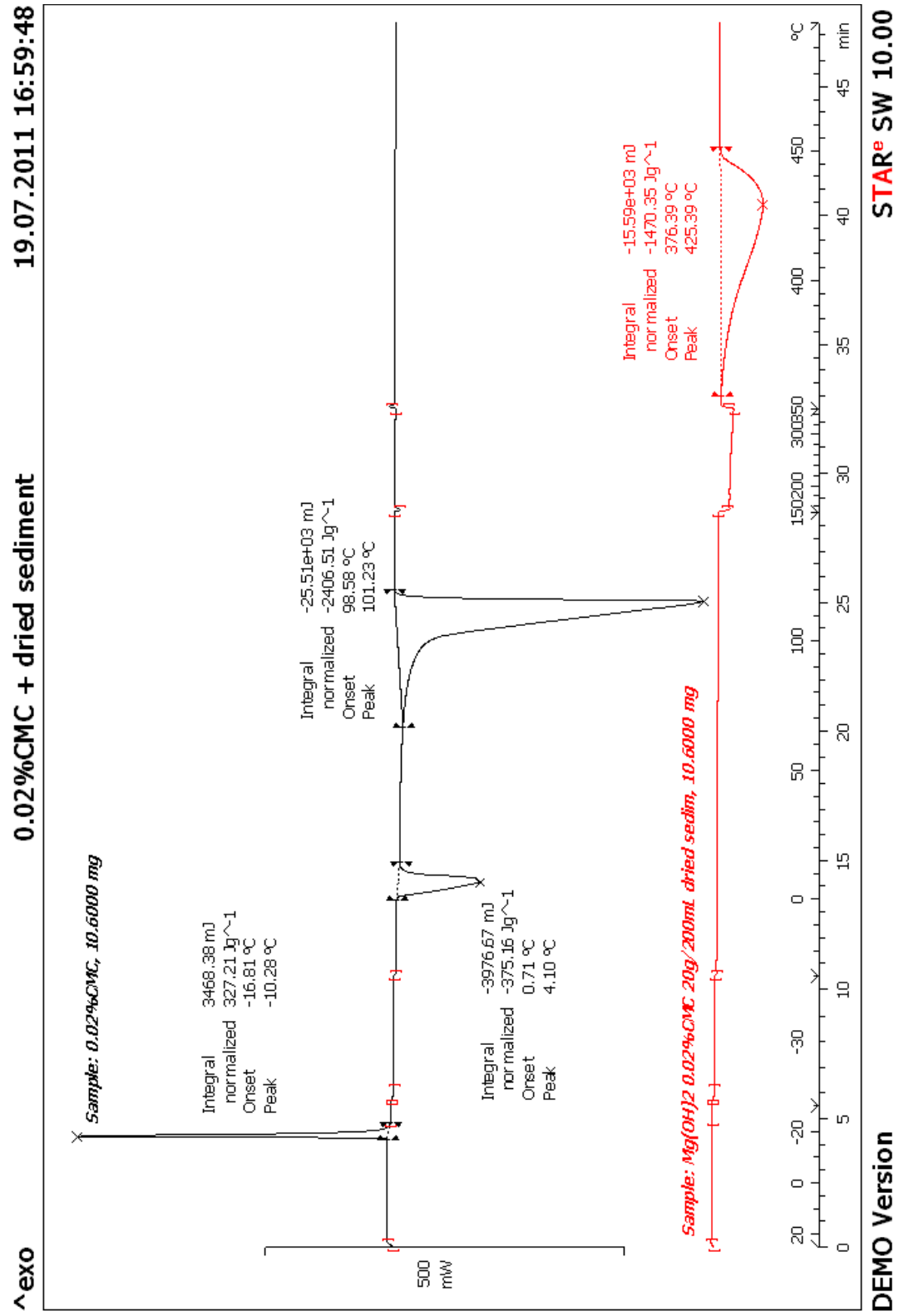

Figure 8.57 DSC thermogram for 0.02% (w/v) CMC and the same suspension sediment dried in a 50 °C oven over night as the reference

It was obvious that all water crystallization peaks shift to a higher temperature in filtered sediments compared to the liquid media, 67.6% for Purified Water USP, 101.2% for 0.005%CMC, 71.1% for 0.01%CMC, and 58.9% for 0.02% CMC. There were no significant changes in all the other peak temperatures. Water content for the suspension in each media was determined by comparison of the heat of crystallization and the heat of fusion with that of the reference dispersing media. This is summarized in Table 8.20. It is quite obvious that the water content increased in the suspensions with CMC solutions. However, this water was only in the free and unbound water from which was retained in the sediment after filtering. The loosely-bound water onto the magnesium hydroxide particles was not able to be determined in this study, even when the samples were cooled to temperatures as low as -50 °C and held at this temperature for more than 20 minutes, due to the instrumentation limitations in temperature program.

Table 8.20 The water content for the suspension in each media

	Water	0.005% CMC	0.01% CMC	0.02% CMC
Relative ΔH_c (%)	43.63	51.46	50.95	46.95
Relative ΔH_f (%)	40.44	44.59	47.75	43.22
Average	42.03	48.03	49.35	45.09

8.2.2 Thermogravimetry (TG) Results

The TG experiments were performed using the method provide in Chapter 7 Section 7.5.2. The TG thermograms for the filtered sediments are given in Figures 8.58 to 8.61. Data obtained form the thermograms are summarized in Table 8.21. The later part of the mass loss was considered to be the decomposition of magnesium hydroxide into magnesium oxide as given in Eqn. 8.1 in Section 8.2.1. This decomposition was verified by X-ray powder diffraction.

Table 8.21 Date summarized from the TG thermograms

	T (Onset) (°C)	T (Endset) (°C)	Mass Loss (%)	T (Onset) (°C)	T (Endset) (°C)	Mass Loss (%)
Water	40.00	117.45	34.8641	359.98	444.63	18.0544
0.005% CMC	48.53	125.26	46.3238	361.42	442.69	14.9234
0.01% CMC	47.69	123.59	48.3233	357.87	440.27	13.8166
0.02% CMC	50.76	124.08	48.1819	367.21	442.90	14.2934

The data were analyzed using the first derivative of the percent (%) mass loss versus temperature in °C and summarized in Table 8.22. It was obvious from the fist derivative plots that there were two distinctive peaks in the mass loss from about 40 to 120 °C, which indicated the possible existence of both unbound and bound water which loosely bounded to the magnesium hydroxide particle.

Table 8.22 Data summarized from the first derivative graph (peak temperatures)

	T_1 (°C)	T_2 (°C)	T_3 (°C)
Water	102.83	110.24	422.86
0.005% CMC	101.77	117.52	423.23
0.01% CMC	105.87	118.51	420.95
0.02% CMC	102.93	117.09	421.70

Therefore, the majority of the water loss occurred during heating. It can be assumed that the first major mass loss was the unbound water in the filtered sediment, and the bound water was lost at a slightly higher temperature. Mass losses for these two types of water are summarized in Tables 8.23 and 8.24.

It indicated that the addition of CMC decreased the bound water content, and with an increasing concentration of CMC, the bound water content decreases. One possible explanation was that the addition of CMC to the dispersion media caused the CMC to bind with the magnesium hydroxide particles occupying the binding sites due to its

polymeric nature, resulting in fewer sites for the bound water.

Table 8.23 The mass losses for the bound and unbound water

	Total Mass loss (%)	Unbound water (%)	Bound water (%)
Water	34.8641	29.0777	5.7864
0.005% CMC	46.3238	40.7598	5.5640
0.01% CMC	48.3233	43.0733	5.2500
0.02% CMC	48.1819	43.4016	4.7803

Table 8.24 The percentage composition for the bound and unbound water

	Unbound water (%)	Bound water (%)
Water	83.40	16.60
0.005% CMC	87.89	12.01
0.01% CMC	89.14	10.86
0.02% CMC	90.08	9.92

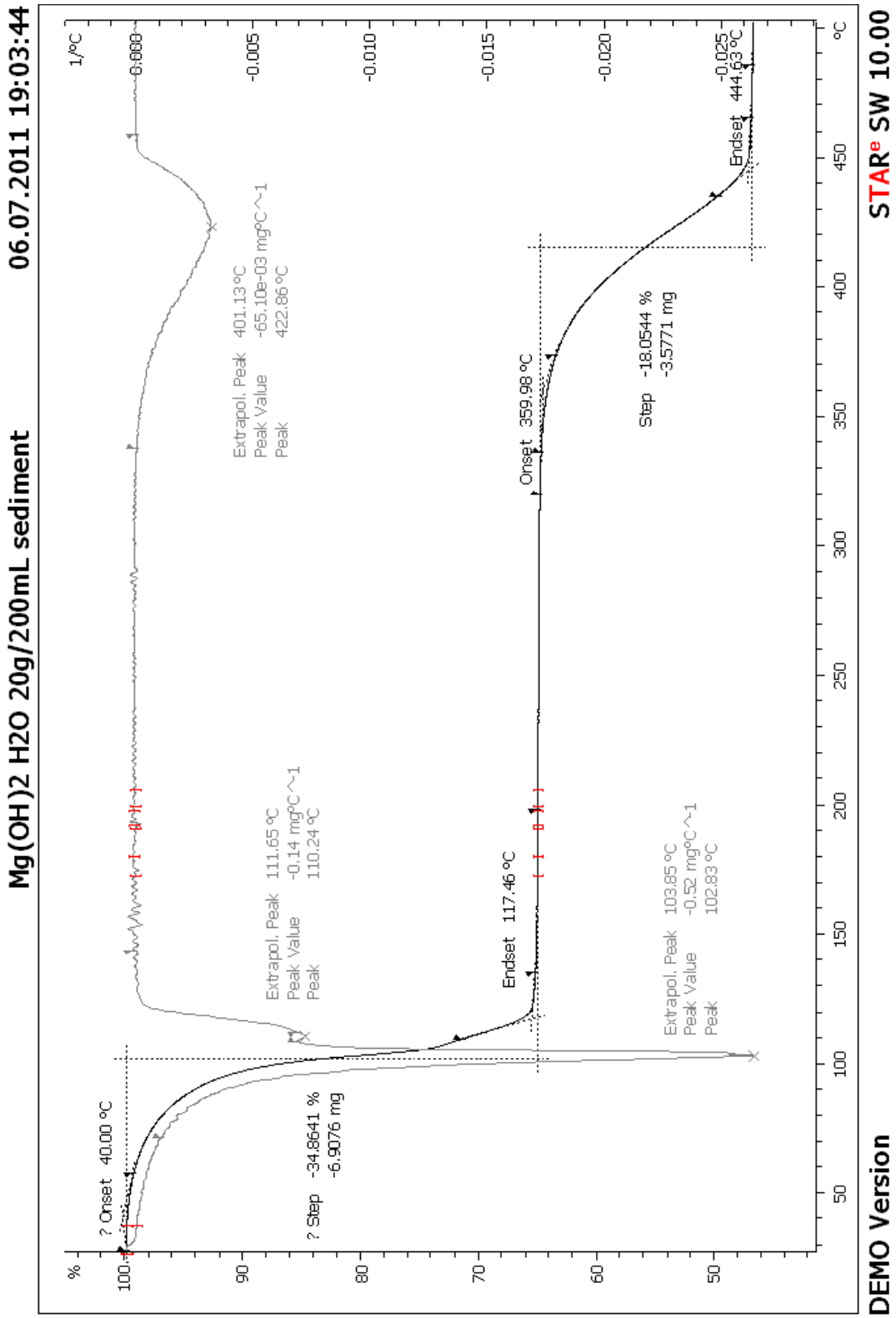

Figure 8.58 TG thermogram for the filtered sediment of dry powder magnesium hydroxide suspension in Purified Water USP at a concentration 20 g/200 mL

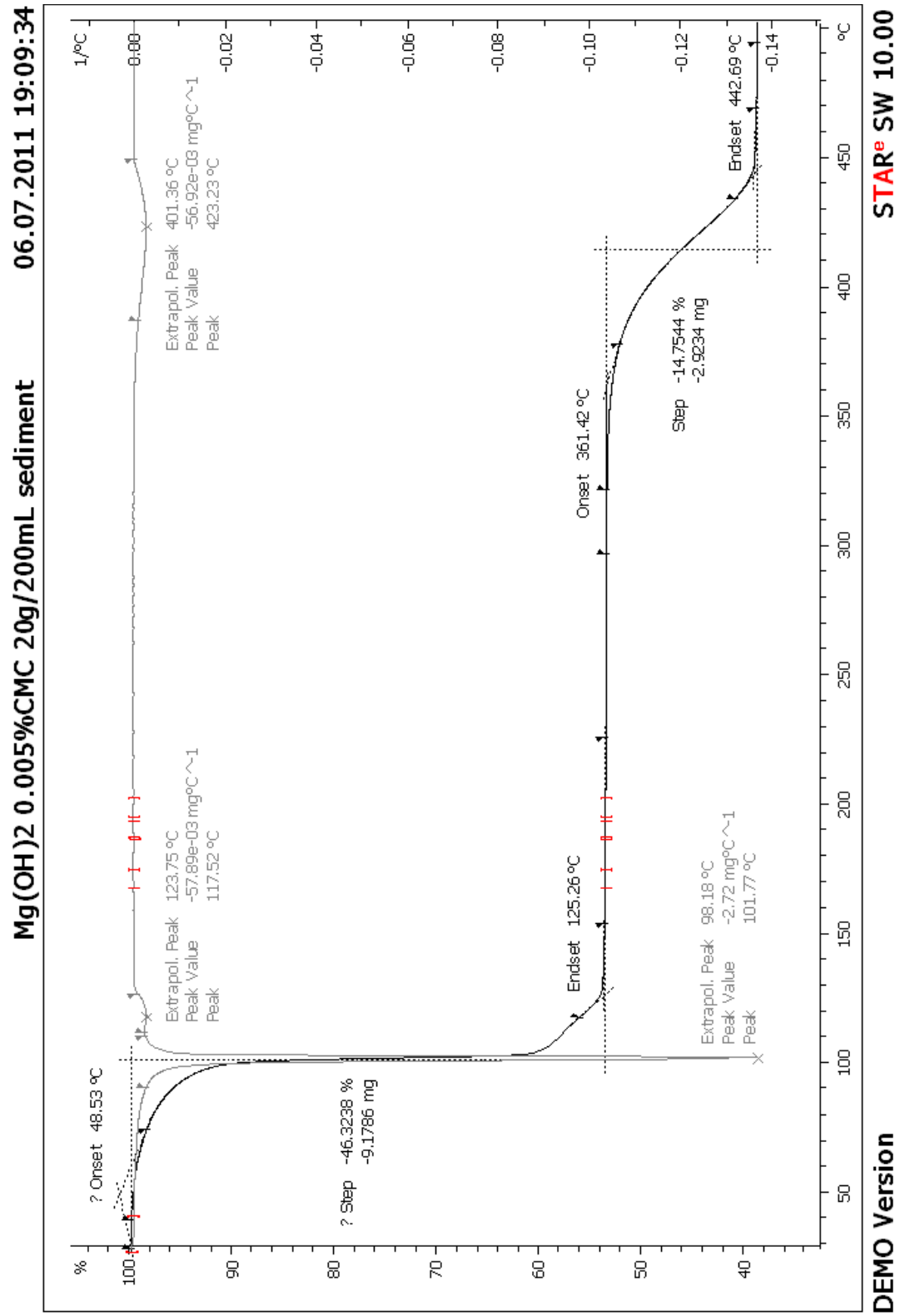

Figure 8.59 TG thermogram for the filtered sediment of dry powder magnesium hydroxide in 0.005% (w/v) CMC suspension at a concentration 20 g/200 mL

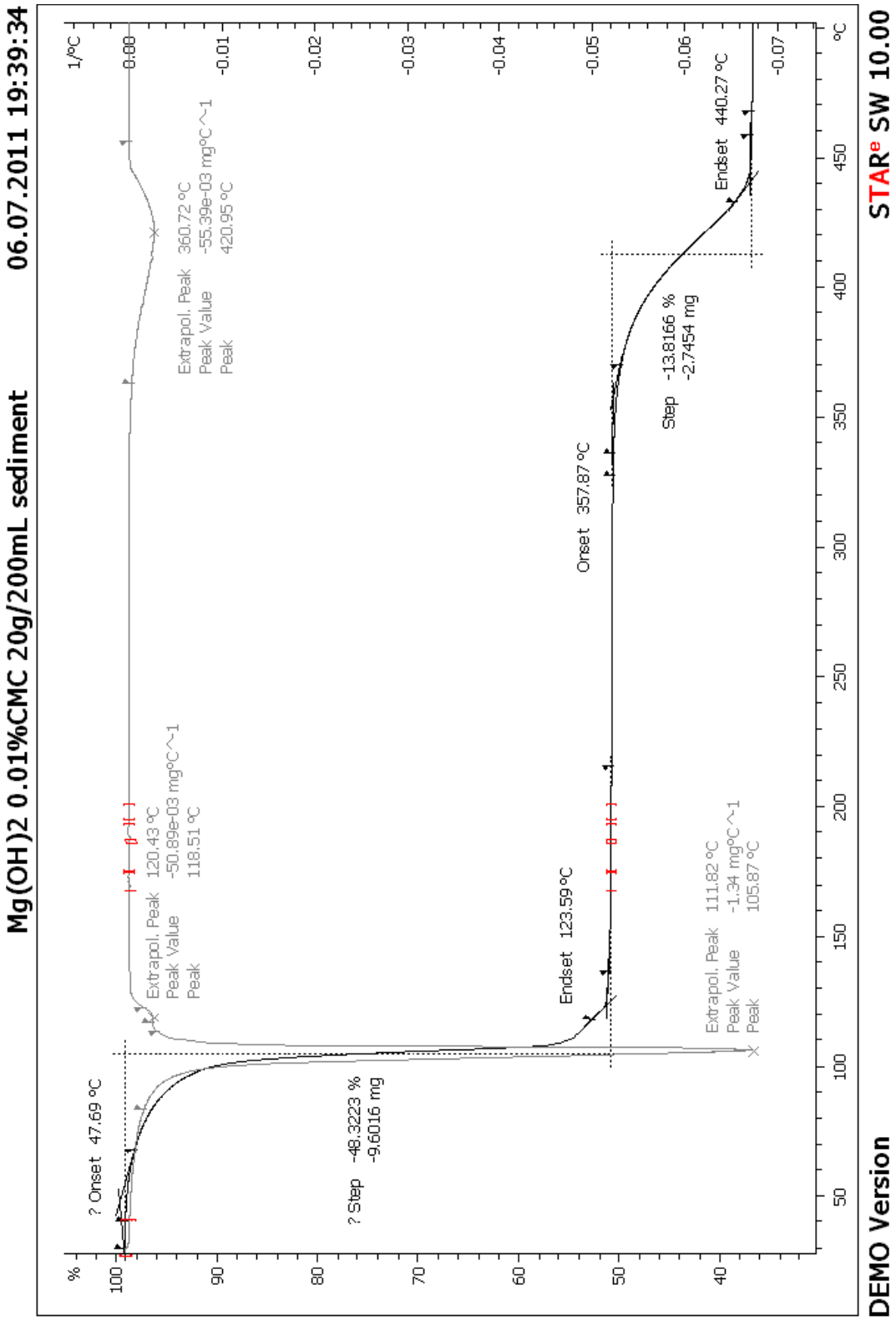

Figure 8.60 TG thermogram for the filtered sediment of dry powder magnesium hydroxide in 0.01% (w/v) CMC suspension at a concentration 20 g/200 mL

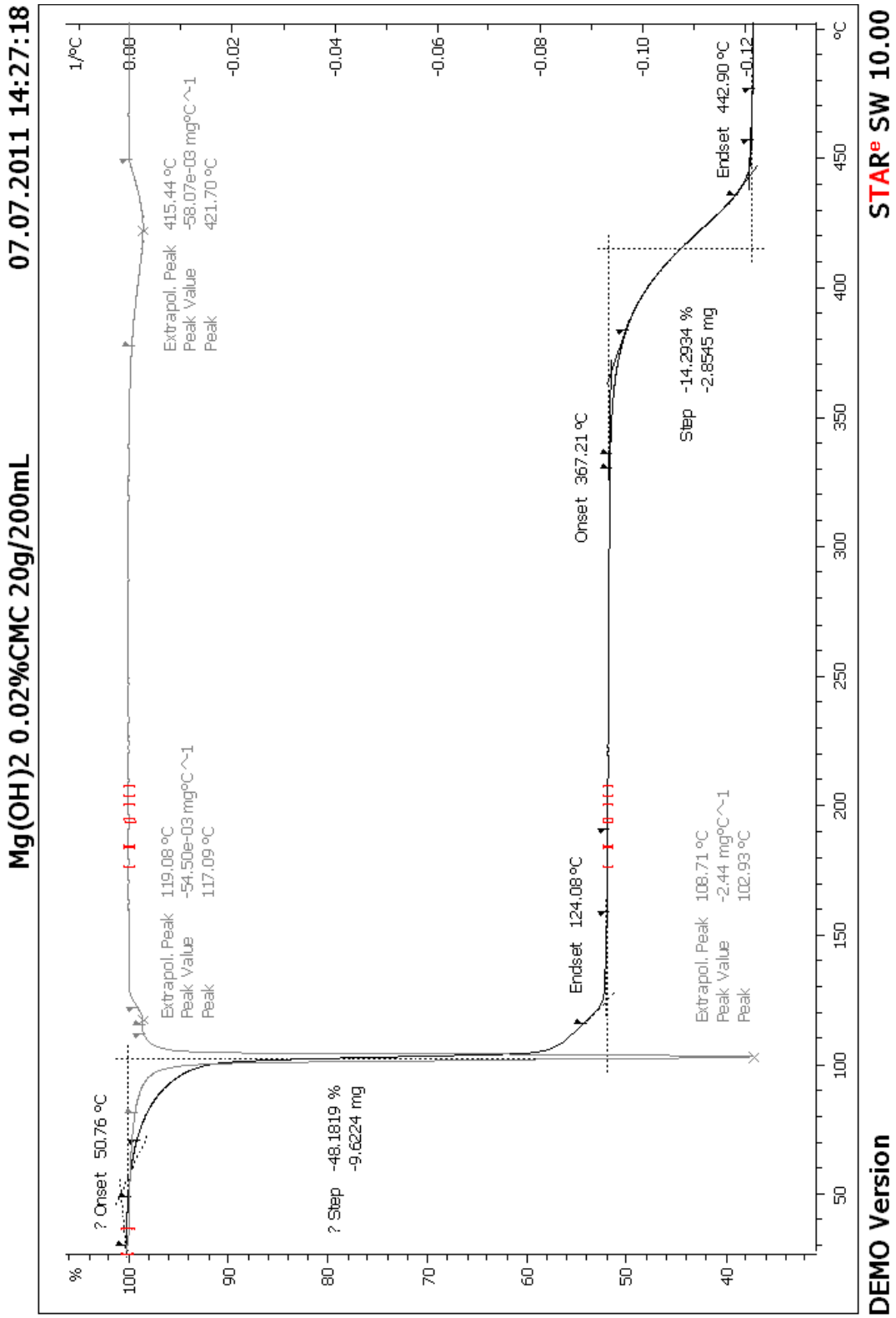

Figure 8.61 TG thermogram for the filtered sediment of dry powder magnesium hydroxide in 0.01% (w/v) CMC suspension at a concentration 20 g/200 mL

8.3 X-Ray Powder Diffraction (PXRD) Results

PXRD experiments were performed using the method provided in Chapter 7 Section 7.6. PXRD diffractograms, seen in Figure 8.62, for the dry powder magnesium hydroxide, dried sediments of suspensions in Purified Water USP and 0.02% (w/v) CMC before heating showed similar diffraction patterns indicating that these three samples were considered to contain exact the same chemical composition.

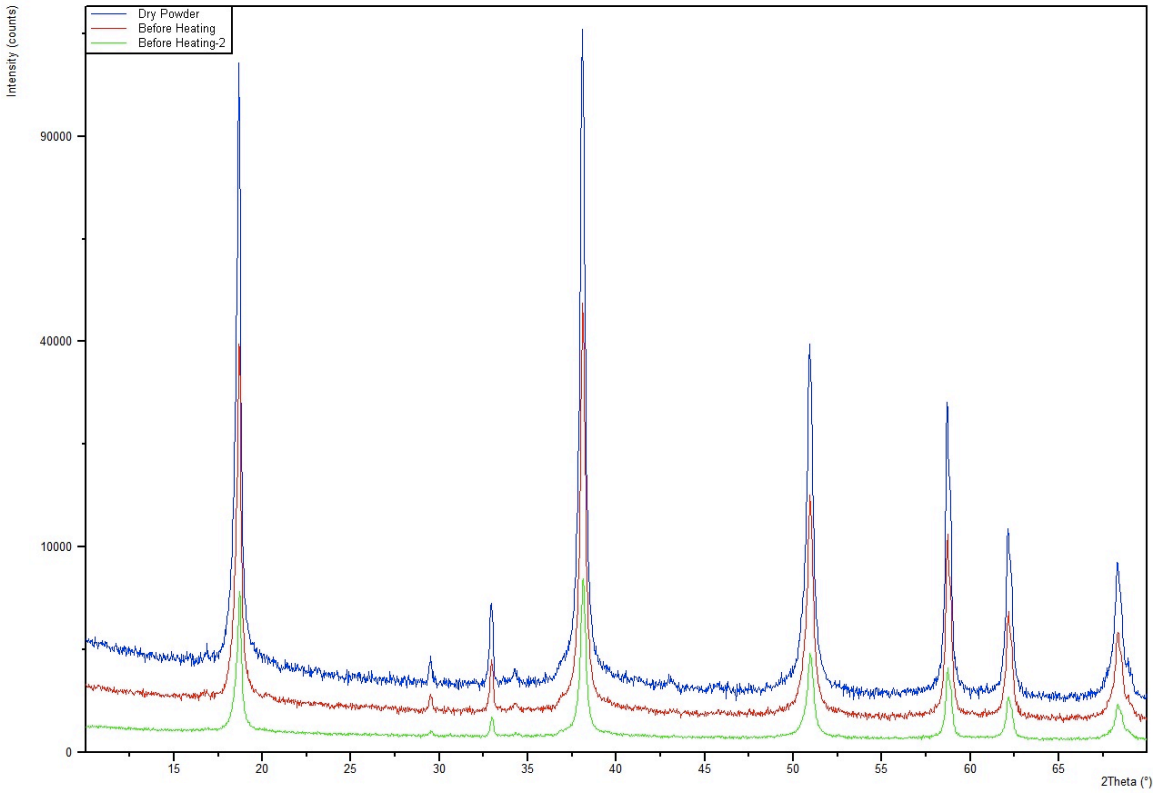

Figure 8.62 PXRD diffractogram for dry powder magnesium hydroxide (Dry Powder), dried sediments of suspensions in Purified Water USP (Before Heating) and 0.02% (w/v) CMC before heating (Before Heating-2)

PXRD diffractogram for dried sediment after heating under high temperature in a TG is given in Figure 8.63. This diffractogram was then compared with the standard diffraction pattern of both magnesium hydroxide and magnesium oxide, as seen in Figure 8.64. It was obvious that both compounds existed in the sample of dried sediment after heating

under high temperature in the TG. Thus, the composition of the residuals after heating indicated that the decomposition starting around 400°C in the TG was incomplete.

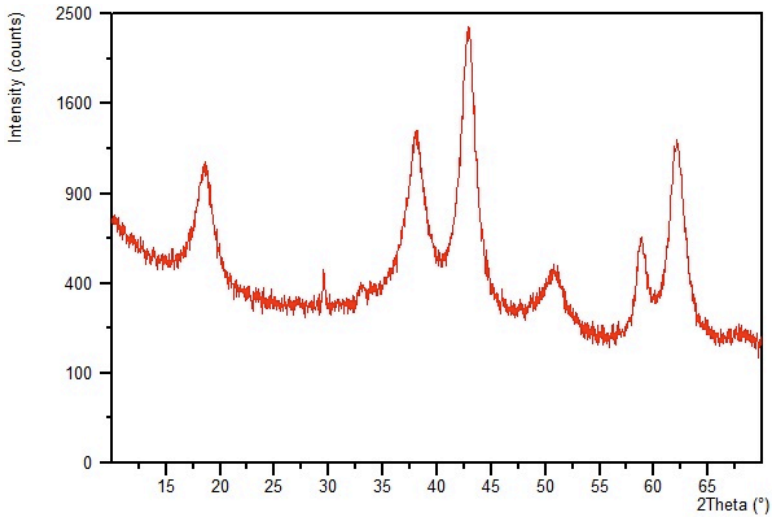

Figure 8.63 PXRD diffractogram for dried sediment after heating

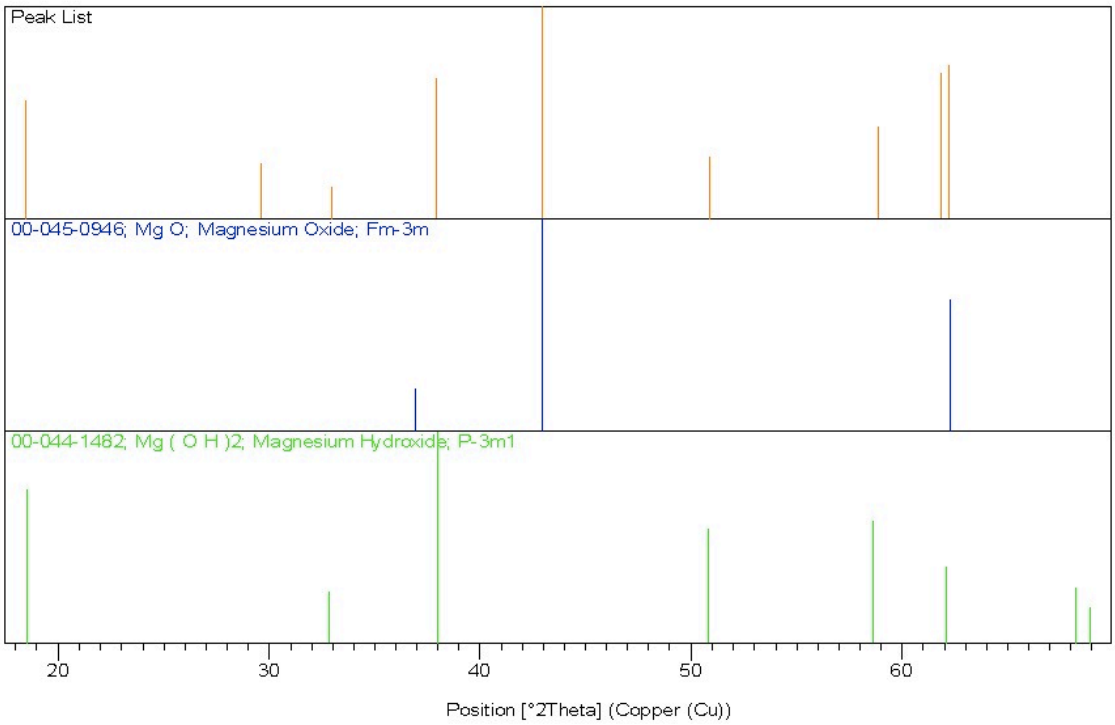

Figure 8.64 Comparison of PXRD diffractogram for dried sediment after heating with the standard diffraction pattern of both magnesium hydroxide and magnesium oxide

Chapter 9

Conclusions & Future Work

9.1 Conclusions

Magnesium hydroxide suspension has been widely used as an antacid and laxative. This study focused on the characterization of the dry powder magnesium hydroxide suspensions. Particle size analysis is one of the most important approaches for such characterization.

The hindered settling method was the major method utilized for of the particle size analysis in this study. Suspensions were prepared to observe the hindered settling with a similar tendency in falling patterns. Three distinctive regions were clearly observed. Three modified equations to Stokes' law, namely Steinour, Richardson and Zaki, Dollimore and McBride, were explored to describe the sedimentation plots for the suspensions at a series of concentrations in various media with an increasing viscosity by adding CMC. The particle size calculated using the results from these three equations gave an increasing tendency with increasing CMC concentrations in dispersion media. The compartment model was attempted to be utilized, however, insufficient data points,

namely only 5 points of the required 10, were obtained from hindered settling, and this attempt failed. The mean particle size calculated in this method were compared with all other methods available.

Among the four most widely used methods chosen for the study of dry powder magnesium hydroxide suspensions, sieve analysis is the most simple method to obtain size distribution, however, it was not the appropriate one to obtain the actual particle size. The clustered and porous nature of the powder, as observed under Scanning electron microscopy (SEM) imaging, caused a mean size (r) to be greater when compared to the other methods used in this study. Sieve analysis was only utilized to obtain the size distribution for only the dry powder and not the suspensions.

Scanning electron microscopy (SEM) was a good imaging method to observe the nature and texture of both the dry powder magnesium hydroxide and the dried sediment from the suspensions prepared with various media. The image for the dry powder magnesium hydroxide greatly explained the cause of the enlarged mean particle size obtained from the sieve analysis. The estimated size range from SEM images was consistent with the calculated particle size using the hindered settling method. However, SEM only gave an estimation of the particle size range but no the actual size distribution. The sampling method could also be modified for better imaging.

A better and more sensitive method, laser diffraction (LD), was utilized to obtain the size distribution of the dry powder magnesium hydroxide dispersed in various media. This

method showed a similar tendency of particle size enlargement with an increasing viscosity after the addition of CMC in the hindered settling method. The mean particle size determined by this method was slightly smaller compared to that by hindered settling method. One limitation of the LD method is that the sonication and dispersion of the suspension into the flow system during measurement will effect the determination of particle size to some extent.

Thermal techniques such as differential scanning calorimetry (DSC) and thermogravimetry (TG) were utilized in this study to determine the water content in the dry powder magnesium hydroxide suspensions prepared in various media. The amount of associated water in the concentrated suspensions is an important parameter for better understanding the nature of such suspensions. With the DSC, however, it was only possible to observe the free unbound water in the dry powder magnesium hydroxide suspension sediments, the loosely-bound water was not able to be observed in this study, even at extreme temperature conditions as -50°C with prolonged holding times, due to the limitation of temperature program in current instrumentation. TG gives a better estimation of the possible associated water in such sediments. The first derivative of the percent (%) mass loss versus temperature in °C was utilized to determine the possible water content of both the unbound and bound water which loosely bounded onto the magnesium hydroxide particles. It indicated that the bound water was lost in slightly higher temperature compared to the unbound water. The addition of CMC decreased the

bound water content. With an increasing concentrations of CMC, the water content decreased. One possible explanation is that the addition of CMC to the dispersion media, with the magnesium hydroxide particles caused the CMC to occupy the binding sites due to its polymeric nature, resulting in fewer sites for water to bind.

X-ray powder diffraction (PXRD) was then a useful method to determine the composition of the residuals after heating under high temperature (up to 500 °C) in TG. The PXRD results verified the fact that decomposition occurred after 350°C. It indicated an incomplete decomposition at such temperature. One possible explanation was that the samples were not heated sufficiently at a hold temperature of 400 °C, due to the fast heating rate in the TG temperature program.

9.2 Future Work

1. As observed in the hindered settling experiments, the decrease in the rate of fall of the interface after preparation of suspensions could be further studied to verify the explanation of insufficient wetting after the first settling reading and extended wetting over time.
2. More concentrations of dry powder magnesium hydroxide could be prepared for hindered settling experiments to make it possible to explore the compartment model, which requires at least 5 data points for each compartment (a total of 10) to obtain a meaningful and precise linearity.
3. Since dry powder magnesium hydroxide suspensions were naturally flocculated, the

flocculating effect of CMC was not obvious in this study. Other types of polymer could be used as viscosity enhancers and protective colloids for further evaluation of the properties of dry powder magnesium hydroxide suspensions.

4. The sampling method in SEM can be also modified for better imaging for the dried sediments.
5. The determination of the water content in the suspension systems by TG and DSC could be further studied to establish better operating conditions to obtain a better resolution of the peaks and estimation of the existence of the bound and unbound water.

References

Chapter 1

1. M. E. Aulton, Pharmaceutics: The Science of Dosage Form Design 2nd Edition, Churchill Livingstone, 2002, p91
2. J. I. Bhatty, L. Davies, D. Dollimore, The Use of Hindered Settling Data to Evaluate Particle Size or Floc Size, and The Effect of Particle-Liquid Association on Such Sizes, Surface Technology, (1982), 15, pp.323-344
3. Terence Allen, Particle size Measurement 5th Edition, Chapman & Hall, 1997, p44
4. R.C. Mackenzie, Nomenclature in Thermal Analysis, Treatise on Analytical Chemistry, John Wiley & Sons, 1983, Part 1, Vol. 12, pp. 1-16

Chapter 2

1. Leon Lachman, Herbert A. Lieberman, Joseph L. Kanig, The Theory and Practice of Industrial Pharmacy 3th Edition, Lea & Febiger, 1986, pp.479-500
2. Alfred Martin, Physical Pharmacy 2nd Edition, Lea & Febiger, 1993, pp.477-487
3. Lan D. Morrison, Sydney Ross, Colloidal Dispersions: Suspensions, Emulsions, and Foams, John Wiley & Sons, Inc., 2002, pp.70-71

4. J. I. Bhatty, L. Davies, D. Dollimore, The Use of Hindered Settling Data to Evaluate Particle Size or Floc Size, and The Effect of Particle-Liquid Association on Such Sizes, Surface Technology, (1982), 15, pp.323-344
5. Clive Washington, Particle size analysis in pharmaceutics and other industries - theory and practice, Ellis Horwood Limited, 1992, p193-195
6. Alfred Martin, Physical Pharmacy 2nd Edition, Lea & Febiger, 1993, pp.432-433
7. J.M. Rosen, Surfactants and Interfacial Phenomena 2nd Edition, John Wiley & Sons, Inc., 1989, p.212
8. L. Davies, D. Dollimore, J. H. Sharp, Sedimentation of Suspensions: Implications of Theories of Hindered Settling, Powder Technology, (1976), 13, pp.123-132
9. Robert B. McKay, Hindered settling of organic pigment dispersions in hydrocarbon liquids, Journal of Applied Chemistry & Biotechnology, (1976), 26(2), pp.55-66.
10. D. Dollimore, G. B. McBride, Alternative methods of calculating particle size from hindered settling measurements, Journal of Applied Chemistry & Biotechnology, (1968), 18(5), pp.136-140
11. Yuantao Wang, Master Thesis: The Investigation of Concentrated Suspensions of Magnesium Trisilicate, The University of Toledo, 2001
12. Harold H. Steinour, Rate of Sedimentation: Non-flocculated Suspensions of Uniform Spheres, Industrial and Engineering Chemistry, (1944), 36(7), pp.618-624
13. J.F. Richardson, W.N. Zaki, The Sedimentation of A Suspension of Uniform Spheres

Under Conditions of Viscous Flow, Chemical Engineering Sciences, (1954), 8, pp.65-73

14. J.F. Richardson, W.N. Zaki, Sedimentation and Fluidisation: Part I, Transactions of the Institution of Chemical Engineers, (1954), 32, pp. 35-53
15. D. Dollimore, G.B. McBride, Comparison of Methods of Calculating Particle Size From Hindered Settling Results and Its Application to Inorganic Oxysalts Precipitates, Analyst, (1969), 94, pp.760-767
16. V. Ramakrishna, S.R. Rao, Particle Size Determination And Hindered Settling, J. Appl. Chem., (1965), 15, pp.473-479
17. D. Dollimore, G.B. McBride, The application of Hindered Settling Methods to Suspensions of Oxysalts, Powder Technology, (1973), 8, pp.207-212
18. D. Dollimore, R.Karimian, Sedimentation of Suspensions: Factors Affecting The Hindered Settling of Alumina In A Variety of Liquids, Surface Technology, (1982), 17, pp.239-250
19. L. Davies, D. Dollimore, G.B. McBride, Sedimentation of Suspensions: Simple Methods of Calculating Sedimentation Parameters, Powder Technology, (1977), 16, pp.45-49
20. L. Davies, D. Dollimore, Theories and Experimental Values For the Parameter k of The Kozeny-Carman Equation, As Applied To Sedimenting Suspensions, J. Phys. Appl. Phys., (1980), 13, PP.2013-2020

21. K. S. Alexander, D. Dollimore, S. S. Tata, V. Uppala, A Comparison of the Coefficients in the Richardson and Zaki's and Steinour's Equations Relating to the Behavior of Concentrated Suspensions, Separation Science And Technology, (1991), 26(6), pp.819-829
22. Kenneth S. Alexander, Jamshid Azizi, David Dollimore, Vykuntam Uppala, Interpretation of the Hindered Settling of Calcium Carbonate Suspensions in Terms of Permeability, Journal of Pharmaceutical Sciences, (1990), 79(5), pp. 401-406
23. Ping Tong, Master Thesis: A Study of Hindered Settling Phenomena and Thermal Analysis on Selected Calcium Oxysalts, The University of Toledo, 1995
24. A. Basu, P. Tong, K.A. Alexander, D. Dollimore, Extension of The Compartment Theory For Hindered Settling Suspensions, S.T.P. Pharma Sciences, (1997), 7(3), pp.215-222

Chapter 3

1. Leon Lachman, Herbert A. Lieberman, Joseph L. Kanig, The Theory and Practice of Industrial Pharmacy 3rd Edition, Lea & Febiger, 1986, pp.480-481
2. Alfred Martin, Physical Pharmacy 2nd Edition, Lea & Febiger, 1993, p.478
3. J. R. Farnand, H. M. Smith, I. E. Puddington, Spherical agglomeration of solids in liquid suspension, The Canadian Journal of Chemical Engineering, (1961), 39(2),

pp.94-97

4. M. E. Aulton, Pharmaceutics: The Science Of Dosage Form Design 2nd Edition, Churchill Livingstone, 2002, pp.337-340
5. M. E. Aulton, Pharmaceutics: The Science Of Dosage Form Design 2nd Edition, Churchill Livingstone, 2002, pp.79-84
6. A.W. Adamson, Physical Chemistry of Surfaces 3rd Edition, Wiley-InterScience, 1976, p.197
7. http://images.pennnet.com/articles/wwi/thm/th_korea%20explores%20f1.gif
8. B. Dobias, Coagulation and Flocculation Theory and Applications, M. Dekker, 1993, pp.391-426
9. B. Dobias, Coagulation and Flocculation Theory and Applications, M. Dekker, 1993, pp.231-243
10. Marjorie J. Vold, The Effect of Adsorption on The van der Waals Interaction of Spherical Colloidal Particles, Journal of Colloid Science, (1961), 16(1), pp.1-12
11. M. E. Aulton, Pharmaceutics: The Science Of Dosage Form Design 2nd Edition, Churchill Livingstone, 2002, pp.91-93
12. E. Verwey, J.Hh.G. Overbeek, Theory of The Stability of Lyophobic Colloids, Elsevier, 1948, p.155
13. Ian D. Morrison, Sydney Ross, Colloidal Dispersion: Suspensions, Emulsions, and Foams, Wiley-InterScience, 2002, pp.506-510

14. Alfred Martin, Physical Pharmacy 2nd Edition, Lea & Febiger, 1993, pp. 482-483
15. J.I. Bhatty, D. Dollimore, A.H. Zahedi, Studies on The Suspending Properties of Aqueous Solutions of Some Natural And Synthetic Hydrocolloids on China Clay Suspensions, Water Research, (1978), 12, pp.1139-1148
16. Asif S. Bhatti, David Dollimore, Lesley Davies, Javed I Bhatty, The Application of Interface Settling Rates In Hindered Settling to The Determination of The Mean Particle Radii, Surface Technology, (1985), 26, pp.287-293

Chapter 4

1. M. E. Aulton, Pharmaceutics: the science of dosage form design 2nd Edition, Churchill Livingstone, 2002, p91
2. Terence Allen, Particle size Measurement 5th Edition, Chapman & Hall, 1997, p44
3. Clive Washington, Particle size analysis in pharmaceutics and other industries - theory and practice, Ellis Horwood Limited, 1992, p10
4. Terence Allen, Particle size Measurement 5th Edition, Chapman & Hall, 1997, p112-113
5. Clive Washington, Particle size analysis in pharmaceutics and other industries - theory and practice, Ellis Horwood Limited, 1992, p215-220
6. M. E. Aulton, Pharmaceutics: the science of dosage form design 2nd Edition,

Churchill Livingstone, 2002, p 156-158

7. Alfred Martin, Physical Pharmacy 2nd Edition, Lea & Febiger, 1993, p431-432
8. H.G. Merkus, Particle Size Measurements, Springer Science+Business Media B.V. 2009, p 205- 209
9. Terence Allen, Particle size Measurement 5th Edition, Chapman & Hall, 1997, p 141
10. A.K. Dua, M. Roy, Principles and Applications of SEM and EDAX, Materials science foundations, Zurich: Trans Tech Publicaions, Vol 49, 2009
11. Barbra L. Gabriel, SEM: A user's manual for materials science, American society for metals, 1985, p 4-25
12. Ray F. Egerton, Physical Principles of Electron Microscopy, Springer Science & Business Media, Inc., 2005, p17
13. http://metallurgyfordummies.com/metallography/scanning-electron-microscope2-2/
14. http://en.wikipedia.org/wiki/Scanning_electron_microscope
15. Ray F. Egerton, Physical Principles of Electron Microscopy, Springer Science & Business Media, Inc., 2005, p 126-129
16. Barbra L. Gabriel,SEM: A user's manual for materials science, American society for metals, 1985, p 81-85
17. Leon Lachman, Herbert A. Lieberman, Joseph L. Kanig, The Theory and Practice of Industrial Pharmacy, Lea & Febiger, 1986, p27
18. H.G. Merkus, Particle Size Measurements, Springer Science+Business Media B.V.

2009, p 220

19. Jens T. Carstensen, Advanced Pharmaceutical Solids, Marcel Dekker Inc., New York, 2001, p55.
20. http://en.wikipedia.org/wiki/Mesh_(scale)
21. Terence Allen,Particle size Measurement 5th Edition, Chapman & Hall, 1997, p 163
22. Harry G. Brittain, Particle-Size Distribution, Part III: Determination by Analytical Sieving, Pharmaceutical Physics, www.pharmatech.com, December 2002
23. Clive Washington, Particle size analysis in pharmaceutics and other industries - theory and practice, Ellis Horwood Limited, 1992, p 75-76
24. Clive Washington, Particle size analysis in pharmaceutics and other industries - theory and practice, Ellis Horwood Limited, 1992, p193-195
25. Clive Washington, Particle size analysis in pharmaceutics and other industries - theory and practice, Ellis Horwood Limited, 1992, p105
26. Marie J. Desroches, Ian A. Castillo, Richard J. Munz, Determination of Particle Size Distribution by Laser Diffraction of Doped-CeO2 Powder Suspensions: Effect of Suspension Stability and Sonication, Part. Part. Syst. Charact. 22 (2005) 310–319
27. Alena Mudroch, Manual of physico-chemical analysis of aquatic sediments. CRC Press Inc. 1997, p. 30.
28. H.G. Merkus, Particle Size Measurements, Springer Science+Business Media B.V. 2009, p 260-269

29. Barabanenkov YN, The Fraunhofer approximation in the theory of multiple wave scattering, Radiophysics and Quantum Electronics, February, 1971, vol. 14, No. 2, 188-194.

30. R. Guardani, C.A.O. Nascimento, R.S. Onimaru, Use of neural networks in the analysis of particle size distribution by laser diffraction: tests with different particle systems, Powder Technology 126 (2002) 42–50

31. http://en.wikipedia.org/wiki/Dynamic_light_scattering

32. http://www.malvern.com/LabEng/technology/dynamic_light_scattering/classical_90_degree_scattering.htm

Chapter 5

1. P. J. Haines, Principles of Thermal Analysis and Calorimetry, Royal Society of Chemistry, 2002, p4

2. A.T. Riga, K.S. Alexander, Thermal Analysis of Drugs and Drug Products, American Pharmaceutical Review, 4(1), 2001, p36

3. M.E. Brown, Introduction to Thermal Analysis, Chapman and Hall, 1988, p4

4. M.E. Brown, Introduction to Thermal Analysis, 2nd Edition, Kluwer Academic Publications, 2001, p3

5. M.E. Brown, Introduction to Thermal Analysis, 2nd Edition, Kluwer Academic

Publications, 2001, p6 Table 1.2

6. D. Giron, Applications of Thermal Analysis in the Pharmaceutical Industry, Journal of Pharmaceutical & Biomedical Analysis, 1986, Vol. 4, No. 6, pp. 755-770
7. G.W. H. Höhne, W. F. Hemminger, H.-J. Flammersheim, Differential Scanning Calorimetry 2nd Edition, Springer-Verlag Berlin Heidelberg 2003, p1
8. Emmett S. Watson, Michael J. O'Neill, Differential Microcalorimeter, US Patent No. 3,263,484, April 1962
9. P. J. Haines, Principles of Thermal Analysis and Calorimetry, Royal Society of Chemistry, 2002, p55, 56 Figure1
10. G.W. H. Höhne, W. F. Hemminger, H.-J. Flammersheim, Differential Scanning Calorimetry 2nd Edition, Springer-Verlag Berlin Heidelberg 2003, p9-10
11. Alan Riga, Dhruthiman R Mantheni, Shravan Thakur, "Using DSC and TGA for Materials Characterization - Creating the Best Results from Your DSC and TGA", Cleveland State University, Cleveland, Ohio, Jun 12, 2011
12. M.E. Brown, Introduction to Thermal Analysis, 2nd Edition, Kluwer Academic Publications, 2001, p59-60
13. Mike Reading, Douglas J. Hourston, Modulated-Temperature Differential Scanning Calorimetry: Theoretical and Practical Applications in Polymer Characterization, Springer, 2006, p1-2
14. P. J. Haines, Principles of Thermal Analysis and Calorimetry, Royal Society of

Chemistry, 2002, p70-75

15. M.E. Brown, Introduction to Thermal Analysis, 2nd Edition, Kluwer Academic Publications, 2001, p55-66
16. Pandini, S.; Pegoretti, A.; Ricco, T., DSC analysis of post-yield deformed pbt. Effects of thermal history, Journal of Thermal Analysis and Calorimetry, 2008, 94 (3), pp.825-833
17. G.W. H. Höhne, W. F. Hemminger, H.-J. Flammersheim, Differential Scanning Calorimetry 2nd Edition, Springer-Verlag Berlin Heidelberg 2003, p4
18. R.C. Mackenzie, Nomenclature in Thermal Analysis, Treatise on Analytical Chemistry, John Wiley & Sons, 1983, Part 1, Vol. 12, pp. 1-16
19. P. J. Haines, Principles of Thermal Analysis and Calorimetry, Royal Society of Chemistry, 2002, p10
20. C.J. Keattch, D. Dollimore, An Introduction to Thermogravimetry 2nd Edition, Heyden & Son Ltd., 1975, p12-21
21. M.E. Brown, Introduction to Thermal Analysis, 2nd Edition, Kluwer Academic Publications, 2001, p19-25
22. M.E. Brown, Introduction to Thermal Analysis, 2nd Edition, Kluwer Academic Publications, 2001, p44-45
23. http://physicalchemistryresources.com/Book5_sections/TA_Applications%20Thermogravimetric%20AnalysisHTML_1.htm

Chapter 6

1. http://en.wikipedia.org/wiki/X-ray_powder_diffraction
2. Ron Jenkins, Robert L. Snyder, Introduction to X-Ray Powder Diffractometry, John Wiley & Sons, Inc., 1996, pp. 1-20
3. C. Suryanarayana, M. Grant Norton, X-Ray Diffraction: A Practical Approach, Plenum Press, 1998, pp. 1-19
4. Ron Jenkins, Robert L. Snyder, Introduction to X-Ray Powder Diffractometry, John Wiley & Sons, Inc., 1996, pp. 47-56
5. R. W. James, The optical principles of the diffraction of x-rays, Crystalline state, Vol. 2, Ithaca, N. Y., Cornell University Press, 1965, pp. 20-73
6. C. Suryanarayana, M. Grant Norton, X-Ray Diffraction: A Practical Approach, Plenum Press, 1998, pp. 50-52
7. http://serc.carleton.edu/research_education/geochemsheets/BraggsLaw.html
8. C. Suryanarayana, M. Grant Norton, X-Ray Diffraction: A Practical Approach, Plenum Press, 1998, pp. 63-80
9. T. C. Huang, W. Parrish, Characterization of Thin Films by X-Ray Fluorescence and Diffraction Analysis, Adv. X-Ray Anal., 1979, Vol. 22, pp. 43-63
10. Ron Jenkins, Robert L. Snyder, Introduction to X-Ray Powder Diffractometry, John Wiley & Sons, Inc., 1996, pp. 231-233
11. Munch, H. Ralph, Powder Sample Preparation For X-Ray Diffraction, Norelco

Reporter, Vol. 10 Issue 2, 1963, p.75.

12. B. D. Cullity, Elements of X-Ray Diffraction 2nd Edition, Addison-Wesley, 1978, p.230-237

13. http://epswww.unm.edu/xrd/xrdclass/01-XRD-Intro.pdf

Chapter 7

1. Martindale: The Complete Drug Reference 32th Edition, Kathleen Parfitt, London: Pharmaceutical Press, 1999
2. The Merck Index, Eighth Edition, Merck & Co., Inc., 1968
3. Ionic Equilibria in Analytical Chemistry, Henry Freiser, Krieger Pub Co., 1963
4. http://en.wikipedia.org/wiki/Magnesium_hydroxide
5. http://en.wikipedia.org/wiki/Brucite
6. http://en.wikipedia.org/wiki/Crystal_habit
7. The Chemistry and technology of magnesia, Mark A. Shand, John Wiley & Sons, Inc., 2006
8. Drug Information Handbook 13th Edition, Charles F. Lacy, Lexi-Comp, 2005
9. http://www.valetimegroup.com/international-trade/chemicals/traded-chemicals/magnesium-hydroxide/
10. http://www.chemicalland21.com/industrialchem/inorganic/MAGNESIUM%20HYDR

OXIDE.htm

11. Remington's Pharmaceutical Sciences 17th Edition, A.R. Gennaro, Mark Publishing Co., Easton, 1987

12. http://www.pharmainfo.net/files/images/stories/article_images/Pharmaceutical%20Ostwald%20Viscometer%20file13.jpg